BROADENING THE SPECTRUM OF ALTERNATIVE FEEDSTOCKS: BIOCATALYTIC METHODS FOR SYNTHESIZING FINE CHEMICALS AND COMMODITY PRODUCTS

By

Yasheen Jadidi

A DISSERTATION

Submitted to
Michigan State University
in partial fulfillment of the requirements
for the degree of

Chemical Engineering – Doctor of Philosophy
Chemistry – Dual Major

2023

ABSTRACT

Shikimic acid (SA) and 3-dehydroshikimate (DHS) are intermediates for synthesizing fine and commodity chemicals including oseltamivir, adipic acid, vanillin, and catechol. Current methods for producing these molecules rely on non-renewable petrochemicals, low-yielding plant extractions, or market-saturated agricultural feedstocks. Data presented in this report encompass multiple efforts to develop alternate routes toward chemicals, including both *in vivo* and *in vitro* methods. The first method entails building an economy from agricultural residues utilizing mixed sugars derived from farm waste for SA biosynthesis. The second method builds on an economy based on methanol by metabolizing methanol for DHS biosynthesis.

Escherichia coli RB791 strains expressing three different glucose transport systems – one phosphotransferase system (PTS), and two non-PTS – were characterized in a fed-batch fermenter for their abilities to co-utilize glucose and xylose for SA overproduction. Strain YJ1.144/pSC6.090B, expressing transport enzymes GlF and GlK, out-performed a strain expressing its native glucose PTS and a strain evolved to take up glucose via one of its non-native transport systems. YJ1.144/pSC6.090B achieved a high SA titer of 94.9 g L^{-1} when grown on a 70:30 (*w*/*w*) mixture of glucose/xylose. YJ1.144/pSC6.090B achieves lower SA titer (55.6 g L^{-1}) and higher quinic acid titer when grown on sugars derived from a ball milling process, which also contained acetate. The exact mechanism of this inhibition was not characterized. CO_2 emission data collected from the fed-batch fermentations motivated a comparative LCA/TEA study. Results of LCA depended on assumptions of allocation. As a waste product, stover contributed 29% more than grain to global warming, 86% less to eutrophication, 96% less to water usage, and 69% less to land usage. With allocation based on economic value of the feedstocks, stover contributed 36% more than grain to global warming and had eutrophication, water usage, and land usage impacts

that were over 2-fold higher than that of corn grain. TEA indicated both biorefinery models were profitable. SA sourced from corn grain is more profitable than SA sourced from corn stover.

Deriving commodity chemicals from methanol suffered from a lack of a genetic toolset for modifying the genome of the host strain *Bacillus methanolicus* MGA3. A method was developed for mutagenesis and mutant screening of shikimate pathway auxotrophs in *B. methanolicus* MGA3. Two strategies were also employed to knockdown shikimate dehydrogenase in MGA3 to accumulate DHS: RNAi (RNA interference) and CRISPRi (CRISPR interference). Quantifiable amounts of DHS have yet to be assayed during the knockout and both knockdown strategies. Results from the knockdown suggest non-mutants are enriched during the mutagenesis procedure. More MGA3 mutants need to be isolated, and/or a more effective knockdown strategy must be developed for accumulating quantifiable amounts of DHS.

In memory of Dr. Kris A. Berglund.
I will always remember you fondly.
Rest in peace.

ACKNOWLEDGEMENTS

First and foremost, I have to thank my father and mother. Dad, you are the one person I can go to and have any conversation with. Without my father I would be lost and aimless in this life with no real path to walk down. My beautiful mother has provided me with unconditional love and support since the day I was born.

I want to thank Dr. John W. Frost. The day I met Dr. Frost marked the most important point of inflection during my graduate study, because without having shaken his hand I could have never met Dr. Karen Draths. Investigators oftentimes help each other in ways that can define one another's research for nothing more than a "thank you". I feel a sense of guilt saying thank you to Dr. Draths, as she goes out of her own way for other people's research more often than most for nothing in return. If I could describe her with one word it would be 'dynamic'. Her willingness to take me on as a student coming from a different department and co-advise me with Dr. Christopher M. Saffron, not to mention funding and letting me conduct virtually all my research in her lab, makes her the most central figure in my endeavors. Thank you, Dr. Draths. Thank you very much to Dr. Saffron for serving as my primary advisor. The knowledge you have given me through coursework and in person allowed me to publish my work and will likely carry me through my post-doctoral career.

Thank you to all the members who are serving on my committee and offered their guidance: Dr. Gary J. Blanchard, Dr. Bruce E. Dale, and Dr. S. Patrick Walton. A special thank you to Dr. Nicole E. Shriner, as well, for allowing me to teach under you almost every semester I have taught at MSU. You are a great friend and mentor. Thank you to my co-authors: Dr. Sabyasachi Das and Henry Frost. Thank you to Dr. Wei Liao, as well, for the collaboration with his lab that allowed me to create some of my best work. Thank you to Dr. Marta Irla, as well, for taking the time to

meet with me (and from Norway, no less) multiple times to discuss the strain *Bacillus methanolicus* MGA3. Also, thank you for graciously donated the MGA3 strain to our lab. Thank you to current and former members of my research group Esther Lee, Katelyn Silva, Bismarck Amaniampong, Katie Kwiatkowski, and Amaya Sirinimal for your support.

I would also like to take this chance to mention a few of my close family members and friends. My sister, Sahar Jadidi, and my brother, Dr. Shaheen Jadidi, I am here for you both no matter what. Mom, dad, and I love you more than you know. Pavlin Dimitrov, you and your family have supported me for many years, and you have always been a great role model for me. Affan Malik, I have always said that you are the most talented chemical engineer in our batch of graduate students. I look forward to seeing the wonderful things that are to come for you. Jorge and Rosa Nevarez, you are two of the most amazing people I have ever met. Thank you Rosa for creating the abstract art that was used for our LCA/TEA paper. Finally, to the Iranian community and the Iranian Students Association (ISA) at MSU – this past semester was not easy for any of us. The kindness you have all showed me during my time in East Lansing was truly memorable.

My work has been financially supported by the Department of Chemistry at Michigan State University (MSU), the CHEMS Department at MSU, and MTRAC.

TABLE OF CONTENTS

LIST OF TABLES

LIST OF FIGURES

LIST OF ABBREVIATIONS

SA	Shikimic acid
DHS	3-dehydroshikimic acid
3-HP	3-hydroxypropionate
*cc*MA	*cis*, *cis*-muconic acid
AA	Adipic acid
ACA	Acetylenecarboxylic acid
ADCA	Acetylenedicarboxylic acid
MSA	Malonate semialdehyde
PEP	Phosphoenolpyruvate
E4P	Erythrose-4-phosphate
S3P	Shikimate-3-phosphate
AroB	DHQ synthase
AroF	tyrosine-sensitive DAHP synthase
AroG	phenylalanine-sensitive DAHP synthase
AroH	tryptophan-sensitive DAHP synthase
AroD	DHQ dehydratase
AroE	Shikimate dehydrogenase
AroL	Shikimate kinase isozyme 1
AroK	Shikimate kinase isozyme 2
$AroF^{FBR}$	Feedback resistant DAHP synthase
DHQ	3-dehydroquinate
GlF	Facilitated diffusion transport protein

GlK	Facilitated diffusion kinase
aroL	Shikimate kinase isozyme 1 gene
aroK	Shikimate kinase isozyme 2 gene
serA	D-3-phosphoglycerate dehydrogenase (first-step enzyme in serine biosynthesis)
aroB	DHQ synthase gene
ptsG	glucose specific enzyme IIB gene
glf	Facilitated diffusion transport protein gene
glk	Facilitated diffusion kinase gene
tktA	Transketolase gene
aroB	DHQ synthase gene
P_{tac}	tac promoter
P_{lac}	lac promoter
aroE	Shikimate dehydrogenase gene
$EIIA^{gluc}$	glucose specific enzyme IIA
$EIICB^{gluc}$	glucose specific enzyme IIB
PTS	Phosphotransferase system
XylFGH	Part of the ABC transporter complex involved in xylose transport
XylAB	Part of the ABC transporter complex involved in xylose transport
Ap^R	Ampicillin resistance
Cm^R	Chloramphenicol resistance
Sp^R	Spectinomycin resistance
Kn^R	Kanamycin resistance
LB	Luria broth (rich media)

SOB	Super optimal broth (rich media)
PCR	Polymerase chain reaction
aTc	Anhydrotetracycline
Rep101(T_s)	Thermosensitive replicon
DO	Dissolved oxygen
OD	Optical density
DCW	Dry cell weight
RID	Refractive index detection
UV-vis	Ultraviolet-visible light
CCR	Carbon catabolite repression
C_j	Number of carbon atoms in compound j
T_j	Titer of compound j
MW_j	Molecular weight of compound j
F_j	Mass of compound j in external feed per initial volume of broth
LCA	Life cycle assessment
TEA	Technoeconomic analysis
NPV	Net present value
MSP	Minimum selling price
LCI	Life cycle impacts
TC	Transportation cost
X	Trucking distance
WSF	Water scarcity footprint
CF_{AWARE}	Characterization factor

w_i	Water usage inventory of equipment, i
$C_{x,yr,cap}$	Equipment cost at particular year and capacity
CEPCI	Chemical Engineering Plant Cost Index
AAI	Average annual investment
P	Initial investment
SV	Salvage value
n	Economic lifetime
DEP	Depreciation
$C_{int,ins}$	Annual cost of interest and insurance
PMH	Productive machine hours
SMH	Scheduled machine hours
MR	Machine rate
PR	Production rate
La	Lang factor
C_x	Cash flow
SP	Selling price
FP	Feedstock price
FR	Feedstock consumption rate
ASR	Annual sales revenue
GP	Gross profit
NP	Net profit
DCFRR	Discount cash flow rate of return
LCIA	Life cycle Impact Assessment

$Stover_1$	Stover allocation scenario one
$Stover_2$	Stover allocation scenario two
$Grain_1$	Grain allocation scenario one
$Grain_2$	Grain allocation scenario two
EMS	Ethyl methanesulfonate
MNNG	N-Methyl-N'-nitro-N-nitrosoguanidine
RNAi	RNA interference
CRISPRi	CRISPR interference
*as*RNA	Antisense RNA
*sg*RNA	Single guide RNA
*d*Cas9	Dead Cas9
RuMP	Ribulose monophosphate pathway
NADH	Nicotinamide adenine dinucleotide
NADPH	Nicotinamide adenine dinucleotide phosphate
ADP	adenosine diphosphate
ATP	adenosine triphosphate
TAE	Tris-Acetate EDTA
SOBsuc	Super optimal broth with sucrose
SR	Survival rate
CFU	Colony forming units
D	Dilution factor
t	Exposure time
PT	Paired termini

RBS	Ribosome binding site
AroG1	DAHP synthase isozyme 1 (MGA3)
AroG2	DAHP synthase isozyme 2 (MGA3)
AroB1	DHQ synthase isozyme 1 (MGA3)
AroB2	DHQ synthase isozyme 2 (MGA3)
P_{mdh}	Methanol-inducible promoter
P_{m2p}	Mannitol-inducible promoter

CHAPTER ONE: INTRODUCTION

1.1. Background & Motivation

It is proposed here that an agricultural residue economy and a methanol economy be developed and elaborated upon within the current bio-economy for chemical synthesis (**Fig. 1.1**). The chemical sector is a massive consumer of petroleum, demanding 14% of total petroleum and 8% of global natural gas consumption.[1,2,30] Petroleum and shale gas are non-renewable resources requiring energy-intensive processing that contribute to the looming threat of climate change.[2,32]

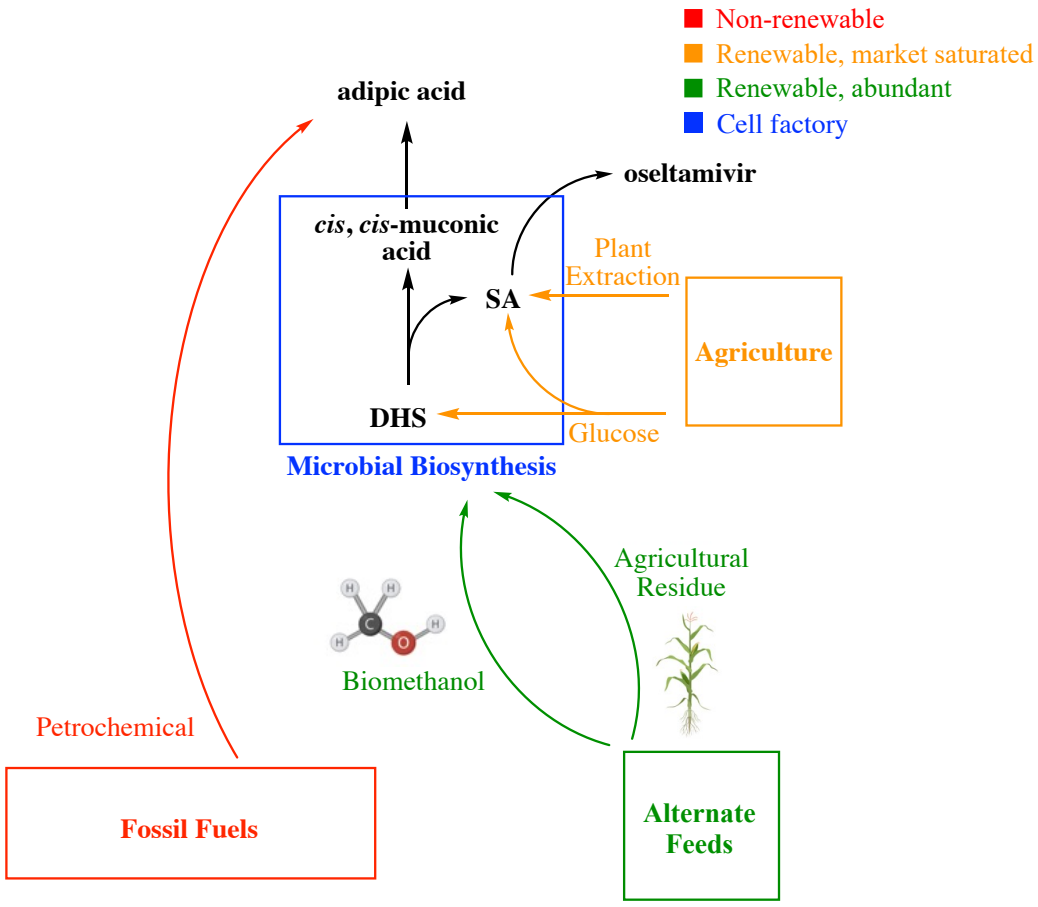

Figure 1.1. Overview of processes biosynthesis of chemical precursors shikimic acid (SA) and 3-dehydroshikimate (DHS) from alternate feeds including agricultural residues and methanol (green) in an effort to phase out fossil fuel economy (red) and avoid competition with agriculture economy. Methods for biosynthesis of these molecules of interest involve engineering a cell factory (blue) for production. Renewable feeds that can be used to synthesize SA and DHS from corn starch or Chinese star anise are boxed in orange.

These non-renewable resources are represented in red in **Fig. 1.1**, while renewable biomass resources are represented in orange and green. Agricultural resources that are produced in limited supply or that directly compete with the food industry are boxed in orange and alternative renewable resources are represented in green as potential "alternate" feeds.[33] Renewable biomass, including forest resources, agricultural resources, and construction/demolition waste, is the largest available source of renewable carbon in the United States.[34,35] Biomass was responsible for the production of over 40% of renewable energy used in the United States in 2015.[3] The *2016 Billion-Ton Report* demonstrated that the availability of biomass resources in the United States has potential to reach one billion dry tons by 2030, enough to displace approximately 30% of the country's reliance on petroleum.[4] Phasing out the economy's dependence on non-renewable resources will surely include efforts to find alternative feedstocks or to enhance the conversion efficiencies of current ones.[5-7]

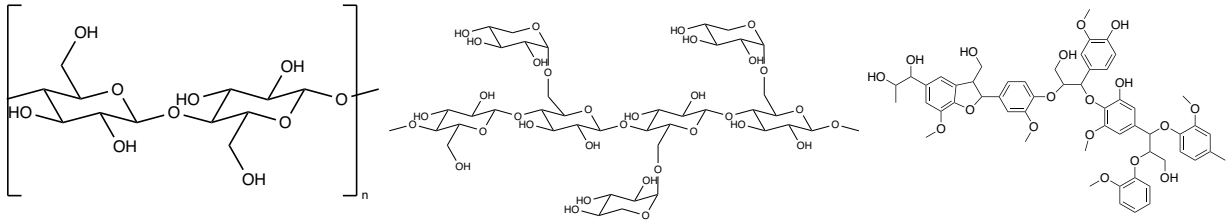

Figure 1.2. Components of lignocellulose chemical structures of **(a)** cellulose, **(b)** hemicellulose in the form of *D*-xylo-*D*-glucan, and **(c)** lignin.

For this work, agricultural residues in **Fig. 1.1** refer to lignocellulosic farm waste that fall into the category of alternative feeds (boxed in green). Lignocellulosic biomass is the most abundant renewable biomass resource on earth. The two major components of lignocellulose are lignin and holocellulose with holocellulose being made up of cellulose and hemicellulose polymers.[8,9] Structural features of these three biopolymers forming lignocellulose are shown in **Fig. 1.2**.

Lignocellulose contains roughly 40% cellulose (**Fig. 1.2(a)**) by mass, which is a biopolymer of *D*-glucose monomeric units connected by β-1→4 glycosidic linkages.[10] Hemicellulose occupies between 20% and 30% of total lignocellulose by mass and is a network biopolymer composed of different hexose and pentose monomeric units.[11] Although hemicellulose can take many forms, a common form containing D-glucose and D-xylose monomeric units, namely D-xylo-D-glucan, is shown in **Fig. 1.2(b)**. Hemicellulose is frequently acetylated, which serves as a natural defense mechanism against enzymes that break down these polysaccharide chains.[12] The remainder of lignocellulose is made up of lignin (**Fig. 1.2(c)**). While cellulose is embedded within hemicellulose networks, lignin tends to act as a binding material for layers of holocellulose. Lignin is also a heteropolymer composed of diverse organic alcohol monomeric units called monolignols. Its interunit linkages give lignin a packed globular structure that gives lignocellulose its recalcitrant nature.[8,12,13]

Single carbon molecules such as methanol can also be derived from renewable biomass resources. Methanol can be bioderived through the gasification of lignocellulosic biomass followed by catalytic hydrogenation of the synthesis gas that results.[14,36] Therefore, methanol can also be sourced from alternative feeds boxed green in **Fig. 1.1**. There is also potential to derive methanol from non-renewable single-carbon molecules that are otherwise flared during cracking processes.[37,38] The global economic burden from wasteful flaring and venting methane gas amounts to $30 billion annually, a figure that fails to account for the practice's contribution to climate change.[19] Thus, more utilization of methane-derived methanol could also enhance the efficiency of current non-renewable processes in an effort to alleviate the total demand for non-renewables. Methane can react with steam under high pressure in the presence of catalyst to produce a mixture of hydrogen and carbon monoxide known as syngas.[39-41] Syngas to methanol technologies (STM)

is a broad field dedicated to the conversion of syngas to methanol typically using a form of a metal-zeolite catayst.[15,16] Methane gas derived from anaerobic digestion (known as biogas, which is 50-75% methane and 25-50% carbon dioxide) is another abundant source of methane that can be used for STM.[17,18,31]

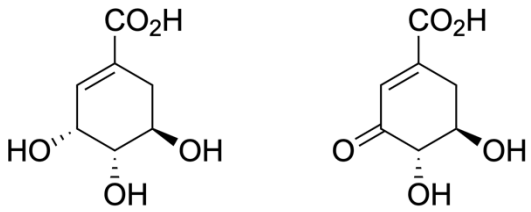

Figure 1.3. Molecules of interest chemical structures of **(a)** shikimic acid and **(b)** 3-dehydroshikimic acid.

Target molecules of interest chosen for this study, shikimic acid (SA) and 3-dehydroshikimic acid (DHS), are shown as chemical structures in **Fig. 1.3**. The natural product SA is the starting material for the synthesis of oseltamivir phosphate (Tamiflu®), an antiviral agent effective against influenza.[22-24] The valuable intermediate DHS can be dehydrated, subsequently decarboxylated, then acted on by a dioxygenase to form *cis*,*cis*-muconic acid (*cc*MA). The molecule *cc*MA is hydrogenated to form adipic acid (AA), a highly demanded dicarboxylic acid that is otherwise made from petroleum-derived benzene.[25] Most AA is used in the synthesis of nylon-6,6.[26] Briefly, two *in vivo* methods are proposed here for the biosynthesis of SA and DHS from lignocellulose and methanol, respectively. Previously, SA has been isolated from plants; however, methods for biosynthesizing SA from glucose via fed-batch fermentation have also been developed.[23,42] Methods for biosynthesizing DHS from glucose via fed-batch fermentation have also been reported.[25,43] **Fig. 1.1** shows however that these methods (orange) suffer from market saturation or competition with the food industry. Also, the product AA is commonly derived from nonrenewable petrochemicals (**Fig. 1.1** in red).[25,44] Production of SA and DHS from lignocellulose and methanol

feedstocks is investigated here to potentially mitigate these issues and broaden the spectrum of biomass resources that are currently used for chemical synthesis.

REFERENCES

[1] IEA, 2020. Energy Technology Perspectives **2020**, Energy Technology Perspectives. International Energy Agency, Paris.

[2] Bauer, F.; Kulionis, V.; Oberschelp, C.; Pfister, S.; Tilsted, J. P.; Finkill, G. D.; & Fjäll, S. "Petrochemicals and Climate Change: Tracing Globally Growing Emissions and Key Blind Spots in a Fossil-Based Industry" *IMES/EESS report* **2022**, 126.

[3] EIA (U.S. Energy Information Administration) **2016**. Short-Term Energy Outlook. https://www.eia.gov/forecasts/steo/report/renew_co2.cfm.

[4] Langholtz, M. H.; Stokes, B. J.; Eaton, L. M. "2016 Billion-Ton Report: Advancing Domestic Resources for a Thriving Bioeconomy" U.S. Department of Energy **2016**, Volume 1: Economic Availability of Feedstocks. (Leads), ORNL/TM-2016/160. Oak Ridge National Laboratory, Oak Ridge, TN. 448p. http://energy.gov/eere/bioenergy/2016-billion-ton-report.

[5] Liu, X.; Yu, D.; Luo, H.; Li, C.; Li, H. "Efficient Reaction Systems for Lignocellulosic Biomass Conversion to Furan Derivatives: A Minireview" *Polymers* **2022**, *14*, 3671.

[6] Veerabadhran, M.; Natesan, S.; MubarakAli, D.; Xu, S.; Yang, F. "Using different cultivation strategies and methods for the production of microalgal biomass as a raw material for the generation of bioproducts" *Chemosphere* **2021**, *285*, 131436.

[7] Liu, Z.; Wang, J.; Nielsen, J. "Yeast synthetic biology advances biofuel production" *Current Opinion in Microbiology* **2022**, *65*, 33-39.

[8] Smith, M. D. "Understanding Lignocellulose: Synergistic Computational and Analytic Methods" ACS Symposium Series, *ACS* **2019**, 1-15.

[9] Martin, A. F.; Tobimatsu, Y.; Kusumi, R.; Matsumoto, N.; Miyamoto, T.; Lam, P. Y.; Yamamura, M.; Koshiba, T.; Sakamoto, M.; Umezawa, T. "Altered lignocellulose chemical structure and molecular assembly in CINNAMYL ALCOHOL DEHYDROGENASE-deficient rice" *Nature* **2019**, *9*, 17153.

[10] Gibson, L. J. "The Hierarchical Structure and Mechanics of Plant Materials" *J. R. Soc., Interface* **2012**, *9* (76), 2749–2766.

[11] Ebringerová, A. "Structural Diversity and Application Potential of Hemicelluloses" *In Macromolecular Symposia; Wiley*; Weinheim, Germany **2005**, *232*, 1–12.

[12] Zoghlami, A.; Paës, G. "Lignocellulosic Biomass: Understanding Recalcitrance and Predicting Hydrolysis" *Front. Chem.* **2019**, *7*, 874.

[13] Boerjan, W.; Ralph, J.; Baucher, M. "Lignin Biosynthesis" *Annu. Rev. Plant Biol.* **2003**, *54* (1), 519–546.

[14] Nakagawa, H.; Harada, T.; Ichinose, T.; Takeno, K.; Matsumoto, S.; Kobayashi, M.; Sakai, M. "Biomethanol Production and CO_2 Emission Reduction from Forage Grasses, Trees, and Crop Residues" JARQ **2007**, *41* (2), 173 – 180. http://www.jircas.affrc.go.jp

[15] Yang, R.; Fu, Y.; Zhang, Y.; Tsubaki, N. "In situ DRIFT study of low-temperature methanol synthesis mechanism on Cu/ZnO catalysts from CO_2-containing syngas using ethanol promoter" *Journal of Catalysis* **2004**, *228*, 23-35.

[16] Bae, J. W.; Kasipandi, S. "Recent Advances in Direct Synthesis of Value-Added Aromatic Chemicals from Syngas by Cascade Reactions over Bifunctional Catalysts" *Advanced Materials* **2019**, *31*, 1803390.

[17] Saur, G.; Milbrandt, A. "Renewable Hydrogen Potential from Biogas in the United States" NREL/TP-5400-60283; *National Renewable Energy Lab*. (*NREL*), Golden, CO (United States), **2014**.

[18] Magnolo, F.; Dekker, H.; Decorte, M.; Bezzi, G.; Rossi, L.; Meers, E.; Speelman, S. "The Role of Sequential Cropping and Biogasdoneright™ in Enhancing the Sustainability of Agricultural Systems in Europe" *Agronomy* **2021**, *11*, 2102.

[19] Rabe, B.; Kaliban, C.; Englehart, I. "Taxing Flaring and the Politics of State Methane Release Policy" *Review of Policy Research* **2020**, 1-33.

[20] Liu, Z.; Wang, K.; Chen, Y.; Tan, T.; Nielsen, J. "Third-Generation Biorefineries as the Means to Produce Fuels and Chemicals from CO_2" *Nat. Catal.* **2020**, *3* (3), 274–288.

[21] Xu, L.; Xiu, Y.; Liu, F.; Liang, Y.; Wang, S. "Research Progress in Conversion of CO_2 to Valuable Fuels" *Molecules* **2020**, *25* (16).

[22] Diaz Quiroz, D. C.; Carmona, S. B.; Bolivar, F.; Escalante, A. "Current perspectives on applications of shikimic and aminoshikimic acids in pharmaceutical chemistry" *Research and Reports in Medicinal Chemistry* **2014**, *4*, 35-46.

[23] Rawat, G.; Tripathi, P.; Saxena, R. K. "Expanding horizons of shikimic acid: Recent progresses in production and its endless frontiers in application and market trends" *Appl. Microbiol Biotechnol.* **2013**, *97*, 4277-4287.

[24] Estévez, A. M.; Estévez, R. J. "A Short Overview on the Medicinal Chemistry of (—)-Shikimic Acid" *Mini-Reviews in Medicinal Chemistry* **2012**, *12*, 1443-1454.

[25] Niu, W.; Draths, K. M.; Frost, J. W. "Benzene-Free Synthesis of Adipic Acid" *Applied and Environmental Microbiology* **2012**, *78*(15), 5170-5181.

[26] Skoog, E.; Shin, J. H.; Saez-Jimenez, V.; Mapelli, V.; Olsson, L. "Biobased adipic acid – The challenge of developing the production host" *Biotechnology Advances* **2018**, *36*, 2248-2263.

[27] Werpy, T.; Petersen, G. *Top Value Added Chemicals from Biomass: Volume I -- Results of Screening for Potential Candidates from Sugars and Synthesis Gas*; DOE/GO-102004-1992, 15008859; 2004; p DOE/GO-102004-1992, 15008859. https://doi.org/10.2172/15008859.

[28] Kumar, V.; Ashok, S.; Park, S. Recent Advances in Biological Production of 3-Hydroxypropionic Acid. *Biotechnol. Adv.* **2013**, *31* (6), 945–961.

[29] Brethauer, S.; Shahab, R. L.; Studer, M. H. "Impacts of biofilms on the conversion of cellulose" *Applied Microbiology and Biotechnology* **2020**, 104:5201-5212.

[30] EIA, US. "Monthly Energy Review, November 2022" **2022**

[31] Li, Y.; Alaimo, C. P.; Kim, M.; Kado, N. Y.; Peppers, J.; Xue, J.; Wan, C.; Green, P. G.; Zhang, R.; Jenkins, B. M.; Vogel, C. F. A.; Wuertz, S.; Young, T. M.; Kleeman, M. J. "Composition and Toxicity of Biogas Produced from Different Feedstocks in California" *Environ. Sci. Technol.*, **2019**, 53, 11569-11579

[32] Gao, J. Fengqi, Y. "Dynamic material flow analysis-based life cycle optimization framework and application to sustainable design of shale gas energy systems." *ACS Sustainable Chemistry & Engineering* 6.9, **2018**, 11734-11752.

[33] Abadam, V.; Yeh, A. "Sugar and Sweeteners Outlook: June 2022" *USDA*, Economic Research Service, **2022**, SSS-M-406

[34] Pelkmans, L. "IEA Bioenergy Countries' Report." *Update*, **2021**.

[35] Bar-On, Y. M.; Phillips, R.; Milo, R. "The biomass distribution on Earth." *Proceedings of the National Academy of Sciences* 115.25, **2018**, 6506-6511.

[36] Deka, T. J., et al. "Methanol fuel production, utilization, and techno-economy: A review." *Environmental Chemistry Letters*, **2022**, 1-30.

[37] Elvidge, C. D., et al. "The potential role of natural gas flaring in meeting greenhouse gas mitigation targets, Energy Strateg. Rev., 20, 156–162." **2018**.

[38] Rehan, M.; Tahir, M. "Recent developments in natural gas flaring reduction and reformation to energy-efficient fuels: a review." *Energy & Fuels* 35.5, **2021**, 3675-3714.

[39] Latimer, A. A., et al. "Direct methane to methanol: the selectivity–conversion limit and design strategies." *ACS catalysis* 8.8, **2018**, 6894-6907.

[40] Priyank, K.; Mewada, R. K. "Single step oxidation of methane to methanol–towards better understanding." *Procedia Engineering* 51, **2013**, 409-415.

[41] Cañete, B., Gigola, C. E.; Nélida, B. B. "Synthesis gas processes for methanol production via CH4 reforming with CO2, H2O, and O2." *Industrial & Engineering Chemistry Research* 53.17, **2014**, 7103-7112.

[42] Ghosh, S.; Chisti, Y.; Banerjee, U. C. "Production of shikimic acid." *Biotechnology advances* 30.6, **2012**, 1425-1431.

[43] Li, K. "Microbial Syntheses of Value-Added Chemicals from *D*-Glucose" **1999**, *A PhD Dissertation*.

[44] Jin, X., et al. "Chemical Synthesis of Adipic Acid from Glucose and Derivatives: Challenges for Nanocatalyst Design." *ACS Sustainable Chemistry & Engineering* 8.51, **2020**, 18732-18754.

CHAPTER TWO: BIOSYNTHESIS OF SHIKIMIC ACID

2.1. Introduction

2.1.1. An Agricultural Residue Economy

Renewable biomass resources in the United States have the potential to reach one billion dry tons by 2030, which could displace approximately 30% of the country's reliance on petroleum.[1,2] Reaching this target will play a central role in phasing out nonrenewable petrochemical feedstocks but requires a large increase in the availability and supply of biomass.[2,38,54,55] Meanwhile, ongoing military actions between Russia and Ukraine (two of the world's largest suppliers of grain) have reduced global food supplies, which is a market that directly competes for biomass.[3,56] Ukraine alone is expected to decrease crop production by 35-45% for the next production year.[4] Utilization of lignocellulosic resources is one means of creating a renewable economy to fight climate change and mitigate today's unpredictable geopolitical climate.[39,40] The study presented here examines new technology for product synthesis from lignocellulosic corn stover.[5,6,7]

A ball-milling and enzymatic hydrolysis strategy to release glucose and xylose from the lignocellulosic, recalcitrant structures of corn stover has been reported.[8] Hydrolysates achieved glucose and xylose conversions and titers of [88.6%, 55.2 g L^{-1}] and [67.3%, 20.1 g L^{-1}]. This particular ball mill process has the advantages of being chemical-free, single-step, and easily scalable, while others tend to require multiple steps and harsh caustic materials.[8,41,42] This work sets up possibilities for the biosynthesis of chemicals from mixed sugar feedstocks. With collaborative help from the Liao group in the Biosystems Engineering Department at Michigan State University, the ball milling approach for releasing sugars from corn stover was combined with strain engineering and fermentation studies performed here. The ease of genetic manipulation

of *Escherichia coli* RB791 made it a practical host for conversion of corn stover hydrolysates to shikimic acid (SA).

SA is a high-value chemical used industrially as a precursor to the antiviral medicine oseltamivir phosphate, or Tamiflu®.[10,11] By itself, SA is reportedly a strong antioxidant and carries antipyretic, anti-inflammatory, and analgesic properties. SA derivatives, including (-)-zeylenone, [Pt(dach)$(SA)_2$], and 3,4-oxo-isopropylidene-SA, carry antitumor, anticancer, antibiotic, and antithrombotic activities.[10,12] Oseltamivir phosphate is a neuraminidase inhibitor of influenza virus surface proteins.[10,11] Traditional methods of extracting SA from *Illicium verum* (Chinese star anise) are low-yielding and depend on the unpredictable natural sources of SA, which sometimes fail to meet growing demands for Tamiflu.[57] It was during the swine flu pandemic that shortages of SA were blamed on plant extraction methods predominantly used for its production.[11] Further, where SA production was about 590 MT yr^{-1} in 2015, an average growth rate of 3.7% has been witnessed over the past several years.[13] To address this issue, prior research produced SA in high titer via bacterial fermentation using a glucose feedstock.[14-16] In alignment with a growing trend to examine alternative biomass feedstocks, recent advances have successfully produced mixtures of glucose and xylose sugars from lignocellulose derived from swine manure and corn stover.[11,17-19] Rational design of a bacterial host strain that can overproduce SA while co-fermenting hexose and pentose sugars derived from lignocellulose presents a window of opportunity to produce SA from farm residue feed sources.

2.1.2. Carbon Source Uptake Mechanisms

E. coli is host to many protein complexes capable of transporting carbohydrates across its phospholipid bilayer. Glucose-specific enzyme IIA ($EIIA^{gluc}$) and ptsG-encoded glucose-specific enzyme IIB ($EIICB^{gluc}$) components of the glucose PTS serve as an active transport protein dimer

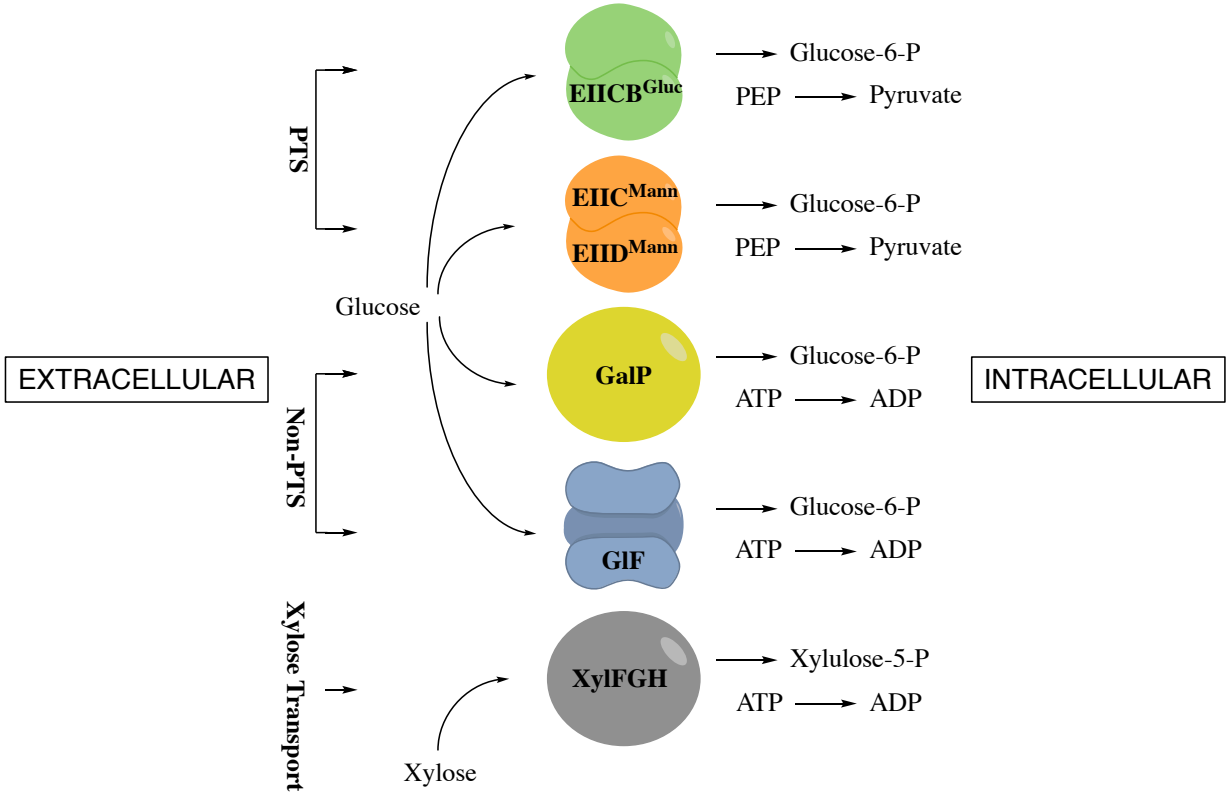

Figure 2.1. Substrate transport in *E. coli* four transport systems shown above are capable of transporting glucose into *E. coli*. GlF and GlK need to be heterologously expressed using a plasmid. XylFGH and XylAB are native transport proteins in *E. coli* for xylose transport into the cell.

and a kinase/transferase, respectively.[45] Wild-type *E. coli* natively utilizes its glucose PTS to transport glucose into the cell where it is phosphorylated, producing glucose-6-P and pyruvate at the expense of one equivalent of PEP.[31] However, two other systems exist in *E. coli* capable of transporting glucose into the cell, namely the mannose and galactose transport systems.[32] All three of these protein complexes can be seen side-by-side in **Fig. 2.1**. Where the native mannose transport system is also a PTS that uses PEP to phosphorylate its substrate, the galactose transport system is a non-PTS that uses ATP as its phosphorus source.[20] Upon deletion of the *ptsG* gene, unless another glucose transport system is being expressed on a plasmid or on the genome, the cell will evolve to use one of its other two transport systems to bring glucose into the cell.[21,32] For the synthesis of shikimate pathway intermediates, a non-PTS system is desired as the consumption of

PEP will reduce the availability of carbon atoms for product synthesis.[49] Furthermore, it is desired to deactivate the native glucose PTS due to its inhibitory effects on the xylose transport system, e.g. glucose will be preferentially taken up to xylose when this transport system is being expressed.[33] This phenomena is known as carbon catabolite repression (CCR).[33,50,51] Non-PTS GlF and GlK transport proteins, natively found in *Zymomonas mobilis*, are commonly expressed on a plasmid in *E. coli* for expression of a non-PTS glucose-uptake system.[29] GlF, GlK, and xylose transport proteins, XylFGH and XylAB, are illustrated in **Fig. 2.1**. Maximum theoretical yields of 3-dehydroshikimic acid (DHS) from glucose and from xylose using PTS and non-PTS transport systems have been previously discussed.[64] Theoretical yield of DHS from glucose when substrate transport is driven by PEP consumption (PTS) is 43% (mol/mol). When substrate transport is driven by ATP consumption, rather, theoretical yield would increase to 86% (mol/mol). Maximum theoretical yield of DHS from xylose was reported as 71% (mol/mol).[64]

2.1.3. Strain Construction for SA Overproduction

Deactivation of a biosynthetic pathway enzyme is used here to afford the accumulation of the substrate the enzyme acts upon. By knocking out an enzymatic step of a pathway the ability of the cell to use the pathway for metabolite biosynthesis can be obstructed or completely shut off, and it is necessary to exogenously provide the products of this pathway to the microbe. In the case of SA production, a block is made in the pathway microbes use to synthesize their aromatic amino acids and aromatic vitamins, known as the shikimate pathway (**Fig. 2.2**). Disruption of two shikimate kinase isozymes (*aroL* and *aroK*) affords SA accumulation and export from the cell.[43] Rational design of host strains have enhanced carbon flux into the shikimate pathway, shown in **Fig. 2.3**, thereby maximizing yields for SA.[20,21,65] The shikimate pathway is initiated when

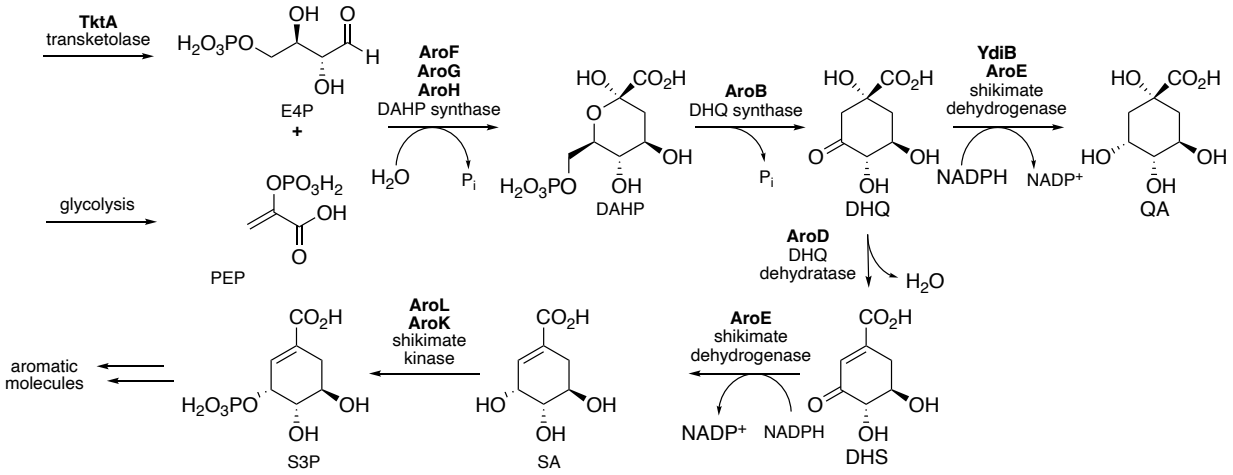

Figure 2.2. Shikimate pathway in *E. coli* shikimic acid biosynthesis proceeds via the common pathway of aromatic amino acid biosynthesis. Participating metabolites include D-erythrose-4-phosphate (E4P), phosphoenolpyruvate (PEP), 3-deoxy-D-arabino-heptulosonic acid 7-phosphate (DAHP), 3-dehydroquinic acid (DHQ), quinic acid (QA), 3-dehydroshikimic acid (DHS), shikimic acid (SA), and shikimate-3-phosphate (S3P). Participating enzymes include tyrosine-sensitive DAHP synthase (AroF), phenylalanine sensitive DAHP synthase (AroG), tryptophan-sensitive DAHP synthase (AroH), DHQ synthase (AroB), DHQ dehydratase (AroD), shikimate dehydrogenase (AroE), and shikimate kinase (AroL, AroK).

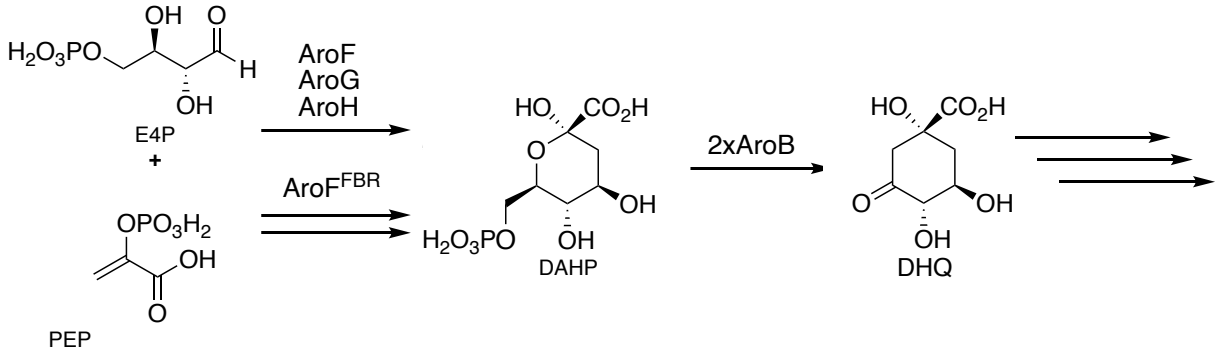

Figure 2.3. Shikimate pathway engineering carbon flux into the shikimate pathway is improved by expressing a feedback-inhibited isozyme of DAHP synthase and twofold higher DHQ synthase activity.

phosphoenolpyruvate (PEP) and erythrose 4-phosphate (E4P) are converted to 3-deoxy-D-arabino-heptulosonate 7-phosphate (DAHP) via one of three feedback-inhibited DAHP synthase isozymes: AroF, AroG, and AroH. They are inhibited by the three aromatic amino acids L-tryptophan, L-phenylalanine, and L-tyrosine, respectively. Carbon flux into the shikimate pathway is enhanced using a feedback-resistant DAHP synthase ($AroF^{FBR}$), developed using UV mutagenesis of AroF.[58]

Upon addressing the issue of feedback inhibition in DAHP synthase activity the non-phosphorylated form of DAHP, 3-deoxy-D-arabino-heptulosonate (DAH), begins to accumulate outside the cell.[59] It is necessary to express twofold 3-dehydroquinate (DHQ) synthase, AroB, activity as illustrated in **Fig. 2.3**.[22] Subsequently, DHQ dehydratase followed by shikimate dehydrogenase (AroD and AroE, respectively) affords DHS en route to producing SA.

Table 2.1. Edits made to *E. coli* RB791 all necessary gene insertions and gene deletions made in the *E. coli* RB791 host strain.

Gene edit	Description	Ref.
serA::aroB	Insertion of DHQ synthase, *aroB*, into *serA* using a homologous recombination strategy	[62]
Δ*aroL*	Deletion of first shikimate kinase isozyme, *aroL*, using No-SCAR method	[25]
Δ*aroK*	Deletion of second shikimate kinase isozyme, *aroK*, using No-SCAR method	[25]
Δ*ptsG*	Deletion of glucose-specific enzyme IIB, *ptsG*, using P1 transduction	[26]

Table 2.1 summarizes the necessary edits made to genes of *E. coli* host strain RB791. References are also provided detailing the recombineering strategy employed for each gene edit. RB791 *serA::aroB* Δ*aroL* Δ*aroK* Δ*ptsG*/pSC6.090B is a SA-overproducing and glucose/xylose co-utilizing that heterologously expresses GlF and GlK facilitated diffusion transport enzymes via plasmid pSC6.090B.[29] Plasmid SC6.090B was developed in a previous study.[29] RB791 *serA::aroB aroL aroK ptsG*/pKD12.138A is a SA-overproducing and glucose/xylose co-utilizing strain that has been forced to evolve for growth on glucose for several generations in minimal glucose media as described in the experimental section. Plasmid pKD12.138A was developed in a previous study.[14] Higher AroB activity is achieved by strategically recombineering the insertion of an *aroB* gene into the genomic *serA* locus of *E. coli* RB791.[22] The *serA* gene is used in the first step necessary for biosynthesis of the amino acid L-serine, so the re-expression of *serA* on a plasmid forces plasmid maintenance of any one of pSC6.090B (**Fig. 2.4(a)**) or pKD12.138A (**Fig. 2.4(b)**)

as they are used in the biosynthesis of serine and overproduction of SA. Deletions in *aroL* and *aroK* genes encoding shikimate kinase are made to accumulate SA. A transport protein-encoding gene, *ptsG*, involved in the glucose phosphotransferase system (PTS), is deleted to render the glucose PTS deactivated. *Z. mobilis*-derived facilitated diffusion genes, *glf* and *glk*, are heterologously expressed in pSC6.090B to take on the vacant role of transporting glucose into the cell.[44,61] Additionally, the plasmid pSC6.090B encodes the aforementioned DAHP synthase gene, $aroF^{FBR}$. An extra copy of the gene *tktA*, transketolase, is expressed to increase the availability of E4P, the first limiting reagent of the shikimate pathway.[62,63] An additional copy of *aroE* is also expressed to further enhance SA-production kinetics. P_{tac} and P_{lac} encode tac and lac promoters, respectively. The plasmid pKD12.138A has all the same features as pSC6.090B minus the two genes, *glf* and *glk*, encoding facilitated diffusion transport proteins.[22,23]

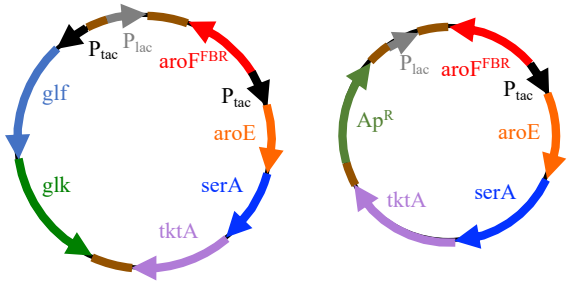

pSC6.090B, 12.8 *k*b **pKD12.138A**, 10.3 *k*b

Figure 2.4. Plasmids for shikimate overproduction (a) pSC6.090B (b) pKD12.138A.

2.2. Results and Discussion

2.3.1. Physiological Properties

SA overproducing *E. coli* strains were designed to harbor different active transport systems for taking up glucose. Two methods were identified for the expression of alternate glucose transport systems in *E. coli*. The first involved recombineering techniques to genetically dismantle the native PTS followed by heterologous expression of *glf* and *glk* genes using the plasmid pSC6.090B. The

second method was evolutionary, where a strain lacking the PTS was forced to grow in an environment where only glucose substrate was available. These two SA production hosts are compared to a base-case production host that produce SA using the native PTS of *E. coli*. **Table 2.2** provides a general genotypic description of these three strains, which are about to be described and referred to as their abbreviated names.

Table 2.2. Three strains capable of SA production two strains engineered to overproduce SA while utilizing two different glucose transport systems are compared to a base case strain that synthesizes SA after transporting glucose using its native glucose PTS.

Abbreviation	Relevant Characteristics	Description
YJ1.130	RB791 *serA::aroB* Δ*aroL* Δ*aroK*	Base case strain (PTS transport)
YJ1.144	YJ1.130 Δ*ptsG*	Engineered strain with plasmid expressed glucose transport
YJ1.148	YJ1.144 evolved to take up glucose	Engineered strain with evolved glucose transport

Strain YJ1.130 was generated starting with RB791 serA::aroB and deleting genes encoding the two isozymes of shikimate kinase, *aroL* and *aroK*, using the No-SCAR recombineering method.[25] YJ1.130 is a strain capable of utilizing its native glucose PTS for the transportation of glucose across its cellular membrane at the expense of one equivalent of PEP. Strains of *E. coli* that utilize their native PTS, such as YJ1.130, are known to exhibit carbon catabolite repression (CRR) when growing on mixed glucose and xylose feeds (i.e., glucose will be completely exhausted in the media before xylose is at all metabolized).[33,50,51] When equipped with pKD12.138A, YJ1.130/pKD12.138A overexpresses enzymes *tktA* and *aroE* as well as a feedback resistant isozyme of DAHP synthase to maximize carbon flux into the shikimate pathway allowing for it to overproduce SA.[22,23] YJ1.144 was generated by creating a deletion in the *ptsG* gene of YJ1.130 using P1 transduction. YJ1.144 is unable to utilize the native PTS of *E. coli* for glucose transport. By the expression of facilitated diffusion transport enzymes GlF and GlK from *Z. mobilis* through

Table 2.3. Summary of fermentation results comparisons of glucose transport mechanisms with respect to SA overproduction in fed-batch fermentations performed in duplicate. Physiological properties include SA titer, DHS titer, QA titer, dry cell weight (DCW) titer, and CO_2 emission titer. Titers are reported after 48 hours of fermentation.

	Glucose, 48 h[a]					**70:30 (*w*/*w*) Glucose : Xylose, 48 h[b]**				
Strain	SA ($g\ L^{-1}$)	DHS ($g\ L^{-1}$)	QA ($g\ L^{-1}$)	DCW ($g\ L^{-1}$)	CO_2 ($g\ L^{-1}$)	SA ($g\ L^{-1}$)	DHS ($g\ L^{-1}$)	QA ($g\ L^{-1}$)	DCW ($g\ L^{-1}$)	CO_2 ($g\ L^{-1}$)
YJ1.130/ pKD12.138A	78.0	8.4	1.5	35	31.9	61.4	5.2	2.6	38	27.8
YJ1.144/ pSC6.090B	54.9	21.2	23.5	36	20.3	91.7	16.1	8.3	34	25.5
YJ1.148/ pKD12.138A	83.9	35.1	15.8	38	22.4	102	28.8	5.8	36	23.7

[a]Initial charge of 30 $g\ L^{-1}$ glucose. Total glucose fed amounted to 330 $g\ L^{-1}$ glucose
[b]Initial charge of 21 $g\ L^{-1}$ glucose and 9 $g\ L^{-1}$ xylose. Total glucose and xylose fed amounted to 231 $g\ L^{-1}$ glucose and 99 $g\ L^{-1}$ xylose

Table 2.4. Key parameters itemized parameters of each fe-batch fermentation experiment including sugar consumed, carbon flux, and selectivity toward SA.

	Glucose, 48 h				**70:30 (*w*/*w*) Glucose : Xylose, 48 h**			
Strain	μ_{max} (h^{-1})	Sugar Consumed[a] (%)	C-Flux[b] (mol)	Selectivity SA (%)	μ_{max} (h^{-1})	Sugar Consumed[a] (%)	C-Flux[b] (mol)	Selectivity SA (%)
YJ1.130/ pKD12.138A	0.40	81	0.50	89	0.43	73	0.40	89
YJ1.144/ pSC6.090B	0.29	87	0.56	56	0.33	93	0.66	79
YJ1.148/ pKD12.138A	0.33	90	0.77	63	0.34	92	0.78	75

[a]Percentage by mass of sugar consumed by microbes over 48 h to sugar fed and initially charged in fermenter
[b]Carbon flux is equivalent to the total moles of SA, DHS, and QA measured in the fermentation broth using HPLC

the plasmid pSC6.090B, YJ1.144/pSC6.090B represents a strain engineered to co-utilize glucose and xylose for SA overproduction. Additionally, GlK will use ATP to phosphorylate glucose as it is brought into the cell rather than PEP.[52] YJ1.148 was generated by forcing YJ1.144 to evolve an alternative glucose transport system for glucose uptake by growing the strain for at least 40 generations in minimal salts media containing glucose as an exclusive source of carbon for growth. After isolating the strain and transforming it with pKD12.138A, it was found that the strain could not only co-utilize glucose and xylose but also produced SA at high titer. YJ1.148/pKD12.138A

utilizes an uncharacterized glucose transport mechanism en route to SA overproduction. Previous findings have suggested that the native mannose PTS and galactose transport systems are capable of glucose uptake into the cell.[8,46-48]

The aforementioned strains were examined in a fed-batch fermenter for their abilities to co-utilize glucose and xylose for SA biosynthesis; YJ1.144/pKD12.138A (expressing a heterologously expressed facilitate diffusion mechanism) and YJ1.148/pSC6.090B (expressing an uncharacterized evolved transport mechanism) were compared to a base case in strain YJ1.130/pKD12.138A (expressing its native PTS glucose transport mechanism) in terms of their physiological properties (**Table 2.3**). Strains were evaluated in 2-L bioreactors at pH 7.0, 33°C, an initial agitation of 50 RPM, and an initial aeration rate of 0.06 L min^{-1}. Once dissolved oxygen (DO) reached 10%, DO was maintained using a two-phase cascade control system. In phase one, agitation was ramped to and held at 750 RPM, followed by ramping of airflow to 1.00 L min^{-1}. In the second phase, airflow was held at 1.00 L min^{-1}, and agitation was ramped up to 1800 RPM. Optical density was measured at 600 nm (OD_{600}) and converted to dry cell weight (DCW) using a 0.43 g DCW conversion factor. Glucose, xylose, SA, and QA were quantified by High-Performance Liquid Chromatography (HPLC) refractive index detection (RID). HPLC UV detection was used to quantify DHS. Headspace exhausts from the fermenter were passed through a condenser and Drierite and then sent to an infrared CO_2 Gas Sensor to quantify CO_2. Data reported on SA sourced from hydrolysate sugars were not replicated due to the limited availability of substrate. Other fermentation data are an average of two replicate experiments. Further details of fermentations are provided in the experimental section. Selectivity toward biomass is presented in terms of maximum specific growth rate, μ_{max}, and titer of dry cell weight (DCW). The desired SA product as well as major byproducts, QA and DHS, are reported as g L^{-1} titers. Carbon dioxide

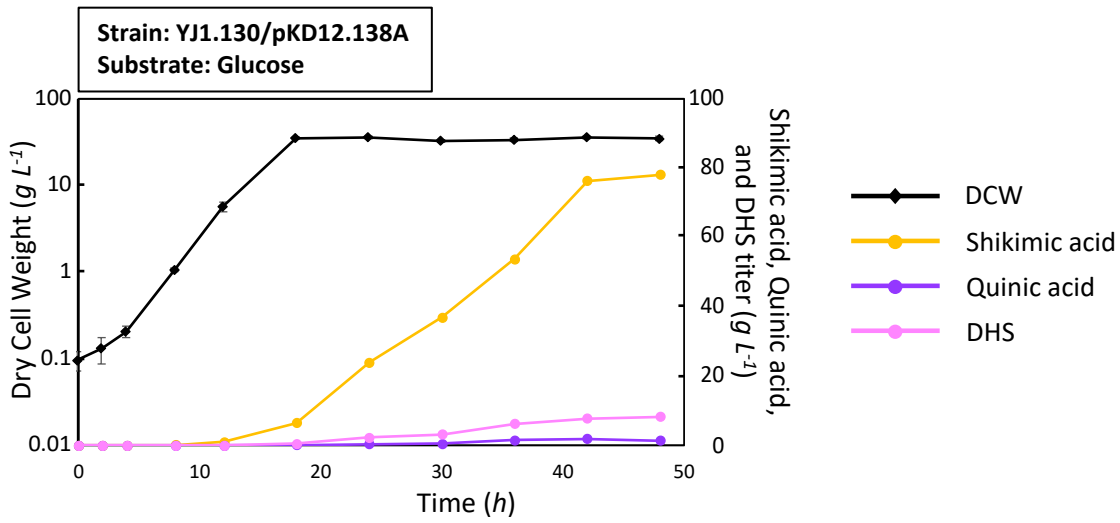

Figure 2.5. YJ1.130/pKD12.138A growth on glucose titers versus time.

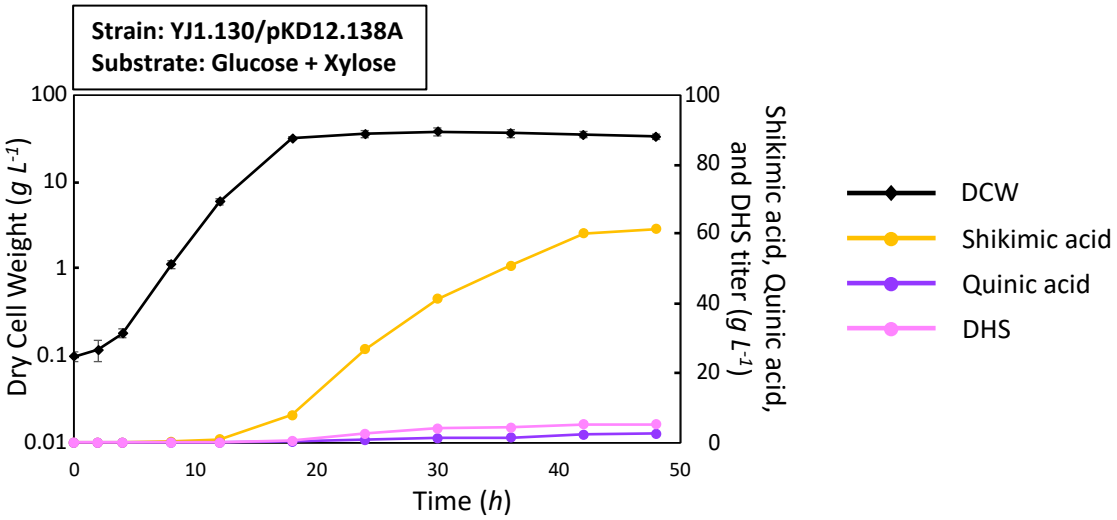

Figure 2.6. YJ1.130/pKD12.138A growth on glucose:xylose (70:30) titers versus time.

emissions from each fermentation were calculated on a per liter of initial fermentation broth basis. Finally, sugar consumed over the 48 h fermentation (%), carbon flux into the shikimate pathway (mol), and selectivity for SA (%) are itemized in **Table 2.4**. Carbon flux is defined as the total moles of SA, DHS, and QA measured in the fermentation broth after 48 h in the respective fermentation.

Fermentation plots of YJ1.130/pKD12.138A can be found in **Fig. 2.5** and **Fig. 2.6** (raw data are provided in **Table A.2.1**, **Table A.2.2**). This strain utilized the native glucose PTS to take

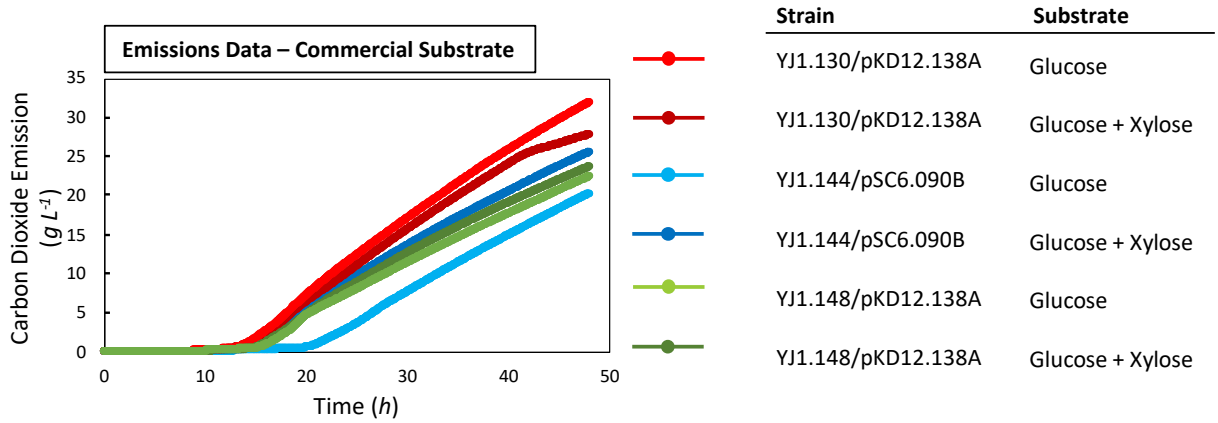

Figure 2.7. CO_2 emissions of strains grown on commercial sugars CO_2 emissions of fermentations from **Fig. 2.5** – **Fig. 2.6** and from **Fig, 2.8** – **Fig. 2.11**. Emissions data were collected for a single run of each duplicate of fermentation experiments.

glucose into the cell and showed the highest μ_{max} values of any strain when grown on pure glucose and mixed glucose/xylose feedstock. DCW was higher than those realized by other strains during growth on mixed glucose/xylose feedstocks. High specific growth rates and DCW indicate a high selectivity toward biomass during the exponential phase of growth. **Fig 2.4** illustrates how the PTS will produce pyruvate at the expense of one equivalent of PEP, which can flow toward other cellular processes such as the TCA cycle. When grown solely on glucose, DCW was lower than other strains due to a shorter duration in exponential and deceleration growth phases even though μ_{max} was the highest for this strain. **Fig. 2.7** displays total CO_2 emissions curve for each fermentation plot of growth on glucose or 70:30 (*w*/*w*) glucose:xylose (raw data are provided in **Table A.2.9**).. On both single carbon and mixed feed sources of carbohydrates, YJ1.130/pKD12.138A had the highest selectivity toward carbon dioxide. With higher selectivity for CO_2 in this strain, less carbon flux remained to flow toward the desired SA product, resulting in lower overall productivity. SA titer (productivity) of 78.0 g L^{-1} (1.63 g L^{-1} h^{-1}) and 61.4 g L^{-1} (1.28 g L^{-1} h^{-1}) were achieved on glucose and mixed glucose/xylose, respectively, in YJ1.130/pKD12.138A. The theoretical yield for SA from xylose is higher than the theoretical yield

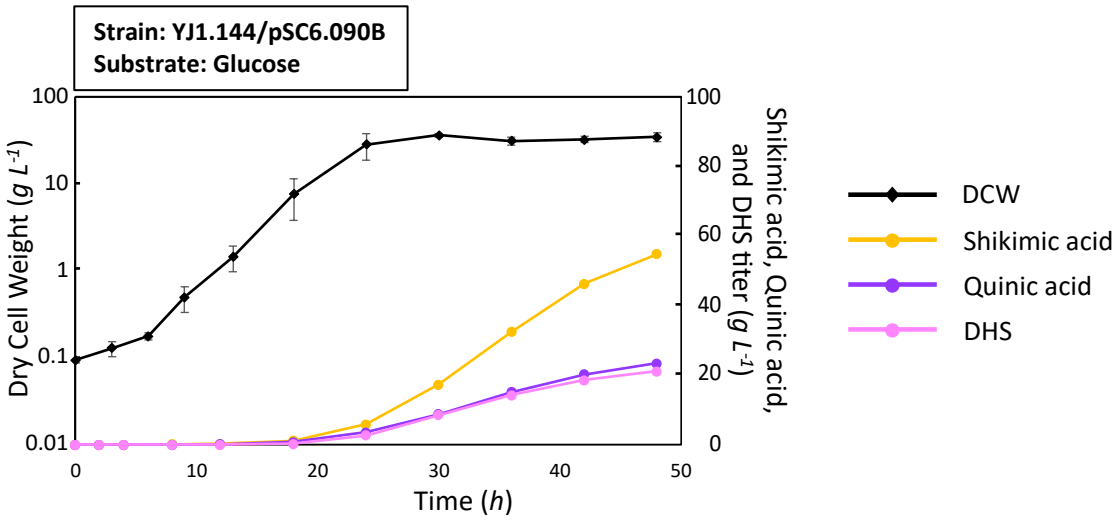

Figure 2.8. YJ1.144/pSC6.090B growth on glucose titers versus time.

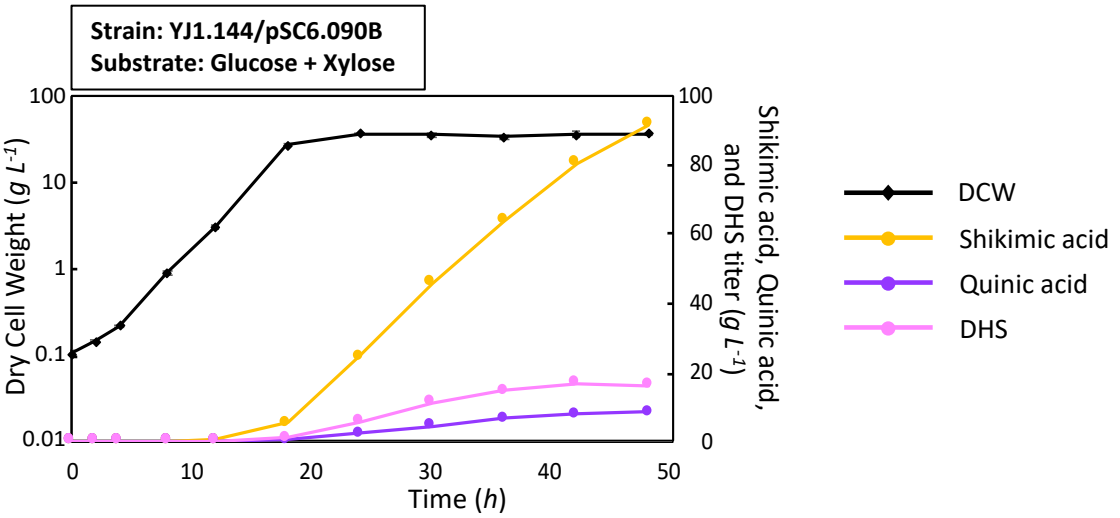

Figure 2.9. YJ1.144/pSC6.090B growth on glucose:xylose (70:30) titers versus time.

for SA from glucose.[64] Lower yields, however, are achieved in YJ1.130 when growing on glucose/xylose mixed feedstocks compared to growth on solely glucose. Due to CCR, a heavy burden is placed on the host cell as it changes its metabolism from glucose to xylose, which reduces the strains overall titer for SA. YJ1.130/pKD12.138A utilized a particularly low percentage of sugars fed to the fermenter when mixed glucose and xylose were cofed (**Table 2.4**). This is due to the preferential consumption of glucose to xylose when native substrate transport systems of *E. coli* are active. It is worth noting that although a low SA titer was realized in

YJ1.130/pKD12.138A, its selectivity toward SA versus the byproducts of the shikimate pathway, DHS and QA, was the highest. DHS and QA were produced in titers of 8.4 g L^{-1} and 1.5 g L^{-1}, respectively. High selectivity toward SA was observed in YJ1.130/pKD12.138A, however, carbon flux into the shikimate pathway (moles of SA and byproducts, QA and DHS) was the lowest observed of the three tested strains.

A deletion in the genomic *ptsG* gene of YJ1.144 dismantles the native glucose PTS, and glucose transport enzymes native to *Z. mobilis* (GlF and GlK) are heterologously expressed from the plasmid pSC6.090B. In the process of deleting *ptsG*, YJ1.144/pSC6.090B is capable of utilizing glucose and xylose simultaneously rather than preferentially consuming glucose over xylose after CCR has been dismantled (growth on glucose and glucose/xylose in **Fig. 2.8** and **Fig. 2.9**, respectively). Raw data are provided in **Table A.2.3** and **Table A.2.4**. An increase in sugar consumption, particularly mixed sugar feedstocks, and an increase in carbon flux into the shikimate pathway when looking from YJ1.130/pKD12.138A to YJ1.144/pSC6.090B is seen (**Table 2.4**). A drop in selectivity for SA is also observed when using both glucose and glucose/xylose feedstocks. YJ1.144/pSC6.090B showed the lowest μ_{max} values of any strain when grown on glucose alone and mixed glucose/xylose feedstock. Low specific growth rates and DCW titer indicate a low selectivity toward cell mass and potentially a higher availability of carbon flux for SA biosynthesis. GlK will phosphorylate glucose as it is transported into the cell at the expense of one equivalent of ATP rather than PEP, and PEP is required for the initiation of synthesis via the shikimate pathway. By using an alternate glucose transport system and making more PEP available to the shikimate pathway, carbon flux flowed toward SA production. However, it was observed that YJ1.144/pSC6.090B had the lowest SA titer (productivity) when grown solely on glucose of 54.9 g L^{-1} (1.14 g L^{-1} h^{-1}). A lower yield on glucose agrees with theoretical yields of SA

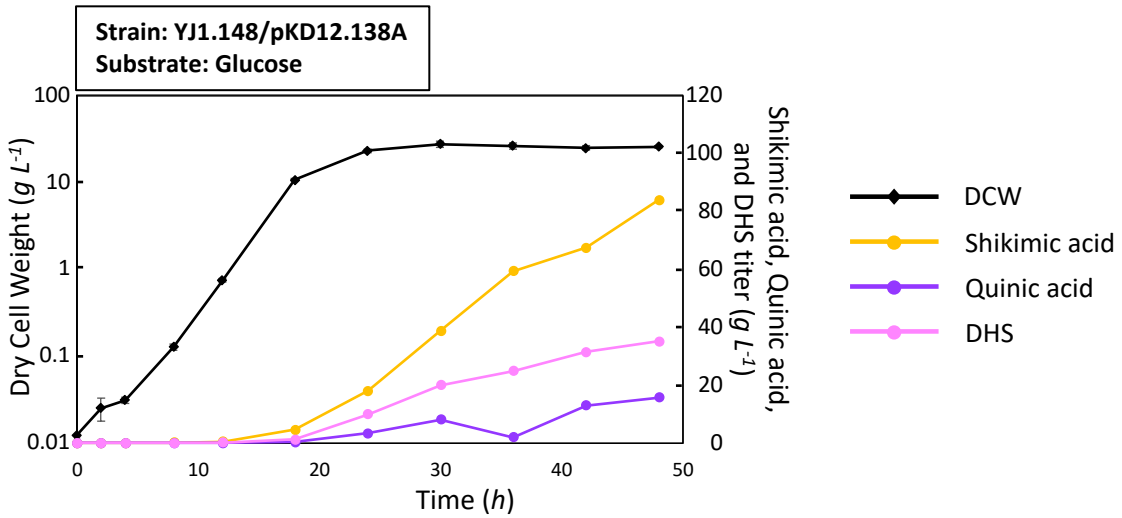

Figure 2.10. YJ1.148/pKD12.138A growth on glucose titers versus time.

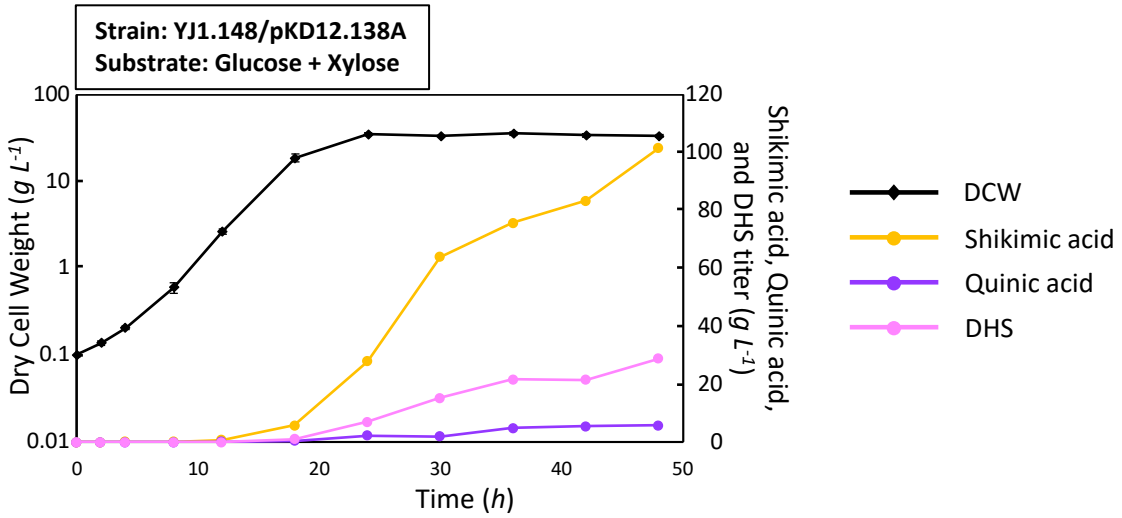

Figure 2.11. YJ1.148/pKD12.138A growth on glucose:xylose (70:30) titers versus time.

from glucose being lower than SA from xylose feedstocks previously discussed.[64] It is also worth pointing out the strain's considerably lower specific growth rate when grown in the absence of xylose. It is possible the strain could have accumulated more SA titer if run for longer than 48 h. DHS and QA were produced in titers of 21.1 g L^{-1} and 23.5 g L^{-1}, respectively. SA titer (productivity) of 91.7 g L^{-1} (1.91 g L^{-1} h^{-1}) were achieved on mixed glucose/xylose in YJ1.144/pSC6.090B, which was slightly lower in selectivity than YJ1.130/pKD12.138A. Byproducts, DHS and QA, were produced in titers of 16.1 g L^{-1} and 8.3 g L^{-1}, respectively.

An evolutionary process was also used to express an alternate glucose transport system to the PTS in the final strain tested, YJ1.148. Fermentation plots for YJ1.148/pKD12.138A are depicted in **Fig. 2.10** and **Fig. 2.11** for growth on glucose and mixed glucose/xylose, respectively (raw data are provided in **Table A.2.5** and **Table A.2.6**). **Table 2.4** shows YJ1.148/pKD12.138A had similar substrate consumption as YJ1.144/pSC6.090B when grown on mixed glucose/xylose feeds. However, where carbon flux into the shikimate pathway and SA titers were higher for YJ1.148/pKD12.138A selectivity toward SA was higher for YJ1.144/pSC6.090B. YJ1.148/pKD12.138A produced byproducts DHS and QA in titers of 35.1 g L^{-1} and 15.8 g L^{-1}, respectively. YJ1.148/pKD12.138A produced SA with impressive titers of 83.9 g L^{-1} (1.75 g L^{-1} h^{-1}) and 102 g L^{-1} (2.13 g L^{-1} h^{-1}) when grown on glucose and glucose/xylose, respectively. However, YJ1.148/pKD12.138A synthesized SA with lower selectivity than both YJ1.130/pKD12.138A and YJ1.144/pSC6.090B. Due to its low selectivity, strain YJ1.144/pSC6.090B was chosen for further analysis on authentic corn stover-derived glucose and xylose. Considering YJ1.148/pKD12.138A can generate greater carbon flux into the shikimate pathway in comparison to YJ1.144/pSC6.090B, it is possible it uses a phosphorus source other than PEP to phosphorylate glucose as it is brought into the cell. Of the two native hexose transport systems in *E. coli* also known to carry activity for transporting glucose, galactose transport system also uses ATP as a source of phosphorus while the mannose transport system utilizes PEP.[8] Therefore, it is possible the galactose transport system may be taking over glucose transport in YJ1.148, however genotype proof of this was not collected.

2.3.2. Hydrolysate Fermentation

The efficiency of the ball milling process on corn stover,[8] including the percentage conversion of cellulose and xylan, as well as the titers of glucose, xylose, and acetate, were determined by the Liao group (**Table 2.5**). Corn stover-derived hydrolysate sugars were donated for this study from

Table 2.5. Milling and fed-batch fermentation data key ball milling and fermentation data.

Ball Milling					
Cellulose Conversion (*w*/*w*)	Xylan Conversion (*w*/*w*)	Glucose Titer (g L^{-1})	Xylose Titer (g L^{-1})	Acetate Titer (g L^{-1})	
82%	47%	55.6	24.0	2.85	

Hydrolysate Fermentation							
Strain	Substrate	μ_{max} (h^{-1})	SA (g L^{-1})	DHS (g L^{-1})	QA (g L^{-1})	DCW (g L^{-1})	CO_2 (g L^{-1})
YJ1.144/ pSC6.090B	Stover Hydrolysate	0.56	55.6	3.4	29.4	30.6	26.3

Dr. Wei Liao's group, as well, but were available in limited supply. Thus, it was not possible to test all three strains' abilities to produce SA sourced from corn stover. Furthermore, corn stover hydrolysate fed-batch fermentation was tested as a single run rather than as duplicate runs. Physiological fermentation data on YJ1.144/pSC6.090B converting corn stover hydrolysate sugars from a ball mill into SA are also shown in **Table 2.5**. A lag phase of roughly 15 h was observed when the shikimate producer was grown on hydrolysate sugars. Following the lag phase, however, specific growth rate increased over time until the fermentation reached a deceleration phase. The μ_{max} achieved was 0.56 h^{-1}. SA titer of 55.6 g L^{-1} was achieved. This decrease in SA yield was coupled with an increase in QA biosynthesis, with DHS and QA accumulating at titers of 3.4 g L^{-1} and 29.4 g L^{-1}, respectively. It was hypothesized that the presence of acetate may have been responsible for more carbon flux directed toward the production of QA, although the exact reason for this is not known. Acetate is known to inhibit microbial growth, but a link has not been made between microbial inhibition by acetate and the shikimate pathway.[34-36] Carbon dioxide emissions data were comparable to that of the strain when grown on commercially bought glucose and xylose. Cell mass titers were lower, however, which can be explained by the aforementioned effect of microbial inhibition. Recent research suggests a quinate/shikimate dehydrogenase (YdiB, *ydiB*) plays an important role in QA production in engineered SA overproducing strains of *E. coli*.[37,66,67]

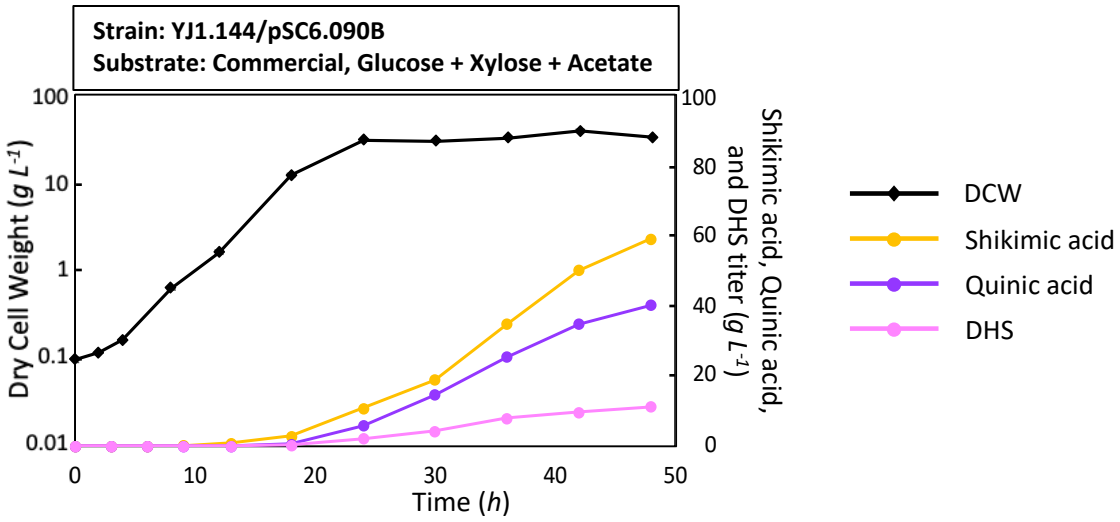

Figure 2.12. YJ1.144/pSC6.090B growth on glucose:xylose:acetic acid (68:29:3.5) titers versus time.

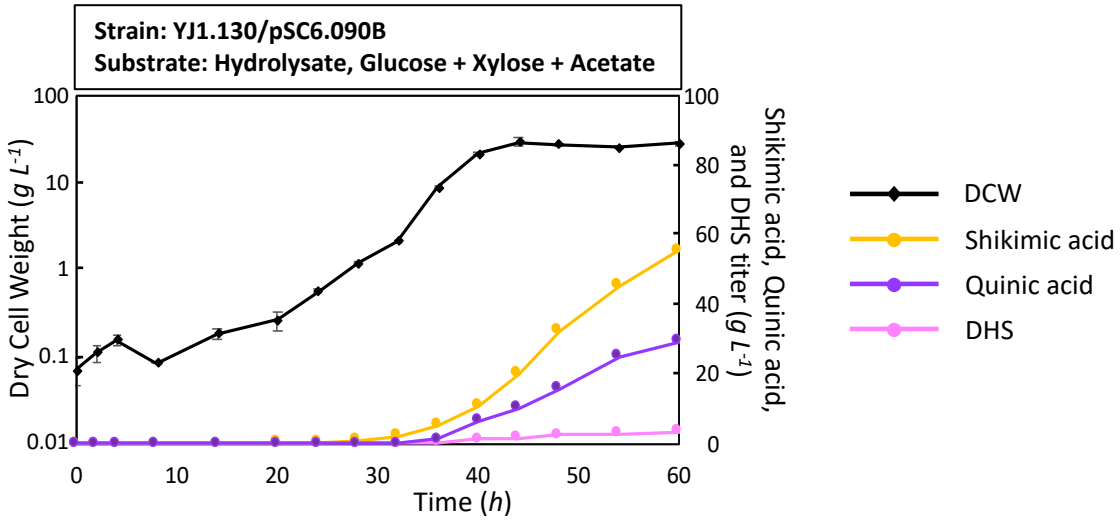

Figure 2.13. YJ1.144/pSC6.090B growth on hydrolysate sugars titers versus time.

Deactivation of *ydiB* reduced the molar yield of QA by 75% and reduced QA yields relative to SA by 6.17% with respect to a parental strain. Overexpression of *ydiB*, on the other hand, resulted in a 500% increase in molar yields of QA and increased QA yields relative to SA by 152%.[37,66,67] These results warrant future investigation of the effects of *ydiB* inactivation on the production of QA during SA fermentations of corn stover-derived glucose and xylose.

The presence of acetate in fermentation media was linked with the decrease in selectivity when YJ1.144/pSC6.090B was grown on hydrolysate sugars. **Fig. 2.12** and **Fig. 2.13** display

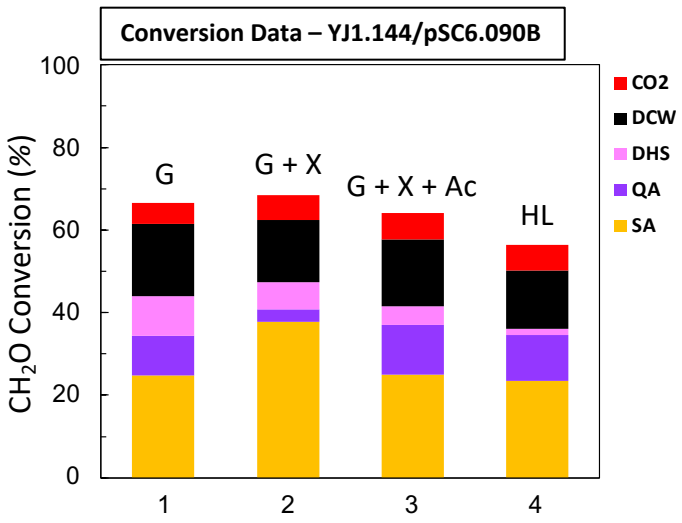

Figure 2.14. Total carbon yields of YJ1.144/pSC6.090B YJ1.144/pSC6.090B percent conversion of sugar to products on a moles of carbon atom basis. (1) Glucose (2) 70:30 (w/w) glucose:xylose (3) 68:29:3.5 (w/w) glucose:xylose:acetic acid (4) Hydrolysate sugar.

fermentation time points for YJ1.144/pSC6.090B growing in mixed, commercially purchased glucose/xylose with added glacial acetic acid as well as its growth on hydrolysate sugars (raw data are provided in **Table A.2.7** and **Table A.2.8**). The effect of acetate can be best understood when sequentially comparing the results of YJ1.144/pSC6.090B grown on glucose, grown on glucose/xylose, grown on glucose/xylose with added acetic acid, and grown on hydrolysate sugars containing acetate. **Fig. 2.14** sequentially displays conversion data (on a basis of moles of carbon) of these four experiments (fermentation plots of these data can be found in **Fig. 2.8**, **Fig. 2.9**, **Fig. 2.12** and **Fig. 2.13**, respectively). Raw data for **Fig. 2.14** are provided in **Table A.2.10**, and **Eq. 2.1** is the key equation for calculating conversions on a carbon atom basis:

$$Conversion = \frac{100\% \cdot {C_j \cdot T_j}/{MW_j}}{\left(\frac{6 \cdot T_{Gi}}{180.16} + \frac{5 \cdot T_{Xi}}{150.13}\right) - \left(\frac{6 \cdot T_{Gf}}{180.16} + \frac{5 \cdot T_{Xf}}{150.13}\right) + \left(\frac{6 \cdot F_G}{180.16} + \frac{5 \cdot F_X}{150.13}\right)} \quad \textbf{(2.1)}$$

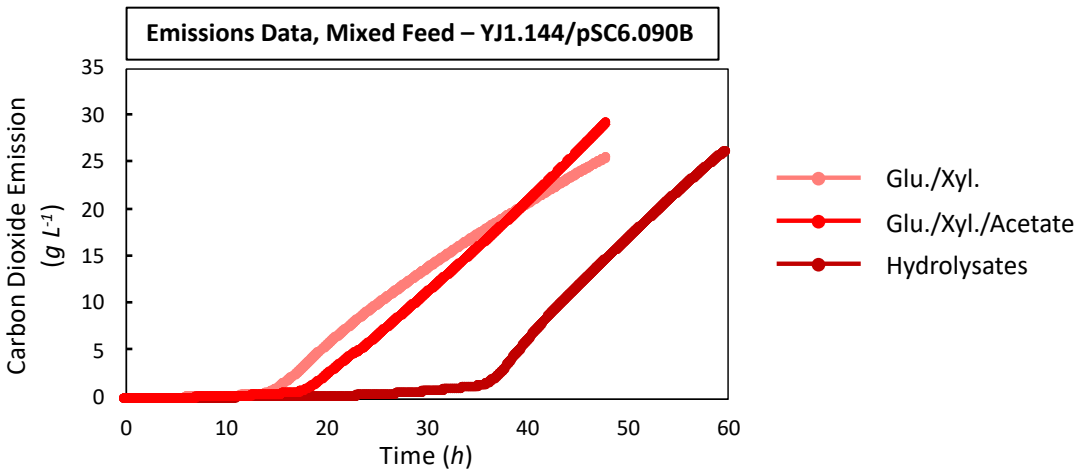

Figure 2.15. CO_2 emissions of YJ1.144/pSC6.090B CO_2 emissions of fermentations from **Fig. 2.9**, **Fig. 2.12**, and **Fig. 2.13**.

Where C_j is the number of carbon atoms in compound j, T_j is the titer of j (g L^{-1}), MW_j is the molecular weight of j (g mol^{-1}), T_{Gi} is the initial titer of glucose (g L^{-1}), T_{Xi} is the initial titer of xylose (g L^{-1}), T_{Gf} is the final titer of glucose (g L^{-1}), T_{Xf} is the final titer of xylose (g L^{-1}), F_G is the amount of external glucose fed per liter of initial fermentation broth (g L^{-1}), and F_X is the amount of external xylose fed per liter of initial fermentation broth (g L^{-1}). About 60% of atomic carbon is accounted for in each of these fermentations when totaling yields for SA (orange), QA (purple), DHS (pink), DCW (black), and CO_2 (red). In stacked bar graph **(1)**, 23.5 g L^{-1} QA (purple) is accumulated when the strain is grown only on glucose. The least amount of QA was produced in bar graph **(2)** when xylose was introduced to the media. Selectivity toward SA is lost to QA in bar charts **(3)** and **(4)**. Similar increases in QA production were realized when acetic acid was introduced to a glucose/xylose fermentation using commercial sugar sources as when hydrolysates were fermented for SA production. Emissions data for YJ1.144/pSC6.090B grown on glucose/xylose, glucose/xylose with acetate, and hydrolysate sugars are shown in **Fig. 2.15** (raw data are provided in **Table A.2.9**). It is worth noting that selectivity toward carbon dioxide, after

the long lag phase, is similar when the strain is grown on hydrolysate sugars to when the strain is grown in the presence of artificially added acetic acid.

2.3. Summary & Future Work

The natural product shikimic acid (SA) is the starting material for the synthesis of oseltamivir phosphate (Tamiflu®), an antiviral agent effective against influenza. Data presented encompass an effort to add to the "agricultural residue economy", utilizing mixed sugars derived from lignocellulosic corn stover for SA biosynthesis. *Escherichia coli* K-12 strains expressing different glucose transport systems – native phosphotransferase (PTS), heterologously expressed *Z. mobilis* GlF and GlK, and an uncharacterized evolved uptake mechanism – were examined in a fed-batch fermenter for their abilities to co-utilize glucose and xylose for SA synthesis. Strain YJ1.144/pSC6.090B expressing GlF and GlK performed better than a strain expressing the native glucose PTS and another PTS^- strain evolved to take up glucose. YJ1.144/pSC6.090B achieved a SA titer of 91.7 g L^{-1} when grown on a 70:30 (*w*/*w*) mixture of glucose/xylose. An evolved strain that took up glucose with either the mannose or the galactose transport systems found in *E. coli* achieved a 102 g L^{-1} titer of SA, although with lower selectivity than YJ1.144/pSC6.090B. YJ1.144/pSC6.090B was grown on corn stover-derived hydrolysates for the biosynthesis of SA, achieving a titer of 55.6 g L^{-1}. QA production was higher when converting hydrolysates in comparison to commercially bought sugars. It is proposed that this reduction in selectivity is due to the presence of acetate. The role of a quinate/shikimate dehydrogenase gene, *ydib*, in QA formation is of particular interest in relation to corn stover hydrolysate fermentations. Literature evidence has shown that inactivation or overexpression of *ydib* results in decreases and increases, respectively, in QA yields relative to SA yields.[37,66,67] Emissions data from the fermentations were used to perform a comparative life-cycle assessment (LCA) and techno-economic analysis (TEA).

REFERENCES

[1] "Short-Term Energy Outlook" *U.S. Energy Information Administration (EIA)*, **2016.** https://www.eia.gov/forecasts/steo/report/renew_co2.cfm

[2] Langholtz, M. H.; Stokes, B. J.; Eaton, L. M. "2016 Billion-Ton Report: Advancing Domestic Resources for a Thriving Bioeconomy" *U.S. Department of Energy* **2016**, Vol. 1: Economic Availability of Feedstocks. Oak Ridge National Laboratory, Oak Ridge, Leads, TN. 448p. http://energy.gov/eere/bioenergy/2016-billion-ton-report.

[3] Ray, D. L.; Sloat, L. L.; Garcia, A. S.; Davis, K. F.; Ali, T.; Xie, W. "Crop harvests for direct food use insufficient to meet the UN's food security goal" *Nature Food* **2022**, Vol. 3, 367-374.

[4] Aminetzah, D.; Baroyan, A.; Kravchenko, O.; Denis, N.; Dewilde, S.; Ferreira, N.; Revellat, J.; Verlan, I. "A reflection on global food security challenges amid the war in Ukraine and the early impact of climat change" *McKinsey & Co.* **2022**. https://www.mckinsey.com/industries/agriculture/our-insights/a-reflection-on-global-food-security-challenges-amid-the-war-in-ukraine-and-the-early-impact-of-climate-change

[5] Garedew, M.; Lam, C. H.; Petitjean, L.; Huang, S.; Song, B.; Lin, F.; Jackson, J. E.; Saffron, C. M.; Anastas, P. T. "Electrochemical upgrading of depolymerized lignin: a review of model compound studies" *Green Chem.* **2021**, *23*, 2868.

[6] Bhalla, A.; Fasahati, P.; Particka, C. A.; Assad, A. E.; Stoklosa, R. J.; Bansal, N.; Semaan, R.; Saffron, C. M.; Hodge, D. B.; Hegg, E. L. "Integrated experimental and technoeconomic evaluation of two-stage Cu-catalyzed alkaline-oxidative pretreatment of hybrid poplar" *Biotechnol Biofuels* **2018**, *11*, 143.

[7] Chen, R.; Rojas-Downing, M. M.; Zhong, Y.; Saffron, C. M.; Liao, W. "Life Cycle and Economic Assessment of Anaerobic Co-digestion of Dairy Manure and Food Waste" *Industrial Biotechnology* **2015**, *11*(2), 127-139.

[8] Zhong, Y.; Frost, H.; Bustamante, M.; Li, S.; Liu, Y. S.; Liao, W. "A mechano-biocatalytic one-pot approach to release sugars from lignocellulosic materials" *Renewable and Sustainable Energy Reviews* **2020**, *121*, 109675.

[9] Centers for Disease Control and Prevention [CDC], "*E. coli* (*Escherichia coli*)" **2020**. National Center for Emerging and Zoonotic Infectious Diseases, Division of Foodborne, Waterborne, and Environmental Diseases.

[10] Diaz Quiroz, D. C.; Carmona, S. B.; Bolivar, F.; Escalante, A. "Current perspectives on applications of shikimic and aminoshikimic acids in pharmaceutical chemistry" *Research and Reports in Medicinal Chemistry* **2014**, *4*, 35-46.

[11] Rawat, G.; Tripathi, P.; Saxena, R. K. "Expanding horizons of shikimic acid: Recent progresses in production and its endless frontiers in application and market trends" *Appl. Microbiol Biotechnol*. **2013**, *97*, 4277-4287.

[12] Estévez, A. M.; Estévez, R. J. "A Short Overview on the Medicinal Chemistry of (—)-Shikimic Acid" *Mini-Reviews in Medicinal Chemistry* **2012**, *12*, 1443-1454.

[13] "Global Shikimic Acid (CAS 138-59-0) Sales Market Report 2020" *Research Allied* **2020**, 120.

[14] Chandran, S. S.; Yi, J.; Draths, K. M.; von Daeniken, R.; Weber, W.; Frost, J. W. "Phosphoenolpyruvate Availability and the Biosynthesis of Shikimic Acid" *Biotechnology Progress* **2008**, *19*(3), 808-814.

[15] Sato, N.; Kishida, M.; Nakano, M.; Hirata, Y.; Tanaka, T. "Metabolic Engineering of Shikimic Acid-Producing *Corynebacterium glutamicum* From Glucose and Cellobiose Retaining Its Phosphotransferase System Function and Pyruvate Kinase Activities" *Front. Bioeng. Biotechnol*. **2020**, *8*, 569406.

[16] Tripathi, P.; Rawat, G.; Yadav, S.; Saxena, R. K. "Shikimic acid, a base compound for the formulation of swine/avian flu drug: statistical optimization, fed-batch and scale up studies along with its application as an antibacterial agent" *Antonie van Leeuwenhoek* **2015**, *107*, 419-431.

[17] Liu, X.; Yu, D.; Luo, H.; Li, C.; Li, H. "Efficient Reaction Systems for Lignocellulosic Biomass Conversion to Furan Derivatives: A Minireview" *Polymers* **2022**, *14*, 3671.

[18] Veerabadhran, M.; Natesan, S.; MubarakAli, D.; Xu, S.; Yang, F. "Using different cultivation strategies and methods for the production of microalgal biomass as a raw material for the generation of bioproducts" *Chemosphere* **2021**, *285*, 131436.

[19] Liu, Z.; Wang, J.; Nielsen, J. "Yeast synthetic biology advances biofuel production" *Current Opinion in Microbiology* **2022**, *65*, 33-39.

[20] Kogure, T.; Kubota, T.; Suda, M.; Hiraga, K.; Inui, M. "Metabolic engineering of *Corynebacterium glutamicum* for shikimate overproduction by growth-arrested cell reaction" *Metabolic Engineering* **2016**, *38*, 204-216.

[21] Fujiwara, R.; Noda, S.; Tanaka, T.; Kondo, A. "Metabolic engineering of *Escherichia coli* for shikimate pathway derivative production from glucose-xylose co-substrate" *Nature Comm*. **2020**, *11*, 279.

[22] Li, K. "Microbial Syntheses of Value-Added Chemicals from *D*-Glucose" **1999**, *A PhD Dissertation*.

[23] Knop, D. R.; Draths, K. M.; Chandran, S. S.; Barker, J. L.; von Daeniken, R.; Weber, W.; Frost, J. W. "Hydroaromatic Equilibration During Biosynthesis of Shikimic Acid" *J. Am. Chem. Soc*. **2001**, *123*, 10173-10182.

[24] Niu, W.; Draths, K. M.; Frost, J. W."Benzene-Free Synthesis of Adipic Acid" Applied and Environmental Microbiology **2012**, *78*(15), 5170-5181.

[25] Prather, K. L. J.; Reisch, C. R. "The no-SCAR (Scarless Cas9 Assisted Recombineering) system for genome editing in *Escherichia coli*" *Science Reports* **2015**, 5:15096.

[26] Saragliadis, A.; Trunk, T.; Leo, J. C. "Producing Gene Deletions in *Escherichia coli* by P1 Transduction with Excisable Antibiotic Resistance Cassettes" *J. Vis. Exp*. **2018**, (139), e58267.

[27] Datsenko, K. A.; Wanner, B. L. "One-step inactivation of chromosomal genes in *Escherichia coli* K-12 using PCR products" *PNAS* **2000**, 97(12), 6640-6645.

[28] Jadidi, Y.; Frost, H.; Das. S.; Liao, W.; Draths, K. M.; Saffron, C. M. "Life cycle and technoeconomic comparisons of shikimic acid sourced from corn grain or corn stover" *Manuscript submitted*

[29] Chandran, S. S. "Manipulation of genes and enzymes in the shikimate pathway" *A Dissertation*, MSU **2000**, 75.

[30] Sambrook, J.; Russell, D. W. Molecular Cloning: A Laboratory Manual 3rd ed.; Cold Spring Harbor Laboratory: Cold Spring Harbor, NY, **2001**.

[31] McCloskey, D.; Xu, S.; Sandberg, T. E.; Brunk, E.; Hefner, Y.; Szubin, R.; Feist, A. M.; Palsson, B. O. "Adaptive laboratory evolution resolves energy depletion to maintain high aromatic metabolite phenotypes in *Escherichia coli* strains lacking the Phosphotransferase System" *Metabolic Engineering* **2018**, *48*, 233-242.

[32] Bennett, G. N.; Zhu, F.; Wang, Y.; San, K. "Metabolic engineering of *Escherichia coli* to produce succinate from soybean hydrolysate under anaerobic conditions" Biotechnology and Bioengineering **2018**,*115*, 1743–1754.

[33] Dev, C.; Jilani, S. B.; Yazdani, S. S. "Adaptation on xylose improves glucose-xylose co-utilization and ethanol production in a carbon catabolite repression (CCR) compromised ethanologenic strain" *Microbial Cell Factories* **2022**, *21*, 154.

[34] Pinhal, S.; Ropers, D.; Geiselmann, J.; de Jong, H. "Acetate Metabolism and the Inhibition of Bacterial Growth by Acetate" *American Society for Microbiology* **2019**, *201*(13).

[35] Wolf, N.; Bussmann, M.; Koch-Koerfges, A.; Katcharava, N.; Schulte, J.; Polen, T.; Hartl, J.; Vorholt, J. A.; Baumgart, M.; Bott, M.; "Molecular Basis of Growth Inhibition by Acetate of an Adenylate Cyclase-Deficient Mutant of Corynebacterium glutamicum" *Front. Microbiol*. **2020**, *11*, 87.

[36] Qiu, X.; Zhang, Y.; Hong, H. “Classification of acetic acid bacteria and their acid resistant mechanism” *AMB Expr*. **2021**, *11*, 29.

[37] García, Sofía, et al. "The role of the ydiB gene, which encodes quinate/shikimate dehydrogenase, in the production of quinic, dehydroshikimic and shikimic acids in a PTS-strain of *Escherichia coli*." *Microbial Physiology* 27.1 (2017): 11-21.

[38] László, F.; Ecker, J. "An overview of biomass conversion: exploring new opportunities." *PeerJ* 8, **2020**, e9586.

[39] Hallgren, L., et al. "Industrial utilization of whole crop sorghum for food and industry." *Utilization of sorghum and millets* 502, **1992**, 121.

[40] Seo, S.; Kim, W. H.; Kim, J. G. "Production and utilization of whole crop barley and whole crop rice in Korea." *Grassland Agriculture: Balancing Production and Environmental Protection----Proceedings of the 2nd China-Japan-Korea Grassland Conference*, **2006**.

[41] Stolle, Achim, et al. "Ball milling in organic synthesis: solutions and challenges." *Chemical Society Reviews* 40.5, **2011**, 2317-2329.

[42] Fuerstenau, D. W., K. S. Venkataraman, and B. V. Velamakanni. "Effect of chemical additives on the dynamics of grinding media in wet ball mill grinding." *International journal of mineral processing* 15.4, **1985**, 251-267.

[43] Draths, K. M., David R. Knop, and J. W. Frost. "Shikimic acid and quinic acid: replacing isolation from plant sources with recombinant microbial biocatalysis." *Journal of the American Chemical Society* 121.7 (1999): 1603-1604.

[44] Liang, Quanfeng, et al. "Comparison of individual component deletions in a glucose-specific phosphotransferase system revealed their different applications." *Scientific reports* 5.1, **2015**, 1-10.

[45] McCoy, Jason G., et al. "The structure of a sugar transporter of the glucose EIIC superfamily provides insight into the elevator mechanism of membrane transport." *Structure* 24.6, **2016**, 956-964.

[46] Stolz, Beat, et al. "The mannose transporter of *Escherichia coli*. Structure and function of the IIABMan subunit." *Journal of Biological Chemistry* 268.36, **1993**, 27094-27099.

[47] Kornberg, H. L., and Claudia Riordan. "Uptake of galactose into *Escherichia coli* by facilitated diffusion." *Microbiology* 94.1, **1976**, 75-89.

[48] Seong, Hyeon Jeong, Ji Eun Woo, and Yu-Sin Jang. "Control of the galactose-to-glucose consumption ratio in co-fermentation using engineered *Escherichia coli* strains." *Scientific reports* 10.1, **2020**, 1-8.

[49] Wu, Sijia, et al. "Metabolic Engineering of Shikimic Acid Biosynthesis Pathway for the Production of Shikimic Acid and Its Branched Products in Microorganisms: Advances and Prospects." *Molecules* 27.15, **2022**, 4779.

[50] Deutscher, Josef. "The mechanisms of carbon catabolite repression in bacteria." *Current opinion in microbiology* 11.2, **2008**, 87-93.

[51] Brückner, Reinhold, and Fritz Titgemeyer. "Carbon catabolite repression in bacteria: choice of the carbon source and autoregulatory limitation of sugar utilization." *FEMS microbiology letters* 209.2, **2002**, 141-148.

[52] Parker, Corrine, et al. "Characterization of the Zymomonas mobilis glucose facilitator gene product (glf) in recombinant *Escherichia coli*: examination of transport mechanism, kinetics and the role of glucokinase in glucose transport." *Molecular microbiology* 15.5, **1995**, 795-802.

[53] Ling, Chen, et al. "Muconic acid production from glucose and xylose in Pseudomonas putida via evolution and metabolic engineering." *Nature Communications* 13.1, **2022**, 1-14.

[54] IPCC "Climate Change 2013: The Physical Science Basis. Contribution of Working Group I to the Fifth Assessment Report of the Intergovernmental Panel on Climate Change" [Stocker, T. F.; Qin, D.; Plattner, G.-K.; Tignor, M.; Allen, S. K.; Boschung, J.; Nauels, A.; Xia, Y.; Bex, V.; Midgley, P. M. (eds.)]. Cambridge University Press, **2013**, Cambridge, United Kingdom and New York, NY, USA, pp. 1535.

[55] Correa, D. F.; Beyer, H. L.; Fargione, J. E.. Hill, J. D.; Possingham, H. P.; Thomas-Hall, S. R.; Schenk, P. M. "Towards the Implementation of Sustainable Biofuel Production Systems" *Renew. Sustain. Energy Rev.*, **2019**, *107*, 250-263.

[56] Shepard, Jun Ukita, and Lincoln F. Pratson. "The myth of US energy independence." *Nature Energy*, **2022**, 1-3.

[57] Hughes, D. L. "9.1 Introduction to Industrial Applications of Asymmetric Synthesis." *Journal: Comprehensive Chirality*, **2012**, 1-26.

[58] Mikola, M. R.; Widman, M. T.; Worden, R. M. "In situ mutagenesis and chemotactic selection of microorganisms in a diffusion gradient chamber." *Biotechnology for Fuels and Chemicals*. Humana Press, Totowa, NJ, **1998**. 905-918.

[59] Ogino, T., et al. "Biosynthesis of aromatic compounds: 13C NMR spectroscopy of whole *Escherichia coli* cells." *Proceedings of the National Academy of Sciences* 79.19, **1982**, 5828-5832.

[60] Hamilton, Carol M., et al. "New method for generating deletions and gene replacements in *Escherichia coli*." *Journal of bacteriology* 171.9, **1989**, 4617-4622.

[61] Snoep, Jacky L., et al. "Reconstruction of glucose uptake and phosphorylation in a glucose-negative mutant of *Escherichia coli* by using Zymomonas mobilis genes encoding the glucose facilitator protein and glucokinase." *Journal of bacteriology* 176.7, **1994**, 2133-2135.

[62] Draths, K. M., et al. "Biocatalytic synthesis of aromatics from D-glucose: the role of transketolase." *Journal of the American Chemical Society* 114.10, **1992**, 3956-3962.

[63] Draths, K. M., and John W. Frost. "Synthesis using plasmid-based biocatalysis: plasmid assembly and 3-deoxy-D-arabino-heptulosonate production." *Journal of the American Chemical Society* 112.4, **1990**, 1657-1659.

[64] Li, Kai, and J. W. Frost. "Microbial synthesis of 3-dehydroshikimic acid: a comparative analysis of D-xylose, L-arabinose, and D-glucose carbon sources." *Biotechnology progress* 15.5 (1999): 876-883.

[65] Martinez, J. A.; Bolivar, F.; Escalante, A. "Shikimic acid production in *Escherichia coli*: from classical metabolic engineering strategies to omics applied to improve its production." *Frontiers in Bioengineering and Biotechnology*, 3, **2015**, 145.

[66] Michel, G.; Roszak, A.W.; Sauvé, V.; Maclean, J.; Matte, A.; Coggins, J.R.; Cygler, M.; Lapthorn, A.J.; "Structures of shikimate dehydrogenase AroE and its paralog YdiB: a common structural framework for different activities." *Journal of Biological Chemistry*, **2003**, 278(21), 19463-19472.

[67] Lindner, H.A.; Nadeau, G.; Matte, A.; Michel, G.; Ménard, R.; Cygler, M. "Site-directed mutagenesis of the active site region in the quinate/shikimate 5-dehydrogenase YdiB of Escherichia coli." *Journal of Biological Chemistry*, **2005**, 280(8), 7162-7169.

CHAPTER THREE: THEORETICAL PERSPECTIVES ON SHIKIMIC ACID

3.1. Introduction

3.1.1. Life Cycle Assessment and Technoeconomic Analysis

The biosynthesis of SA from sugars sourced from corn grain and corn stover is compared here. Comparative life-cycle assessment (LCA) and a technoeconomic analysis (TEA) were performed on two biorefinery models. Empirical data were based on ball-milling and fed-batch fermentation data previously described.[1] To date, this is the first LCA/TEA study comparing the efficacy of different milling and microbial fermentation methods for SA production on an industrial scale. Two biorefinery models were designed based on how sugar feedstocks are sourced: the first model sourced glucose from corn grain via a dry milling process. The second model sourced a mixture of glucose and xylose from corn stover via a ball milling process. Environmental effects of the two refineries were compared using LCA in four impact categories: land usage, carbon emissions, water usage, and eutrophication. The TEA portion compares the profitability of each biorefinery using profitability metrics including net present value (NPV) and minimum selling price (MSP). Here, the LCA/TEA results of SA sourced from stover and grain are discussed to examine what relative environmental impacts and technoeconomics can be achieved using corn stover.

3.1.2. Block Flow Diagram

A spreadsheet model was formulated extending from corn cultivation to the sale of SA (cradle-to-gate). A block flow summary of the corn stover processing system is shown in **Fig 3.1(a)**. After cultivation, corn stover is sent to a facility central to the surrounding farmland. Glucose, xylose, acetic acid, and lignin are produced after enzymatic hydrolysis by cellulase and xylanase in a ball mill. Lignin and residual cellulose/xylan are separated by centrifugation and fed to a combustion engine for energy recycling, after which glucose and xylose are spray dried and trucked offsite for

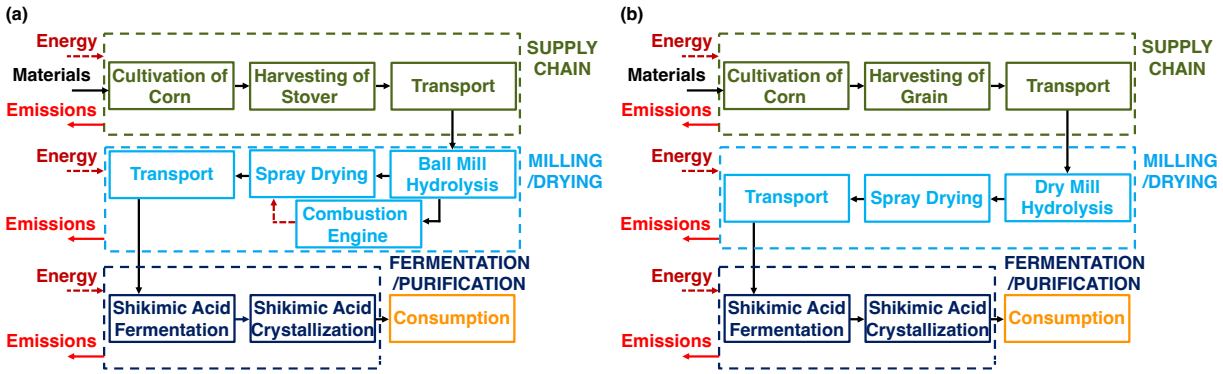

Figure 3.1. LCA/TEA block flow diagrams shikimic acid sourced (a) from corn stover and (b) from corn grain. Color scheme as follows: supply chain (green), milling and drying process (light blue), and fermentation/purification (navy blue). Solid arrows signify material/emission streams. Dashed arrows signify energy streams.

fermentation and purification. Assumptions of perfect separation were made during all centrifugation steps. For SA fermentation, strains that optimized the LCA/TEA models were selected (YJ1.144/pSC6.090B from the stover refinery and YJ1.130/pKD12.138A for the grain refinery). Spray-dried glucose and xylose are used as substrate for YJ1.144/pSC6.090B, an *E. coli* strain equipped to co-utilize hexose and pentose sugars for SA production.[2] After deletion of the native glucose transport system, alternate transport proteins are expressed in YJ1.144/pSC6.090B to better utilize sugars of mixed sugar feedstocks (**Fig. 3.2(a)**). Without disruption of the native phosphotransferase system (PTS) and expression of an alternate glucose transport system, glucose and xylose would not be simultaneously consumed. Rather, sequential consumption of glucose prior to xylose would take place.[3] Glucose facilitated diffusion transporter (GlF) and glucokinase (GlK) are natively found in *Zymomonas mobilis* and heterologously expressed in YJ1.144/pSC6.090B.[2,4] Data describing strain performance when grown on a 70:30 (*w*/*w*) ratio of pure glucose and xylose are used in modeling SA sourced from corn stover. Fermentation data were also collected after growth on authentic corn stover hydrolysates, which will be referenced later in the study. Reduction in SA yield and selectivity is believed to have been caused by the

presence of acetic acid in the hydrolysates, although the mechanism for this has not been determined. Separation and purification of SA via recrystallization utilizes technology patented by Van der Does et al, which has been described for industrial scale SA purification.[5] The byproducts, DHS and QA, are removed as waste during SA purification and not considered further. Fermentation broth is centrifuged to separate cell mass. Nonpolar impurities are removed by passing the supernatant over activated carbon. After spray drying, a water content of 3% (*w*/*w*) is retained in the product. The viscous medium is purified to at least 95% (*w*/*w*) via recrystallization from *n*-butanol.

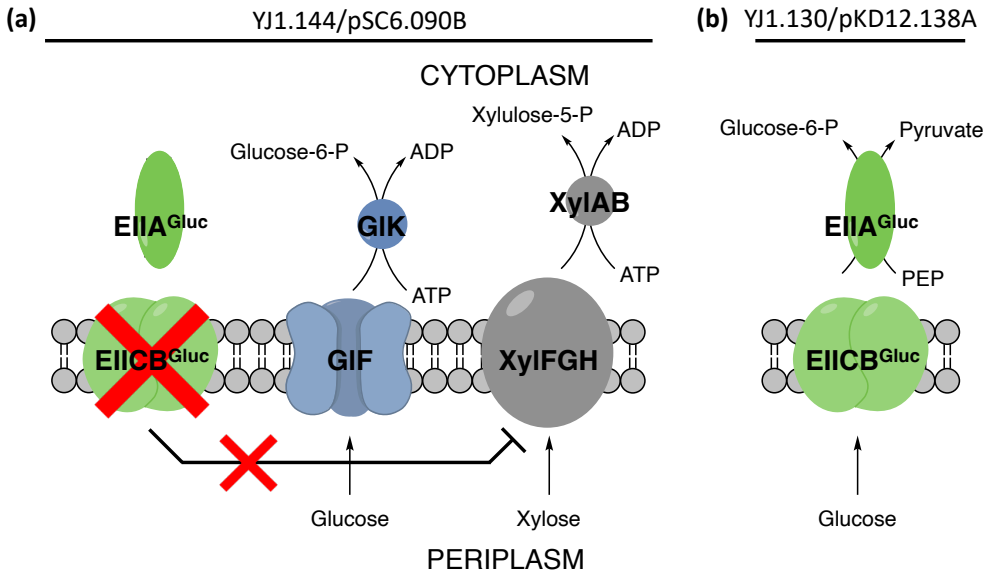

Figure 3.2. Corn stover-derived glucose and xylose and corn grain-derived glucose transport into the cytoplasm schematic representation of corn stover-derived glucose and xylose and corn grain-derived glucose transport into the cytoplasm for strains *E. coli* YJ1.144/pSC6.090B and YJ1.130/pKD12.138, respectively: (a) Mutation of ptsG-encoded EIICBGluc inactivates PTS-mediated glucose transport and eliminates repression of xylFGH expression by glucose. Instead, facilitated diffusion of glucose and subsequent phosphorylation to glucose-6-phosphate is mediated by GlF and GlK, which are expressed heterologously. Xylose transport and phosphorylation are mediated by XylFGH and XylAB, respectively, and occur simultaneous with glucose transport. (b) Glucose transport and phosphorylation is mediated by EIICBGluc and EIIAGluc, respectively.

Using dry milling followed by fermentation/purification, SA can be sourced from corn grain (**Fig. 3.1(b)**). The grain is harvested and trucked to a refinery that is surrounded by corn-growing

farmland. The dry mill begins with crushing corn grain into corn meal via a hammer mill followed by slurrying, liquefaction, and saccharification processes. The resulting solution is centrifuged, spray dried, and trucked to an offsite fermentation/purification facility. The strain YJ1.130/pKD12.138A, a strain of *E. coli* engineered to overproduce SA and transport glucose via its native transport system, is used to synthesize SA sourced from starch-derived glucose.[2] Dry milling solely produces glucose, hence YJ1.130/pKD12.138A does not need to be engineered to co-utlilize glucose and xylose (**Fig. 3.2(b)**). Physiological properties of for YJ1.130/pKD12.138A when grown on glucose are provided (**Table 3.1**). The same technology is utilized for separation and purification of SA as with the previously described process.[5] Separation begins with centrifugation of the fermentation broth to separate cell biomass. The supernatant is passed over activated carbon to further remove nonpolar impurities. The medium is sent to a second spray dryer with an effluent water content of 3% (*w*/*w*). Recrystallization from *n*-butanol affords a final SA product that is at least 95% (*w*/*w*) pure.

Stream summary tables for both corn grain and stover systems can be found below their respective flow diagrams in the Appendix (**Fig. A.3.1** and **Fig. A.3.2**). Data from the previous chapter, given a fixed annual SA production capacity, were used to complete mass balances around each system. Feedstock flowrates, capital expenses, machine hourly rates, and environmental data can be back-calculated once a mass balance is complete. These calculations are described in more detail in the Economic Model section.

3.2. LCA and TEA Models

3.2.1. Goal and Scope

Biocatalytic synthesis of SA is essential in mitigating issues with high cultivation costs and limited SA availability from Chinese Star Anise.[6] The goal of this study was to compare recent

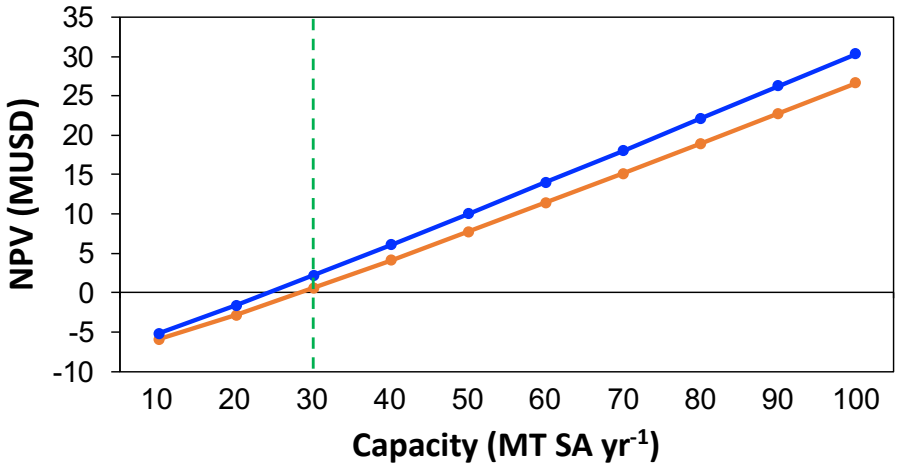

Figure 3.3. NPV of SA refineries in millions of US dollars (MUSD) sourcing corn grain (blue) and corn stover (orange) versus production capacity in metric tons SA per year (MT SA yr^{-1}). Supporting data included in Appendix.

technologies for SA biosynthesis from corn stover with established technologies for biosynthesis from corn grain. An LCA and a TEA were performed comparing methods for SA synthesis from these two feed sources. The scope for this assessment starts at corn planting and ends at selling SA to consumers. This scope includes all processes in manufacturing and recycling of materials within the refineries themselves. Backset water constitutes 30% of water used in the corn grain dry milling and corn stover ball milling processes.[7,8] Lignin coproduct in the corn stover ball milling process is combusted for energy to be recycled to power spray drying of hydrolysates. The geographic scope includes high-density farming areas in Illinois, so data chosen for power consumption and water scarcity were selected from Illinois or Midwestern databases.[22,23] A temporal horizon of 10 years was chosen to evaluate parameters for rates of return over a greater than per annum basis. A functional unit of 1 MT (metric ton) of SA was chosen to evaluate the biorefineries on a consistent scale. Annual SA production of 30 MT yr^{-1} was found to be the minimum capacity at which SA sourced both from corn grain and corn stover would have a positive net present value (NPV) (**Fig. 3.3**). With SA being a low demand (650 ton yr^{-1} in 2015 with an average growth rate of 3.65%

over the years that followed), high value fine chemical, this was chosen as the annual capacity for the two models.[33]

3.2.2. Allocation

A scenario for allocation between stover and grain was needed to perform the LCA portion of the study because they are coproducts of the same plant. As coproducts, allocation determines how much burden or benefit in terms of land use, water use, fertilizer use, emissions and sequestration is allocated toward each feedstock. Carbon sequestration involves photosynthetic carbon capture followed by carbon deposition into the soil through root matter, root exudation, and stover decay. Two allocation scenarios are reported for each life cycle impact (LCI) category. In scenario 1, corn stover is treated as waste rather than a coproduct, meaning allocation is not necessary. In scenario 2, corn stover is a coproduct that has some inherent value (for example, as animal feed or fertilizer), and thus environmental burdens and benefits must be assigned to its cultivation/harvesting. The most common allocation methods are based on either mass ratios or economic value. With the

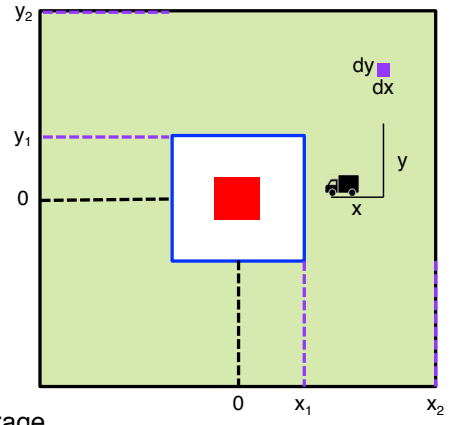

Figure 3.4. Trucking distance model average transportation distance calculation from neighboring farms to feedstock processing refinery.

product of interest being a fine pharmaceutical chemical, allocation was assigned using the economic value of the feedstock. Further, it is believed that the future of producing chemicals and fuels from agriculture will be burdened with competition from the food industry.[9] Allocation with respect to economic value will factor the effects of market pressures, whereas allocation by mass is constant with time.

A price of 4.00 USD per bushel of corn has been used for this study, which was converted to approximately 15.7 ¢ kg^{-1} corn grain.[10] Another recent article monetized the economic value of corn stover as 9.15 ¢ kg^{-1} corn stover.[11] The costs of transportation were added to the reported values of each feedstock. Average trucking distance was calculated as depicted by **Fig. 3.4**. Rectangular coordinates were assumed, because plots of land and the orientation of roads are generally rectangular in nature. The refinery was assumed to occupy the center of a 2.01 x 2.01 km^2 area not designated for cultivation. Areas surrounding the refinery beyond this 2.01 x 2.01 km^2 area were assumed to have 25% of their land dedicated to corn cultivation.[12] Furthermore, it was assumed that only 60% of stover cultivated could be harvested and sold to refinery, as stover left behind is necessary for soil nutrients and for reducing air velocity at the soil surface to reduce wind erosion.[13] Partial removal of stover may result in slight increases in corn yields in some areas.[41] However, total removal of stover from corn fields has been shown to reduce crop yields.[42,43] One major environmental concern is the effect of stover removal on soil organic carbon (SOC), which impacts the global carbon cycle. The amount of SOC that accumlates in the subsurface depends on the tillage severity and the amount of unharvested corn stover on the field surface.[44] This study assumed that 40% of cultivated corn stover is left behind on the fields. The described area is subsequently used to solve the integral in **Fig. 3.4**. The calculated trucking distance is related to transportation cost by **Eq. 3.1**[14]:

$$TC = \frac{299.4}{119.5} \cdot [2.59 \cdot 10^{-5} + (6.20 \cdot 10^{-5}) \cdot X] \quad \textbf{(3.1)}$$

where TC is transportation cost (USD kg^{-1}) and X is trucking distance (km). Energy consumption per pound of feed transported was 1.3 kJ kg^{-1}. The 299.4/119.5 factor was used to account for changes in producer price indices for general freight trucking.[15] Cost of feedstocks delivered to the milling facility for corn grain and corn stover were calculated to be 16.4 ¢ kg^{-1} and 9.80 ¢ kg^{-1}, respectively. 63% of the burdens and benefits of cultivating/harvesting corn crops were allocated to corn grain and 37%, or 1.68 times less, were allocated to corn stover. Allocation toward corn using this method can increase in times of crisis or if future supplies of corn grain fail to meet growing demands for the feedstock.

3.2.3. Life Cycle Impact Categories

Four impact categories were selected for analysis: global warming, eutrophication, land usage, and water usage. All impacts are reported per functional unit basis (per ton SA produced annually). Global warming effects of different emissions are compared in units of carbon dioxide equivalents using LCA equivalency factors for each emission. All components of the biorefinery contributing to eutrophication will be compared in terms of nitrogen equivalents of that compound. Equivalency factors for quantifying global warming and emission potentials will be obtained using the TRACI model.[16] For example, phosphorus is a key component used in fertilizer and from the TRACI model has an equivalency factor of 7.29 kg N eq. $(kg\ P)^{-1}$. Thus, phosphorus has a greater impact than nitrogen toward eutrophication by a factor of 7.29. The GREET model was used to quantify emissions from cultivation and harvesting.[45]

Water requirements of different process elements were weighted depending on the scarcity of water in the designated area. The AWARE (available water remaining) model provides such characterization factors that, when multiplied by water usage of an element, better indicate the

potential to deplete water.[17] The average AWARE characterization factors for major corn producing states were 10.20 and 9.59 for agricultural and non-agricultural areas, respectively. These factors are used to calculate the water scarcity footprint (WSF) using **Eq. 3.2**:

$$WSF = CF_{AWARE} \cdot w_i \quad \textbf{(3.2)}$$

where CF_{AWARE} is the characterization factor and w_i is the water usage inventory of a particular piece of equipment. Cultivation/harvesting and milling were performed in agricultural areas. Conversely, fermentation/purification were performed off-site, in a non-agricultural area. Here, water usage analysis is limited to direct process inputs for cultivation/harvesting (including water usage from irrigation), dry milling, ball milling, and fermentation/purification. Land usage was compared based on hectares (ha) used by each process section. Land use of cultivation/harvesting was determined based on the assumption that a hectare of land provides 430 bushels of corn.[18] The calculated amount of land was subsequently multiplied by the appropriate allocation factor to find the land usage impact. Two hectares of land were purchased for the milling/spray drying refineries and two hectares of land were purchased for the fermentation/purification refineries in both systems being compared. The LCA and TEA models neither included crop productivity changes nor land usage change.

3.2.4. Life Cycle Inventory

Ball milling and shikimic acid fermentation data were obtained experimentally.[1] When designing the dry mill process, equipment sizing and costing were obtained from work by Tyner et al.,[7,8] which incorporated values from the textbook *Plant Design and Economics for Chemical Engineers*.[19] Data quality were quantified using the Weidema pedigree matrix.[20] The data quality indicators of reliability, completeness, temporal correlation, geographical correlation, and further technological correlation were used to score the data used for this LCA (see Appendix **Table**

A.3.1). The TRACI and GREET models were used to quantify global warming potential.[16,45] The TRACI model was used to quantify eutrophication potential.[16] The AWARE model was used to quantify water usage impacts.[17]

3.2.5. Economic Model

To make a complete assessment of eco-efficiency, a TEA was performed over the 10-year temporal horizon. Fixed cost was itemized into depreciation, local taxes, insurance, and rent costs. Chemical Engineering Plant Cost Indices (CEPCI) were used to adjust past year equipment prices to the most recent available index (2018).[29] Combining temporal cost adjustments with the "six-tenths" rule, equipment costs could be adjusted to the correct size (**Eq. 3.3**)[40]:

$$C_{x,yr_2,cap_2} = C_{x,yr_1,cap_1} \cdot \left(\frac{CEPCI_{yr_2}}{CEPCI_{yr_1}}\right)\left(\frac{capacity_2}{capacity_1}\right)^{0.6} \quad \textbf{(3.3)}$$

Average annual investment (AAI) was calculated for each piece of equipment by **Eq. 3.4**:

$$AAI = \frac{(P - SV) \cdot (n + 1)}{2 \cdot n} + SV \quad \textbf{(3.4)}$$

For initial investment (P), salvage value (SV), and economic lifetime (n). Subsequently, depreciation (DEP) was calculated using **Eq. 3.5**:

$$DEP = \frac{(P - SV)}{n} \quad \textbf{(3.5)}$$

where n was assumed equal to the 10-year temporal horizon of the project. Annual interest and insurance were values needed to determine the fixed cost per scheduled machine hour (SMH) using **Eq. 3.6**.

$$C_{int,ins} = \big(interest\ (\%) + insurance\ (\%)\big) \cdot AAI \quad \textbf{(3.6)}$$

$C_{int,ins}$ is annual cost of interest and insurance. Fixed costs per SMH are converted to a productive machine hourly rate by relating productive machine hours (PMH) to SMH (**Eq. 3.7** and **Eq. 3.8**):

$$Fixed\ cost\ per\ SMH = \frac{DEP + C_{int,ins}}{SMH} \quad \textbf{(3.7)}$$

$$SMH = \frac{PMH}{U} \quad \textbf{(3.8)}$$

where U is utilization rate, a measure of the productivity of workers. Fixed costs and operating costs were calculated for process equipment in milling/spray drying and fermentation/purification sections of each biorefinery. Repair and maintenance costs for pieces of equipment were calculated as 50% of the cost of depreciation. For both systems, two operators were hired in the milling/spray drying sections and three operators were hired in the fermentation/purification sections. Operators were paid 25 USD SMH^{-1} with an assumed fringe rate of 40%. Machine rate per SMH (MR) was calculated as the sum of fixed cost per SMH, operating cost per SMH, and wage rate.

Profitability is reported as NPV and MSP in this study. First, production cost per kilogram of SA produced was calculated (**Eq. 3.9**):

$$Production\ cost = \frac{Utilities + Price\ Feedstocks + MR_{harv} + MR_{M/S} + MR_{F/P}}{PR} \quad \textbf{(3.9)}$$

where MR_{harv} (USD SMH^{-1}), $MR_{M/S}$ (USD SMH^{-1}), and $MR_{F/P}$ (USD SMH^{-1}) are machine rates per SMH for cultivation/harvesting, milling/spray drying, and fermentation/purification, respectively. Production rate (PR) has units kg SA SMH^{-1} giving production cost units of USD $(kg\ SA)^{-1}$. An initial investment of total capital spending and available inventory needed on hand was assumed to be incurred at year -1. Capital spending and available inventory were calculated using **Eq. 3.10** and **Eq. 3.11**:

$$Capital\ Investment = La \cdot \sum_{x} C_x \quad \textbf{(3.10)}$$

$$Available\ Inventory = (SP \cdot PR + FP \cdot FR) \cdot 24\frac{h}{d} \cdot 30\frac{d}{m} \quad \textbf{(3.11)}$$

Table 3.1. Listed assumptions assumptions for LCA/TEA model.

Description	Value	Unit	Ref.
Functional Unit	1	US ton SA	-
Temporal Horizon	10	yr	-
MAX Production	55	US ton yr^{-1}	-
Sales Price	54.88	USD $(lb\ SA)^{-1}$	[21]
Corn Grain Price	7.45	¢ lb^{-1}	[9]
Corn Stover Price	4.45	¢ lb^{-1}	[10]
Utility Price	11.6	¢ kWh^{-1}	[22]
Fresh Water Price	0.049	¢ lb^{-1}	[23]
n-Butanol Price	35.4	¢ lb^{-1}	[24]
Activated Charcoal Price	1.25	USD lb^{-1}	[25]
Interest	7	% of AAI	-
Insurance	4	% of AAI	-
Tax	21	% of AAI	[26]
Discount Factor	10	%	-
Fringe	40	%	-
Repair and Maintenance	50	% of DEP	-
Wages	25	USD SMH^{-1}	-
Utilization Factor	98	%	-
Salvage Value	20	% of purchase cost	-
Emission per kWh	1.56	lb CO_2 kWh^{-1}	[27]
Lang Factor	4.36	-	[28]

with newly defined variables Lang factor (La), selling price (SP), feedstock price (FP), and feedstock consumption rate (FR). Each biorefinery was assumed to begin production at maximum PR starting at year 0. Annual sales revenue (ASR) was found using **Eq. 3.12**:

$$ASR = SP \cdot PR \cdot 24\frac{h}{d} \cdot 365\frac{d}{yr} \tag{3.12}$$

Gross profit (GP) and Net Profit (NP) were defined by **Eq. 3.13** and **Eq. 3.14**:

$$GP = ASR - (Production\ cost) \cdot 50{,}000\ \frac{kg\ SA}{yr} \tag{3.13}$$

$$NP = GP \cdot (1 - income\ tax\ \%) \tag{3.14}$$

Finally, net profits were accrued over the ten-year temporal horizon. Annual net profits were discounted (discount cash flow rate of return, DCFRR) and summed to determine NPV (**Eq. 3.15**).

$$NPV = \sum_{t=1}^{10} \left(\frac{1}{1 + DCFRR}\right)^{t} \cdot NP \quad \textbf{(3.15)}$$

To calculate MSP for a set of conditions, DCFRR was fixed at 18% and NPV was set to 0 USD. SP was solved by back-calculating from the above equation for NPV to determine MSP. Thus, MSP was defined as the minimum selling price per pound of SA that achieved a rate of return of 18%. Other assumptions are listed in **Table 3.1**.

3.3. Results and Discussion

3.3.1. Life Cycle Impact Assessment

In the Life Cycle Impact Assessment, the environmental impacts of each system are tallied for the life cycle impact categories of global warming potential, eutrophication potential, water usage, and land usage. In allocation scenario 1, corn stover feedstock is treated as a waste, and no burdens (*e.g.* eutrophication from fertilizer) or benefits (*e.g.* carbon sequestration during cultivation) are credited toward it. In allocation scenario 2, burdens and benefits of one in every 2.68 hectares of land are credited toward corn stover, because the price ratio of grain to stover is approximately 1.68 to 1 (See allocation section). Impact values for SA sourced from stover in scenario 1 will be referred to as $Stover_1$, and impact values for SA sourced from grain in scenario 1 will be referred to as $Grain_1$. Values for SA sourced from stover in scenario 2 will be referred to as $Stover_2$, and impact values for SA sourced from grain in scenario 2 will be referred to as $Grain_2$.

Global warming potential was chosen as an impact category due to inherent energy requirements for chemical production. The TRACI model was used to calculate the carbon dioxide equivalents for each system.[16] The GREET model was used to calculate emissions for each system

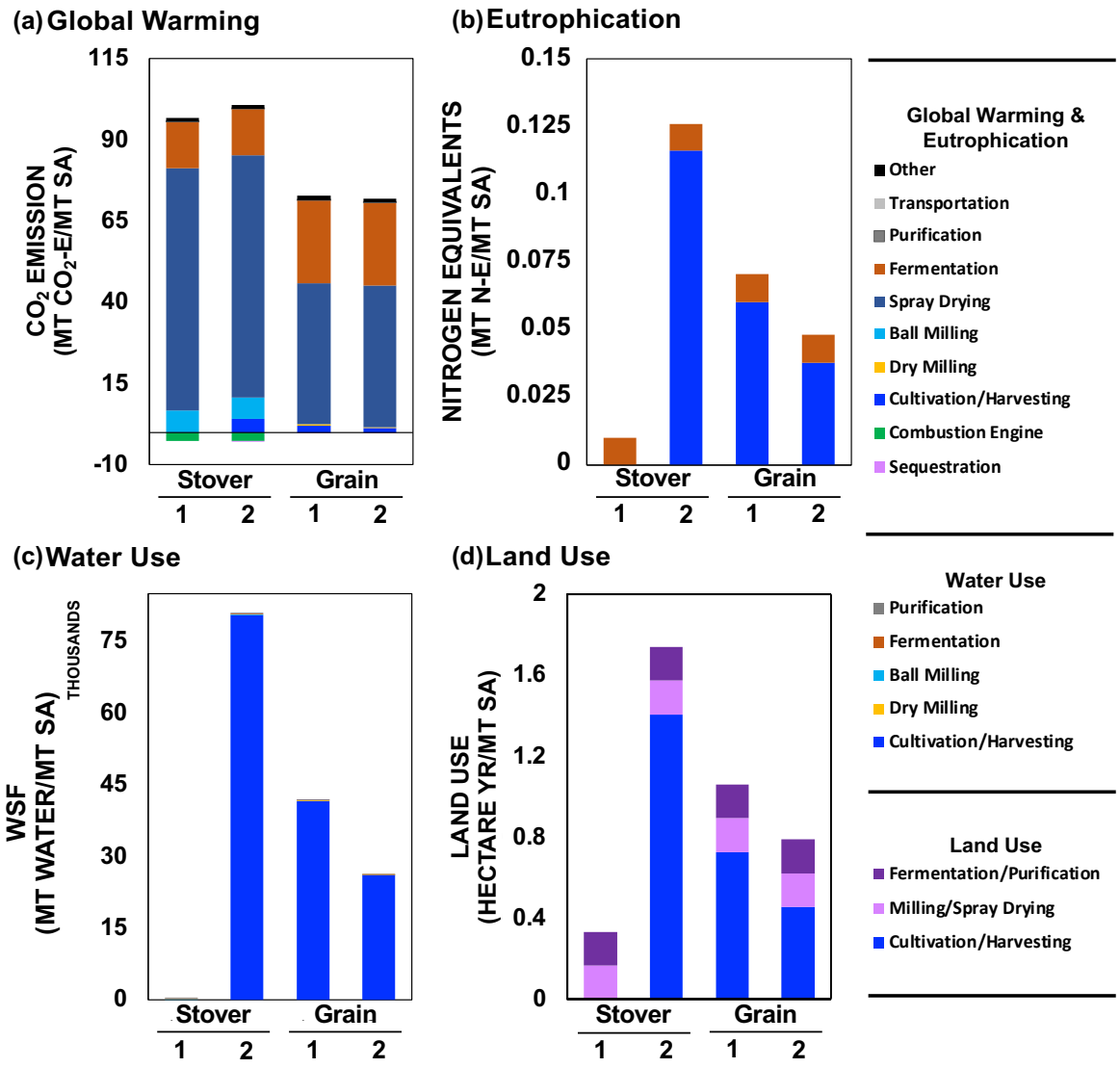

Figure 3.5. Life cycle impacts (a) global warming potential, (b) eutrophication potential, (c) water usage, and (d) land usage impacts of SA production from corn grain (system A) and corn stover (system B). Numbers signify allocation scenarios 1 (no allocation toward stover) or 2 (economic allocation).

due to cultivation and harvesting, revealing that nitrous oxide was the largest contributor.[45] Not unexpectedly, the corn stover system had a higher impact on global warming potential (**Fig 3.5(a)**) by 29% in allocation scenario 1 and by 36% in allocation scenario 2. This is due to a requirement for more corn stover relative to corn grain since sugars are not as readily released from the recalcitrant structure of stover. 174 kg ha^{-1} yr^{-1} of carbon sequestration was assumed during the

cultivation of corn.[47] 100% of sequestration and emissions from cultivation were allocated to $Grain_1$ and 63% to $Grain_2$ (some impacts of sequestration and emission are barely visible because the impacts of some equipment operations are much larger). Sequestration and emissions were allocated 0% to $Stover_1$ and 37% to $Stover_2$. Negative emission benefits are also credited to $Stover_1$ and $Stover_2$ for power generated from a lignin combustion engine used for powering the spray dryer. Within the stover refinery, spray drying had the largest impact followed by the ball mill. Interestingly, the fermentation process for the corn stover processing model had lower emissions than the corn grain processing model. This is owing to the engineered glucose/xylose co-utilizing, SA-overproducing *E. coli* strain YJ1.144/pSC6.090B being more productive than YJ1.130/pKD12.138A.

Eutrophication impacts from fertilizer use during cultivation are a major concern. Fermentation processes also have a eutrophication impact from the nitrogen that bacteria require to grow. Eutrophication was determined using the TRACI model by finding the compounds that contribute to eutrophication and converting the mass flow into kg N/kg to find the final impacts.[34] The eutrophication potentials for grain and stover processing in both allocation scenarios were compared side-by-side (**Fig. 6(b)**). The slight decrease in eutrophication for corn grain from system $Grain_1$ to $Grain_2$ is because allocation toward corn is shifting from accepting 100% of the burdens and benefits for cultivation/harvesting to accepting 63%. Meanwhile, allocation toward corn stover increases from 0% in $Stover_1$ to 37% in $Stover_2$. For $Stover_2$, larger volumes of corn stover to corn grain are purchased to produce equal amounts of SA. The cultivation step of these purchased feeds results in a 2.6-fold higher eutrophication impact in $Stover_2$ than $Grain_2$.

The water usage impact category was chosen because multiple systems in both biorefineries demand fresh water, which will leave a water scarcity footprint (**Fig. 6(c)**). Similarly to a pattern

seen in eutrophication, $Stover_1$ was lower than $Grain_1$ and $Stover_2$ was higher than $Grain_2$. The primary contributor to water usage is in cultivation except in $Stover_1$ where it was in ball milling. Other components of the two refineries that use water include dry milling, ball milling, fermentation, and SA purification processes. The water usage impact of $Stover_2$ was 3.1-fold higher than that of $Grain_2$. The primary contributor to land usage is also in the cultivation step, except in $Stover_2$, where it is in the fermentation process (**Fig. 6(d)**). Equal amounts of land, two hectares, were used for milling/spray drying and fermentation/purification in both refineries and allocation scenarios. Land usage in $Stover_2$ was 2.2-fold higher than land usage in $Grain_2$. A similar trend can be seen in **Fig. 6(b)**, **6(c)**, and **6(d)** where, because of the difficulty in releasing sugars from stover in comparison to grains, a larger volume of feedstock is required to produce SA from stover. The yield of SA from stover is 8.5% (*w*/*w*) while the yield of SA from grain is 15% (*w*/*w*), which explains why the environmental impacts of stover tend to be two to three times higher than corn grain. Allocation is an important factor in determining which technology is more environmentally burdensome. A large spike in eutrophication, water usage, and land usage is realized in $Stover_2$ when corn stover is no longer treated as a waste product.

3.3.2. Life Cycle Sensitivity

The sensitivity of each impact category to key variables was investigated for allocation scenario 2 ($Grain_2$ and $Stover_2$). In **Fig. A.3**, percentage changes in global warming potential (green), eutrophication (red), water usage (blue), and land usage (orange) vary against fixed percentage changes in SA fermentation yield, milling efficiency, and production capacity. The data show for equivalent percentage changes in SA yield, the LCI variables of $Stover_2$ substantiate marginally higher percentage changes compared to $Grain_2$. For equivalent changes in milling efficiency, $Stover_2$ demonstrated larger changes in land usage, global warming potential, and

eutrophication and similar changes in water usage. The data suggest that vast improvements in SA yield and milling efficiency are necessary for stover SA to be competitive with grain SA in these impact categories. Both systems are least sensitive to changes in production capacity, which has no impact on global warming potential, eutrophication potential, and water usage and little impact on land usage. Allocation with respect to economic value of feedstocks is a key assumption when reaching the conclusions of this life cycle sensitivity analysis.

3.3.3. Profitability

The profitability outcomes of each system are understood by itemizing each system into their respective equipment and production costs. **Fig. 3.6(a)** and **Fig. 3.6(b)** below summarize the equipment costs for corn grain and corn stover processing. An equipment summary table, including associated sizes and machine hourly rates, is presented in the Appendix (**Table A.3.2**). In total, corn stover processing requires a larger capital investment due to the large volume feed streams that are being handled. Although it has been suggested that ball milling is a user friendly and easily implemented process for farmers, the size of the ball mill needed to process the necessary corn stover causes it to be more expensive than the dry milling equipment needed for a 55 ton SA annual capacity. Furthermore, the total production cost for corn stover processing is higher than that of corn grain processing.

Fig. 3.6(c) and **Fig. 3.6(d)** itemize production costs into their constituents for the corn stover and the corn grain systems. Production costs associated with every component in corn stover processing, except for fermentation/purification, is higher than the respective component for corn grain processing. Generally, the costs of feedstock (stover and grain) occupy a great percentage of production costs. However due to the small scale of this high profit margin chemical, feedstock price was small in comparison to the price of fermentation supplements, milling/spray drying, and

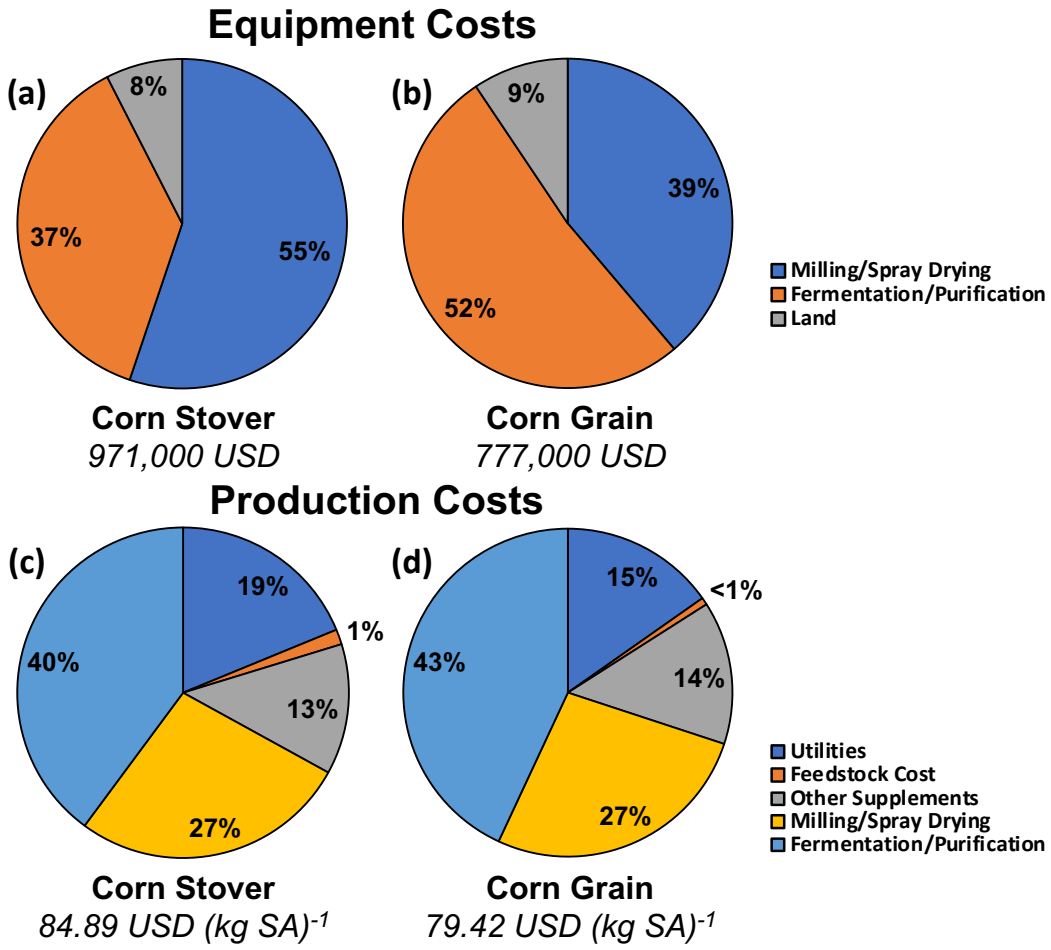

Figure 3.6. Equipment and production costs equipment costs realized in (a) biorefinery sourcing corn stover and (b) biorefinery sourcing corn grain. Production costs realized in (c) biorefinery sourcing corn stover and (d) biorefinery sourcing corn grain.

fermentation/purification. To establish a path for achieving more competitive technoeconomics using corn stover, a sensitivity analysis was performed between the MSP profitability metric and key variables: SA fermentation yield, production scales, milling yields, electricity costs, fermentation supplement costs, feedstock costs, and fresh water costs.

3.3.4. Technoeconomic Sensitivity

After the MSP was determined for a DCFRR of 18%, the change in the MSP was determined for +/- 20% increases or decreases in variables that were thought to affect profitability (**Fig. 3.7**).

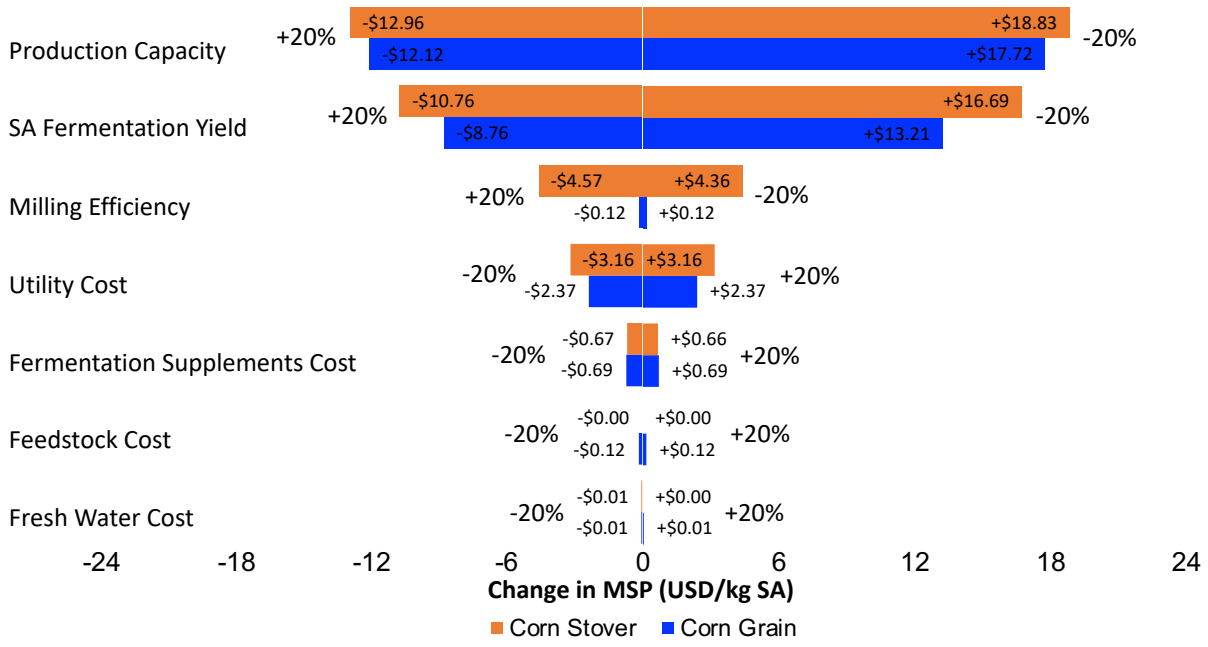

Figure 3.7. Technoeconomic sensitivity tornado plot of the sensitivities of key contributing variables to minimum selling price (MSP). Changes in MSP are labeled on each bar.

These variables included SA yield, production capacity, milling efficiency, utility cost, fermentation supplement cost, feedstock cost, and fresh water cost. The most sensitive variable for SA production was its fermentation yield. The importance of yield will always be emphasized when synthesizing fine chemicals with high margins of profit. Feedstock costs are also relatively low in sensitivity due to the high profit margin realized for SA. One other processing variable that could lead to higher profitability is the milling efficiency, which is important when considering areas for process improvement. For a majority of the variables examined, the profitability of SA sourced corn stover is more sensitive than corn grain, suggesting that process optimization of corn stover SA is needed.

3.3.5. Waterfall Plot Analysis

A path to make ball milled corn stover feedstocks competitive with dry milled corn grain feedstocks is outlined in **Fig. 3.8**. A waterfall plot analysis shows a path based on ideal process

improvements for SA production. Here, MSP is once again calculated for a zero NPV achieving a DCFRR of 18%. In essence, best-case scenarios were designed for both systems based on the independent variables investigated in the sensitivity analysis. Before examining these scenarios however, the results of strain YJ1.144/pSC6.090B grown on authentic corn stover hydrolysates are implemented as a first step. For ball milling strategies of agricultural residues to be implemented, we must first overcome barriers presented by non-sugar coproducts of enzymatic hydrolysis such as acetic acid. As acetyl bonds in hemicellulose release acetic acid during the milling process,[31] either an intermediate process for removal of acetic acid must be implemented (pretreatment of stover to remove acetyl groups or acetic acid purification post-milling) or a strain must be further engineered to be acetic acid tolerant.[32]

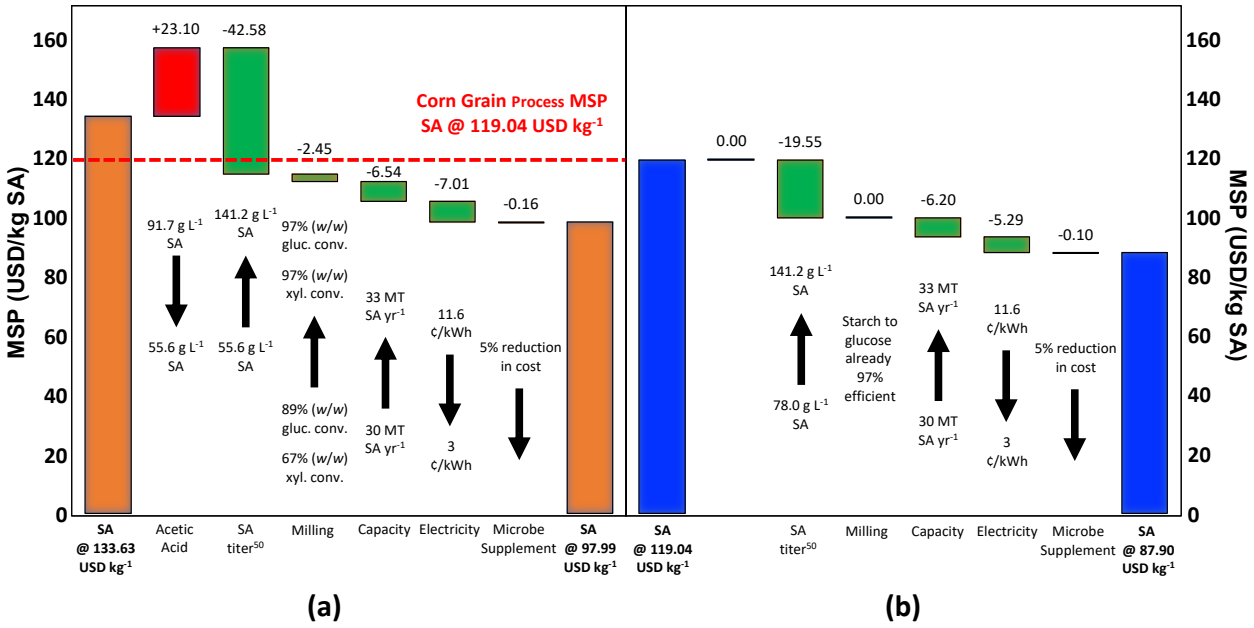

Figure 3.8. Future outlook for SA production waterfall plot analysis with MSP of corn stover processing in (a) biorefinery sourcing corn stover and (b) biorefinery sourcing corn grain.

Should these barriers of implementation be overcome, an engineered SA overproducing strain of *Corynebacterium glutamicum* can achieve SA titers of up to 141.2 g L^{-1} in fed-batch fermentation.[50] To generate an ideal condition for SA yields, physiological properties from Inui et

al. were simulated in the TEA for stover and grain processing. This improvement in fermentation yield results in an MSP for corn stover SA that is lower than the original MSP achieved in corn grain SA. Ball milling yields were optimized by matching the 97% yields achieved in the dry milling process (See **Table 1**). An expected increase in future SA demand suggests the capacity of the proposed refineries can be increased. SA production in 2015 was about 590 MT yr^{-1} and had an average growth rate of 3.65% over the years that followed.[51] An additional 3 MT yr^{-1} in annual production for both systems was carried out as a next step in the analysis. Furthermore, the price of wind and solar energy has been forecast to reduce by about 60% by 2031.[52] To depict related reductions in costs for electricity, utility price was reduced to 3 ¢ kWh^{-1} from its initial value of 11.6 ¢ kWh^{-1} for both systems. The waterfall plot was finalized by enabling a 5% reduction in costs of fermentation supplements to show MSP is not very sensitive to these feedstock prices. It must be highlighted that higher SA fermentation yields and ball milling yields are the most important process improvements. New lignocellulosic feedstock milling technology was assessed here for upgrading feedstocks that would otherwise be used as soil nutrients or animal feed. To reach a point where bioprocesses might add a ball milling strategy to their current chemical process, barriers of implementation must be overcome and the gap in economics from currently implemented methods of biosynthesis must be reduced. In order to marginally increase the profit margin of their land and increase their volume of product, farmers or process engineers may still consider using ball-milling technology at a lower DCFRR than what can be achieved with corn grain (in this study, assumed 18%) for whole-crop utilization.

3.4. Summary & Future Work

LCA and TEA compared SA biosynthesis from corn stover using developmental methods to corn grain via dry milling. Corn stover or corn grain feedstocks were funneled into a milling

facility central to neighboring farms. A ball mill was used in the corn stover process whereas a dry mill was used for corn grain. After the sugar intermediates were spray dried and trucked to a second off-site refinery, they underwent a SA fermentation/refining process to then be sold to consumers. Only when stover was treated completely as a waste feedstock, could advantages in land use, water use, and eutrophication potential be realized. Realistically, corn stover does have inherent value and SA biosynthesis from stover became more environmentally burdensome than biosynthesis from grain when allocating burdens/benefits based on economic value of the feedstocks. SA sourced from both stover and grain can be profitable. However, higher volumes of feed necessary for stover processing result in higher equipment costs and production costs per pound of SA produced. It is hypothesized that ball milling technology can someday be of interest to farmers looking for whole-crop utilization to marginally benefit profit margins of their land rather than use agricultural residues for soil nutrients and animal feed. Currently, it is not recommended the corn stover process be adopted before barriers of acetic acid inhibition are overcome and environmental impacts and technoeconomics are further improved.

REFERENCES

[1] Zhong, Y.; Frost, H.; Bustamante, M.; Li, S.; Liu, Y. S.; Liao, W. "A mechano-biocatalytic one-pot approach to release sugars from lignocellulosic materials" *Renewable and Sustainable Energy Reviews* **2020**, *121*, 109675.

[2] Jadidi, Y.; Frost, H.; Liao, W.; Saffron, C. M.; Draths. K. M. "Examination of Glucose Transport Systems for Upgrading Farm Residue-Derived Hydrolysates to Fine Chemicals" *Manuscript in Preparation*.

[3] Liang, Q.; Zhang, F.; Li, Y.; Zhang, X.; Li, J.; Yang, P.; Qi, Q. "Comparison of individual component deletions in a glucose-specific phosphotransferase system revealed their different applications" *Scientific Reports* **2015**, 5(1), 1-10.

[4] Chandran, S. S.; Yi, J.; Draths, K. M.; Von Daeniken, R.; Weber, W.; Frost, J. W. "Phosphoenolpyruvate Availability and the Biosynthesis of Shikimic Acid" *Biotechnol. Prog.* **2003,** *19*, 808–814.

[5] Van der Does T, Booij J, Kers EE, Leenderts EJAM, Sibeijn M, Agayn V "Process for the recovery of shikimic acid" Patent WO02/06203.

[6] Rawat, G.; Tripathi, P.; Saxena, R. K. "Expanding horizons of shikimic acid: Recent progresses in production and its endless frontiers in application and market trends" *Appl. Microbiol Biotechnol.* **2013**, *97*, 4277-4287.

[7] Tyner, W. E.; Dale, R. T. "Economic and Technical Analysis of Ethanol Dry Milling: Model Description" **2006**, Purdue University, *6*(4), 1-25.

[8] Tyner, W. E.; Dale, R. T. "Economic and Technical Analysis of Ethanol Dry Milling: Model User's Manual" **2006**, Purdue University, *6*(4), 1-25.

[9] Tenenbaum, D. J. "Food vs. Fuel: Diversion of Crops Could Cause More Hunger" **2008**, *Environ Health Perspect*, *116*(6): A254-A257.

[10] Langemeier, M. "Projected Corn and Soybean Breakeven Prices" *farmdoc daily*, **2018**, Department of Agricultural and Consumer Economics, University of Illinois at Urbana-Champaign, (8), 66.

[11] Edwards, W. "Estimating a Value for Corn Stover" *Ag Decision Maker*, **2020**, Iowa State University Extension and Outreach.

[12] Mumm. R. H.; Goldsmith, P. D.; Rausch, K. D.; Stein, H. H. "Land usage attributed to corn ethanol production in the United States: sensitivity to technological advances in corn grain yield, ethanol conversion, and co-product utilization" *Biotechnology for Biofuels*, **2014**, *7*(61). http://www.biotechnologyforbiofuels.com/content/7/1/61

[13] Wortmann, C.; Klein, R.; Shapiro, C. "Harvesting Crop Residues" *NebGuide* **2012**, Nebraska Extension, G1846.

[14] Sokhansanj, S.; Mani, S.; Turhollow, A.; Kumar, A.; Bransby, D.; Lynd, L.; Laser, M. "Large-scale production, harvest and logistics of switchgrass (*Panicum virgatum L.*) – current technology and envisioning a mature technology." Biofuels, Bioprod. Bioref. **2009**, 3, 124–141.

[15] U.S. Bureau of Labor Statistics, "Producer Price Index by Industry: General Freight Trucking, Long-Distance Truckload [PCU484121484121]" *FRED* **2021**, Federal Reserve Bank of St. Louis. https://fred.stlouisfed.org/series/PCU484121484121

[16] Bare, J. C. "TRACI 2.0 - The Tool for the Reduction and Assessment of Chemical and other environmental Impacts" *CLEAN TECHNOLOGIES AND ENVIRONMENTAL POLICY* **2011**, Springer-Verlag, New York, NY, *13*(5):687-696.

[17] Boulay A-M., Bare J., Benini L., Berger, M.; Lathuilliere, M. J.; Manzardo, A.; Margni, M.; Motoshita, M.; Nunez, M.; Pastor, A. V.; Ridoutt, B.; Oki, T.; Worbe, S.; Pfister, S. "The WULCA consensus characterization model for water scarcity footprints: assessing impacts of water consumption based on available water remaining (AWARE)." *Int J Life Cycle Assess* **2018**, *23*, 368–378.

[18] "Crop Production 2018 Summary" *USDA* **2019**, National Agricultural Statistics Service.

[19] Peters, M.S., Timmerhaus, K.D., and West, R.E. "Plant Design and Economics for Chemical Engineers". *McGraw-Hill* **2003**, New York, NY.

[20] Weidema, B. P.; Wesnæs, M. S. "Data quality management for life cycle inventories – an example of using data quality indicators" *Journal of Cleaner Production* **1996**, *4*, 167-174.

[21] Saxena, R. K.; Tripathi, P.; Rawat, G. "Expanding horizons of shikimic acid" *Appl. Microbiol Biotechnol*. **2013**, *97*, 4277–4287.

[22] "Illinois Electricity Rates" *EnergyBot*, **2020**, https://www.energybot.com/illinois-energy.html#:~:text=In%202019%2C%20the%20average%20Illinois,lower%20than%20the%20national%20average).

[23] "Water and Sewer Rates" *Chicago* **2021**, City of Chicago. https://www.chicago.gov/city/en/depts/fin/supp_info/utility-billing/water-and-sewer-rates.html

[24] "Butanol Price Analysis" *Echemi Technology Co., Ltd* **2021**. https://www.echemi.com/productsInformation/pid_Seven2824-butanol.html

[25] Leon, M.; Silva, J.; Carrasco, S.; Barrientos, N. "Design, Cost Estimation and Sensitivity Analysis for a Production Process of Activated Carbon from Waste Nutshells by Physical Activation" *Processes* **2020**, *8*(8), 945.

[26] "Corporate Tax Rates 2021" *Deloitte* **2021**. www.deloitte.com

[27] "Greenhouse Gases Equivalencies Calculator – Calculations and References" *EPA* **2021**. https://www.epa.gov/energy/greenhouse-gases-equivalencies-calculator-calculations-and-references

[28] Sokhansanj, S.; Turhollow, A.; Wilkerson, E. "Development of the Integrated Biomass Supply Analysis and Logistics Model (IBSAL)." *Oak Ridge National Lab* **2008**. ORNL/TM-2006/57

[29] "CEPCI Updates" *Chemical Engineering Magazine* **2021.**

[30] Kogure, T.; Kubota, T.; Suda, M.; Hiraga, K.; Inui, M. "Metabolic engineering of *Corynebacterium glutamicum* for shikimate overproduction by growth-arrested cell reaction" *Metabolic Engineering* **2016**, *38*, 204-216.

[31] Aghazadeh, M.; Ladisch, M. R.; Engelberth, A. S. "Acetic Acid Removal From Corn Stover Hydrolysate Using Ethyl Acetate and the Impact on *Saccharomyces cerevisiae* Bioethanol Fermentation" *Biotechnol. Prog.* **2016**, *32*(4), 929-937.

[32] Chen, X.; Shekiro, J.; Franden, M. A.; Wang, W.; Zhang, M.; Kuhn, E.; Johnson, D. K.; Tucker, M. P. "The impacts of deacetylation prior to dilute acid pretreatment on the bioethanol process" *Biotechnology for Biofuels* **2012**, 5, 8.

[33] "Global Shikimic Acid (CAS 138-59-0) Sales Market Report 2020" *Research Allied* **2020**, 120.

[34] "U.S. Department of Energy sets goal to cut solar costs by 60% within next 10 years" *Legal Monitor Worldwide* **2021**, SyndiGate Media Inc.

[35] Lijó, L.; González-García, S.; Bacenetti, J.; Fiala, M. "Life Cycle Assessment of Electricity Production in Italy from Anaerobic Co-Digestion of Pig Slurry and Energy Crops." *Renewable Energy* **2014**, *68*, 625–35.

[36] Baker, C. G. J.; McKenzie, K. A. "Energy Consumption of Industrial Spray Dryers" *Drying Technology* **2005**, *23*(1), 2, 365-386.

[37] Ricci, Bernardino, and Seok-Min Jung. "Energy storage levelized cost assessment: Lithium-ion vs. combustion turbine." *IEEE* **2015**, 15th International Conference on Environment and Electrical Engineering (EEEIC) 357–362.

[38] IRENA "Renewable Energy Technologies: Cost analysis Series: Biomass for Power Generation" **2012**. www.irena.org/DocumentDownloads/Publications/RE_Technologies_Cost_Analysis-BIOMASS.pdf.

[39] Akdemir, S. “Energy Consumption of an Experimental Cold Storage” *Bulg J Agric Sci* **2012**, *18*(6), 991-996.

[40] Humphrey, J. L.; Keller, G. E. “Separation process technology”. New York: McGraw-Hill, **1997**.

[41] Karlen, D. L.; Birrell, S. J.; Johnson, J. M.; Osborne, S. L.; Schumacher, T. E.; Varvel, G. E.; Ferguson, R. B.; Novak, J. M.; Fredrick, J. R.; Baker, J. M.; Lamb, J. A. "Multilocation corn stover harvest effects on crop yields and nutrient removal." *BioEnergy Research*, **2014**, 7, 528-539.

[42] Agomoh I. V.; Drury, C. F.; Reynolds, W. D.; Woodley, A.; Yang, X.; Phillips, L. A.; Rehmann, L. "Stover harvest and tillage effects on corn seedling emergence." *Agronomy Journal*, **2021**, 113(4), 3688-3696.

[43] Adler, P. R.; Rau, B. M.; Roth, G. W. "Sustainability of corn stover harvest strategies in Pennsylvania." *BioEnergy Research*, **2015**, 8, 1310-1320.

[44] Mann, L.; Tolbert, V.; Cushman, J. "Potential environmental effects of corn (Zea mays L.) stover removal with emphasis on soil organic matter and erosion." *Agriculture, ecosystems & environment*, **2002**, 89(3), 149-166.

[45] Argonne National Laboratory, 2022. The Greenhouse gases, Regulated Emissions, and Energy use in Technologies (GREET) Model

[46] Das, S.; Anderson, J. E.; De Kleine, R.; Wallington, T. J.; Jackson, J. E.; Saffron, C. M. “Comparative life cycle assessment of corn stover conversion by decentralized biomass pyrolysis-electrocatalytic hydrogenation versus ethanol fermentation.” *Sustainable Energy & Fuels*, **2023**.

CHAPTER FOUR: SEARCHING FOR A B. METHANOLICUS MGA3 SHIKIMATE DEHYDROGENASE MUTANT

4.1. Introduction

4.1.1. A Methanol Economy

The most notable bioprocess proposed for the production of bio-methanol involves the gasification of carbonaceous biomass followed by catalytic hydrogenation of the resulting synthesis gas.[1-3] Further, catalytic hydrogenation of carbon dioxide will afford one equivalent of methanol, and research in carbon capture technology has been rapidly growing since 2008.[4,5,39] One particular strain of methylotrophic bacterium has potential to be a production host organism for industrial chemical synthesis in a growing methanol economy. *Bacillus methanolicus* MGA3 is a Gram-positive, thermophilic, endospore-forming, and facultative methylotrophic strain of bacteria (Images taken using confocal microscopy shown in **Fig. 4.1**).[6] Methylotrophic bacteria tend to produce approximately 3.5 times more heat per gram of biomass than typical glucose-metabolizing organisms. Analysis of culturing MGA3 at its optimum growth temperature of 50-

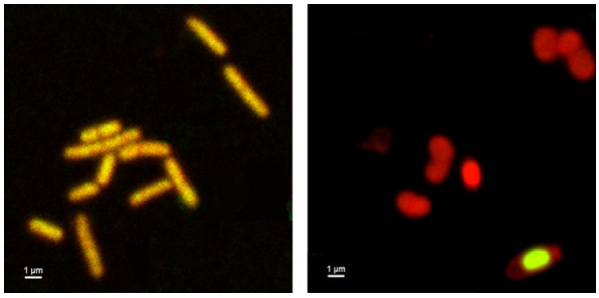

(A) **(B)**

Figure 4.1. Images of gram-stained *B. methanolicus* MGA3 (a) before microbes were placed under sporulating conditions, (b) 26 hours after being under sporulating conditions. Taken using confocal microscopy at the Center for Advanced Microscopy.

55°C in reactor sizes greater than 200 m^3 showed a significant cost-benefit from cooling water reduction in comparison to organisms that grow on glucose at 35°C.[7] Further economic losses are avoided due to a low probability of contamination when running MGA3 fermentations. Microbial contamination during methanol metabolism at elevated temperatures of 50°C is so uncommon that MGA3 has been successfully cultured on seawater-based media (if sea water were successfully implemented in growth media, raw material costs would be reduced further).[7,8] This study examines the possibility of producing 3-dehydroshikimate (DHS) using MGA3 as a host strain.

4.1.2. Strain Construction for DHS Production

The genome of MGA3 encodes all the enzymes required in the shikimate pathway.[9] Deactivation of shikimate dehydrogenase can afford the accumulation of DHS as shown in other DHS producing host strains.[10,40-42] Upon accumulation of this intermediate molecule, *cis*, *cis*-muconic acid (*cc*MA) can be synthesized via heterologous gene expression.[10] First, DHS dehydratase, AroZ, dehydrates DHS to afford protocatechuic acid (PCA). Then, PCA is decarboxylated to catechol by PCA decarboxylase, AroY. Finally, catechol 1,2-dioxygenase acts on catechol to produce *cc*MA. *cc*MA can then be readily hydrogenated in 97% molar yield to adipic acid, a monomer for the synthesis of nylon-6,6 produced in extremely high volume from petroleum.[10] Similar studies have been done in *E. coli* by Frost and coworkers in which 22% molar

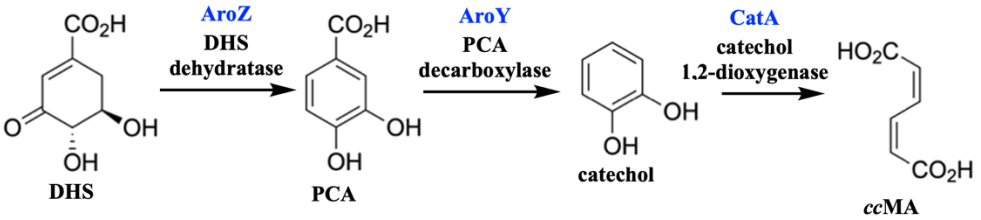

Figure 4.2. Engineering MGA3 for *cc*MA production heterologous expression of DHS dehydratase, PCA decarboxylase, and catechol 1,2-dioxygenase affords ccMA. DHS, 3-dehydroshikimate; PCA, protocatechuic acid; ccMA, *cis*, *cis*-muconic acid.

yields of *cc*MA were achieved using glucose feedstocks.[10-12] **Fig. 4.2** shows what additional reactions would be needed to *cc*MA. Previously, Frost and coworkers bio-catalytically derived vanillin and catechol from *E. coli*, which also required a DHS intermediate.[13, 14]

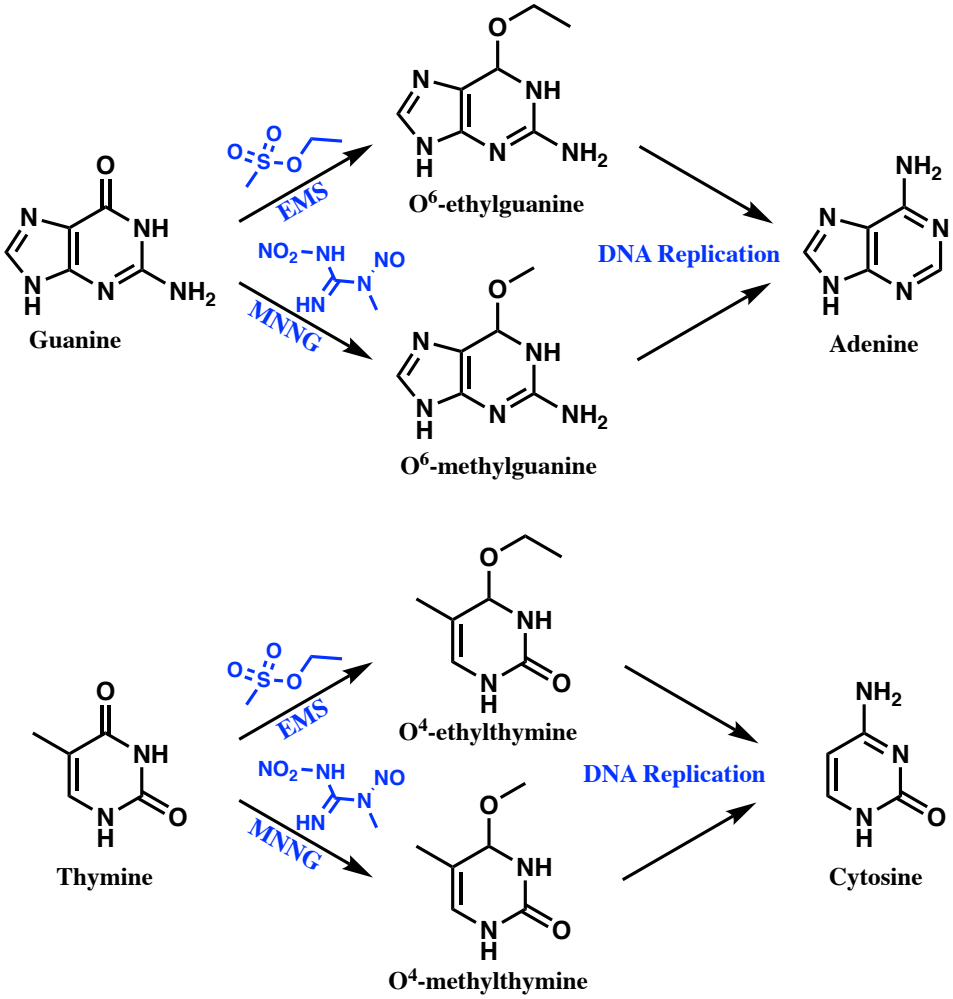

Figure 4.3. Transition mutations facilitating the mutagenesis of purines to purines and pyrimidines to pyrimidines. EMS and MNNG facilitate GC↔AT mutations.

The genetic toolset of MGA3 is limited compared to more commonly used production hosts such as *E. coli*.[15] The only published techniques for creating gene knockouts in MGA3 to date involve classical mutagenesis.[16] Specifically, exposure of MGA3 to mutagens ethyl methanesulfonate (EMS) or *N*-methyl-*N'*-nitro-*N*-nitrosoguanidine (MNNG) facilitates transition

mutations (GC ↔ AT). Both EMS and MNNG work by alkylating the O^6 and the O^4 of guanine and thymine, respectively, as shown in **Fig. 4.3**.[17] Alkylation of these carbonyl groups causes them to be misinterpreted by DNA polymerase as primary amine groups, thus causing guanine to be replaced with adenine and thymine to be replaced by cytosine. Certain "nonsense mutations", which are point mutations that give rise to a premature stop codon, have the potential to render affected genes partially or completely inactivate.[43,44] Chemical mutagenesis was used to knockout shikimate dehydrogenase and force carbon flux, formerly dedicated to the cell's own synthesis of aromatic amino acids and supplements, toward DHS biosynthesis.[17,18]

Techniques that do not completely knockout shikimate dehydrogenase can still provide information about carbon flux into the shikimate pathway. For example, one group achieved gene knockdown using CRISPRi to affect sporulation in *B. methanolicus*.[19] Briefly, CRISPR, or clustered regularly-interspaced short palindromic repeats, are repeating sequences of DNA identified in prokaryotes that tended to encode foreign DNA (viral or phage) that the cell needed to defend itself against.[45-47] CRISPR was coupled with a family of Cas enzymes, which together could create modifications to foreign DNA and ultimately fight infectious particles.[48,49] One particular Cas enzyme is Cas9, which is capable of making targeted double-stranded breaks in DNA. Cas9 is has been used in the genetic recombineering of *E. coli*, but in MGA3 only inactive forms of the enzymes have been identified.[50,51] A deactivated version of Cas9 (dCas9), which is unable to make double-stranded breaks, is guided to its genomic target with the help of *sg*RNA, or single-guide RNA. CRISPRi is shown in **Fig. 4.4** to affect translation of a protein of interest. Interactions between *d*Cas9 and specific targeted sequences of DNA inhibit translation of the genomic target. Additionally, synthetic antisense RNAs (*as*RNAs) have been used in sensor-regulator systems in *E. coli* to direct evolution toward a shikimate dehydrogenase knockdown and

achieve *cc*MA titers of 1.8 g L^{-1}.[20,21] This technique, known as RNA inhibition (RNAi), utilizes RNAs that are antisense to the *m*RNA transcript of interest to target a transcript of interest. The interaction of these *as*RNAs is said to "knock down" the transcription of a targeted *m*RNA (**Fig. 4.4**) Other works have identified transcriptome sequencing has been exploited in *E. coli* to find genes that are transcribed in proportion to levels of DHS within the bacterium.[22] Such transcriptional regulators can be used to develop synthetic biosensors for DHS or generate sensor-regulator systems that could be used for the directed evolution DHS auxotrophs.[21]

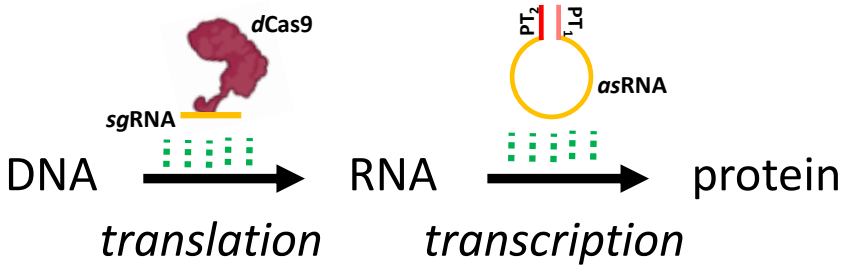

Figure 4.4. Methods for enzyme activity knockdown where CRISPRi would have a targeted effect using its *sg*RNA to guide the *d*Cas9 along the genome, RNAi would affect transcription of the protein using an interaction between *as*RNA and an *m*RNA transcript. Green dashed lines are meant to indicated the down regulation of a translation of transcriptional process.

4.1.3. Biosynthesis in B. methanolicus MGA3

Three methanol assimilating pathways are known: the serine cycle, the ribulose bisphosphate (RuBP) cycle, and the ribulose monophosphate (RuMP) cycle. The core pathway operating in *B. methanolicus* MGA3 is the RuMP pathway shown in **Fig. 4.5**.[23] Three molecules of methanol are consumed to form one molecule of pyruvate, starting with the dehydrogenation of methanol to make formaldehyde. Following the number of carbon atoms in each molecule from methanol assimilation to pyruvate dissimilation helps understand the RuMP cycle. In **Fig. 4.5**, single-carbon molecules are highlighted yellow whereas five-carbon molecules are highlighted in blue. Hexulose phosphate synthase acts on formaldehyde and ribulose-5-P to form the six-carbon molecule

hexulose-6-P. Six-carbon molecules are highlighted green. Pyruvate is subsequently produced via a glyceraldehyde-3-P intermediate and ribulose-5-P is replenished via a xylose-5-P or ribose-5-P intermediate. Pyruvate can be consumed in the TCA cycle. The non-oxidative pentose phosphate pathway (PPP) plays replenishes ribulose-5-P when needed.[24] One interesting aspect of the RuMP in contrast to the serine and RuBP cycles is the presence of E4P within the RuMP cycle. If MGA3 expresses an orthogonal pathway for regenerating E4P used in the RuMP pathway, it could make this particular methylotroph an ideal host for shikimate pathway auxotrophy. To date, such an orthogonal pathway for regenerating E4P in MGA3 has not been identified. However, two separate transketolase isozymes have been characterized in MGA3.[52]

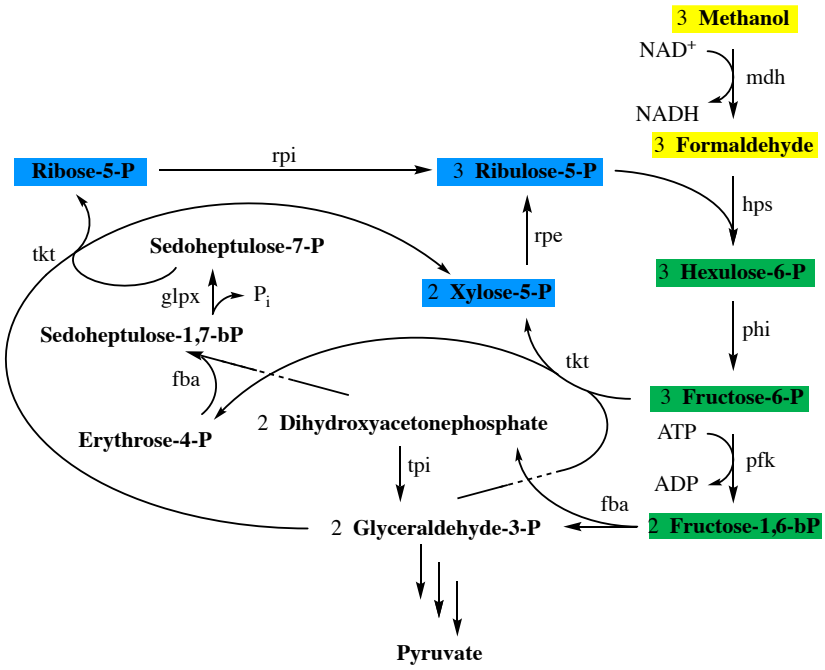

Figure 4.5. Ribulose monophosphate (RuMP) cycle mdh, methanol dehydrogenase; hps, hexulose phosphate synthase; phi, phosphohexulose isomerase; pfk, phosphofructokinase; fba, fructose-bisphosphate aldolase; tkt, transketolase; rpe, ribulosephosphate-3-epimerase; tpi, triosephosphate isomerase; glpx, sedoheptulose-1,7-bisphosphatase; rpi, ribose-5-phosphate isomerase. Single-carbon molecules are highlighted in yellow. Five-carbon molecules are highlighted in blue. Six-carbon molecules are highlighted in green.

Beginning from formaldehyde and ending at pyruvate, the precursor and products to the RuMP cycle of **Fig. 4.5**, the input of one equivalent of NAD^+ and one equivalent of ADP is required, as shown in **Eq. 1**.[25]

$$3HCHO + NAD^+ + ADP + P_i \rightarrow \text{pyruvate} + NADH + ATP \quad \textbf{(4.1)}$$

The serine cycle requires an investment of two molecules of ATP and two molecules of NADH or each equivalent of pyruvate produced. The RuBP cycle requires seven molecules of ATP and one molecule of NAD^+ for every equivalent of pyruvate produced.[25] MGA3 is deserving of the interest it has garnered due to the energetically favorable RuMP pathway it is host to. Chemically mutated MGA3 strains have achieved maximum L-glutamate and L-lysine titers of, 69 g L^{-1} and 65 g L^{-1}, respectively.[26] Cadaverine was produced from an L-lysine intermediate, achieving titers of up to 11.3 g L^{-1}.[27] Finally, methanol-based γ-aminobutyric acid (GABA) production was demonstrated for the first time in MGA3, achieving maximum titers of 9 g L^{-1}.[28]

4.2. Results and Discussion

4.2.1. Methanol Fermentation of MGA3

One of the first experiments performed with MGA3 was to confirm growth independence from exogenously added aromatic amino acids. In a 1.0 L fermentation, all non-aromatic amino acids were supplemented as well as vitamins *D*-biotin and vitamin B12 (vitamins MGA3 cannot grow without).[31] For reasons not yet investigated, aromatic amino acids and vitamins cannot be supplemented to MGA3 without witnessing a severely diminished growth phenotype. Thus, growth in the presence of aromatics was tested by supplementing with yeast extract instead of purified supplements. Methanol was maintained at 150 mM in situ. MVcM minimal medium supplemented with 5 g L^{-1} yeast extract was used as a control reaction containing aromatic amino

acids. Growth in a fermentation containing MVcM minimal medium supplemented with all non-aromatic amino acids supplemented at similar levels to what is found in 5 g L^{-1} yeast extract (1XYEMAA) was used to test the ability for MGA3 to produce its aromatic supplements. Growth was quantified at conditions of 50°C, pH 6.50, and 30% DO. A two-phase cascade control system was used to maintain DO. In phase one, agitation beginning at 400 RPM was ramped up to 1000 RPM and airflow beginning at 0.50 L min^{-1} was ramped up to 1.00 L min^{-1}. In phase two, agitation was further increased to 1800 RPM and aeration was enriched to 60% O_2. Headspace exhausts from the fermenter were passed through a condenser and Drierite and then sent to an infrared optical sensor to quantify CO_2. Fermentations were run until the CO_2 exhaust concentration dropped considerably. Dry cell weight (DCW) was calculated from optical density using a 0.4 g DCW conversion factor. More experimental details regarding methanol fermentation are provided in the experimental section. Biomass titers in both fermentations reached between 35-37 g DCW L^{-1} (**Fig. 4.6**). Growth without aromatic supplementation achieved a growth rate of 0.51 h^{-1} while growth with yeast extract achieved a growth rate of 0.52 h^{-1}. In fed-batch fermentations, MGA3 has been cited to achieve growth rates around 0.49 h^{-1}.[31] Diminished growth in the presence of commercially bought aromatic amino acids L-tryptophan, L-phenylalanine, and L-tyrosine was not only a barrier during fermentation experiments but also during mutagenesis and mutant screening. Nonetheless, similar biomass yields and specific growth rates were demonstrated with and without supplements that exist in yeast extract, which include aromatic amino acids and vitamins.

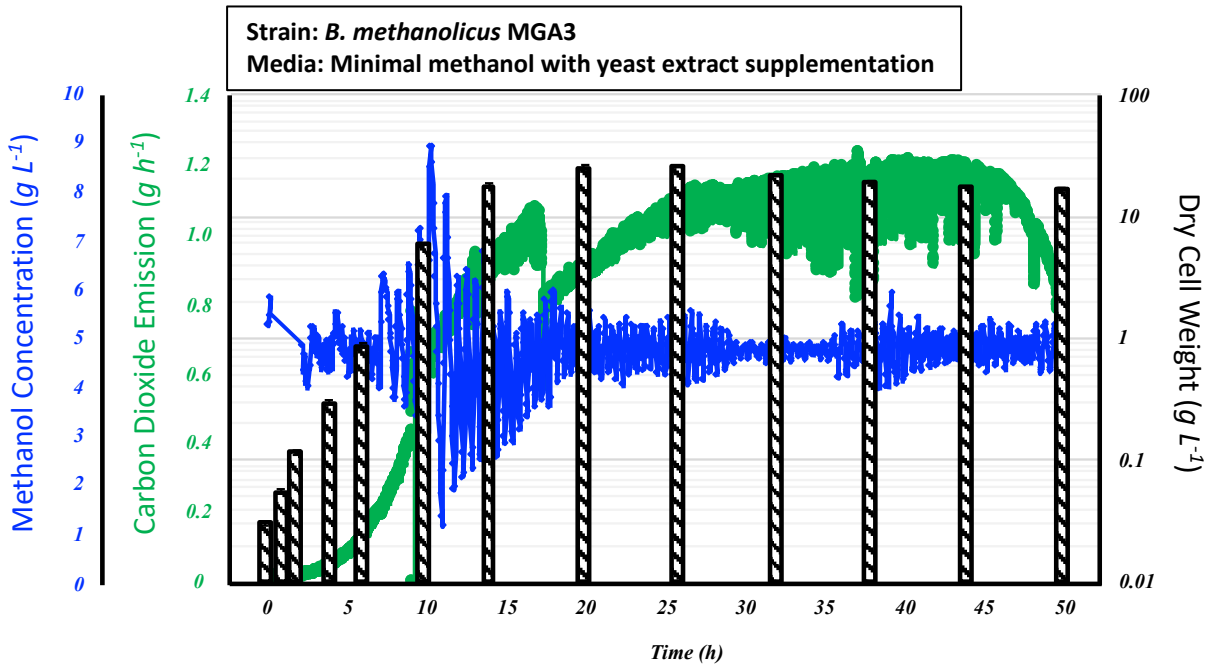

(a)

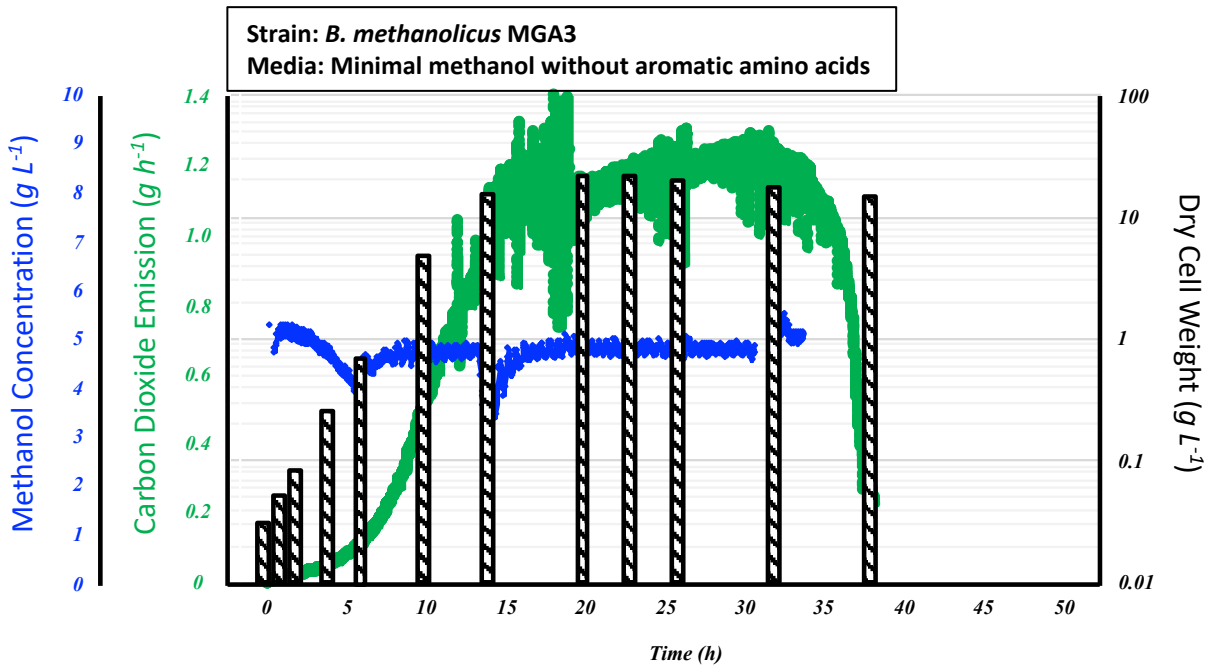

(b)

Figure 4.6. MGA3 fermentation experiments fed-batch fermentation of MGA3 **(a)** run in MVcM buffer with yeast extract supplementation (5 g L^{-1}) **(b)** run in MVcM buffer without aromatic amino acids. Non-aromatic amino acids in same amount and proportion as found in yeast extract were supplemented.

4.2.2. Attempt to Isolate Shikimate Dehydrogenase Knockout in MGA3

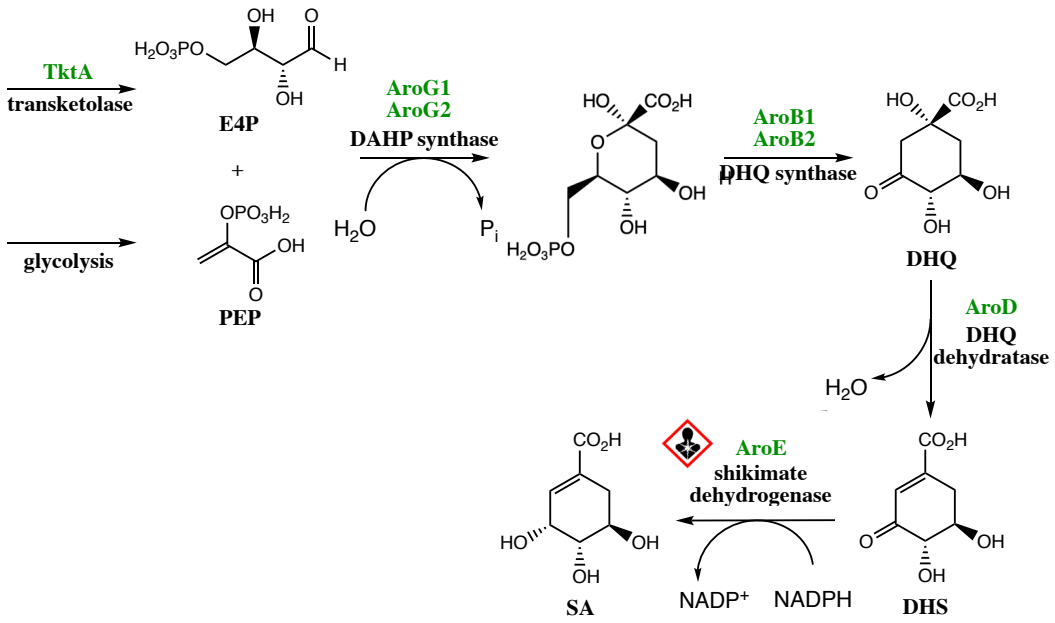

Figure 4.7. Mutagenesis in MGA3 shikimate pathway PEP, phosphoenolpyruvate; E4P, D-erythrose 4-phosphate; DHS, 3-dehydroshikimate; SA, shikimic acid; AroF, tyrosine-sensitive 3-deoxy-D-arabino-heptulosonate 7-phosphate (DAHP) synthase; AroF, phenylalanine-sensitive DAHP synthase; AroH, tryptophan-sensitive DAHP synthase; AroB, 3-dehydroquinate (DHQ) synthase; AroD, DHQ dehydratase; AroE, shikimate dehydrogenase; AroL and AroK, shikimate kinase. Enzymes are highlighted green to signify they are different than those of the previously outlined shikimate pathway for *E. coli*.

A growth phenotype in *B. methanolicus* MGA3 that could not grow in the absence of aromatic amino acids or supplementation of other metabolic intermediates from the shikimate pathway (**Fig. 4.7**) was sought after (a DHS producer, however, would be of particular interest). Genome sequencing of *B. methanolicus* MGA3 previously revealed genetic information encoding shikimate pathway isozymes similar to that found in *E. coli*.[9] However, MGA3 has only two isozymes of DAHP synthase, AroG1 and AroG2, and two isozymes of DHQ synthase, AroB1 and AroB2. For the sake of example, should AroD activity be eliminated using chemical mutagenesis, the growth of this new strain of MGA3 would depend on exogenous DHS, SA, or some downstream aromatic supplementation of metabolites from the common pathway for aromatic

amino acid biosynthesis. Thus, if a mutant MGA3 were able to grow with supplementation of SA but not without, it could indicate a deleterious mutation in one of the genes preceding the formation of SA. An implicit assumption of this procedure is that MGA3 has the ability to transport SA from external media into the cell. Throughout these procedures assume MGA3 cells are cultured at 50°C with 200 RPM agitation unless otherwise noted. In the first procedure, cells underwent one round of chemical mutagen exposure, were sporulated, were washed, then were screened for shikimate pathway auxotrophy. A 40 mL culture containing MVcM supplemented with 200 mM methanol and 5 g L^{-1} yeast extract was grown to late log phase in a six-baffled, 250 mL Erlenmeyer flask. 2.5 mL of the same culture media supplemented with either EMS or MNNG was combined with 2.5 mL of culture. Mutagen exposure was allowed for up to 20 min in a four-baffled, 50 mL Erlenmeyer flask. For recovery, chemical mutants were subsequently diluted 50-fold to 100 mL in a six-baffled, 500 mL Erlenmeyer flask. After 6 h, 1.5 mg $MnCl_2 \cdot 4H_2O$, 0.1 g $MgCl_2 \cdot 6H_2O$, and 0.08 g $CaCl_2$ were added, and culturing continued at 37°C to induce sporulation. After 48 h of shaking, spores were pelleted at 12,000×g, washed twice with sterile water, and stored at 4°C. It was found that the viability of stored mutant spores would diminish after two weeks. Mutants were screened on the first set of selective media described previously. Minimal media containing 5 g L^{-1} was used as a control plate containing aromatic amino acids, and minimal media lacking aromatic vitamins and containing YEMAA supplementation rather than yeast extract was used as a selective plate. Lack of growth on the selective plate but growth on the control plate would indicate auxotrophy for the shikimate pathway.

A so-called "kill curve" was used to determine cell viability exposure times to and concentrations of EMS (**Table 4.1**). Cells were grown to late log phase in media with aromatic supplementation in the form of either 5 g L^{-1} yeast extract or 80 mg L^{-1} SA. 2.5 mL of the same

Table 4.1. Kill curve for mutagenesis of MGA3 MGA3 exposure to varying levels of EMS.

	Concentration (*v/v* % EMS)			
Time (min)	*0*	*1*	*3*	*5*
10	-	150 %	-	-
15	-	67 %	-	-
20	100 %	49 %	0 %	0 %

culture media supplemented with either EMS or MNNG was combined with 2.5 mL of the cell culture. A control experiment was conducted where 2.5 mL of fresh culture with no mutagen was combined with 2.5 mL of the same cell culture. Following mutagenesis, dilutions of the mutants were plated onto SOB solid media. Dilutions of the control culture were similarly plated out. The following day, plates that had distinguishable CFU were tallied.

$$\mathrm{SR}_{C,t} = 100\% \cdot \frac{CFU_M}{CFU_C} \cdot \frac{D_M}{D_C} \qquad \textbf{(6.1)}$$

Eq. 6.1 shows how survival rate, SR, for a given mutagen concentration, C, and exposure time, t. CFU_M is the number of CFU formed on a given plate of mutants. D_M is the dilution factor for that plate. CFU_C is the number of CFU formed on a plate of non-mutants. D_C is the dilution factor for that plate. A working concentration of 1 % (v/v) with an exposure time of 20 min was used during mutagenesis, which was found to have a 49% survival rate. A total of 5,434 mutant spores were examined which were exposed to a single round of exposure to mutagen. Of these 5,434 mutants, 48 mutants showed a growth dependence on yeast extract during the screening. These 48 mutants were re-screened using the same screening protocol. During the second screen, 47 of the 48 candidates were found to be false positives. The single mutant that passed the second screen was

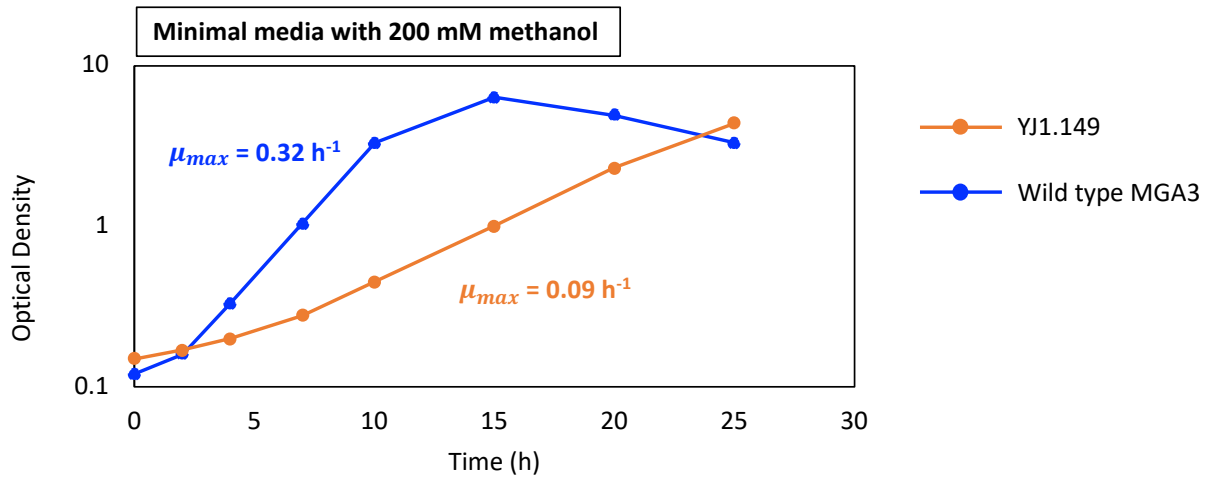

Figure 4.8. YJ1.149 vs. MGA3 growth of YJ1.149 (orange) compared to growth of wild-type MGA3 (blue) on minimal media containing 200 mM methanol.

named YJ1.149 and stored at -80°C. Growth of YJ1.149 was subsequently compared to the growth of wild-type MGA3 in liquid minimal MVcM minimal media containing 200 mM methanol, minimal media containing 200 mM methanol and 1X YEMAA supplements, and minimal media containing 200 mM methanol and 5 g L^{-1} yeast extract (**Fig. 4.8** – **Fig. 4.10**).

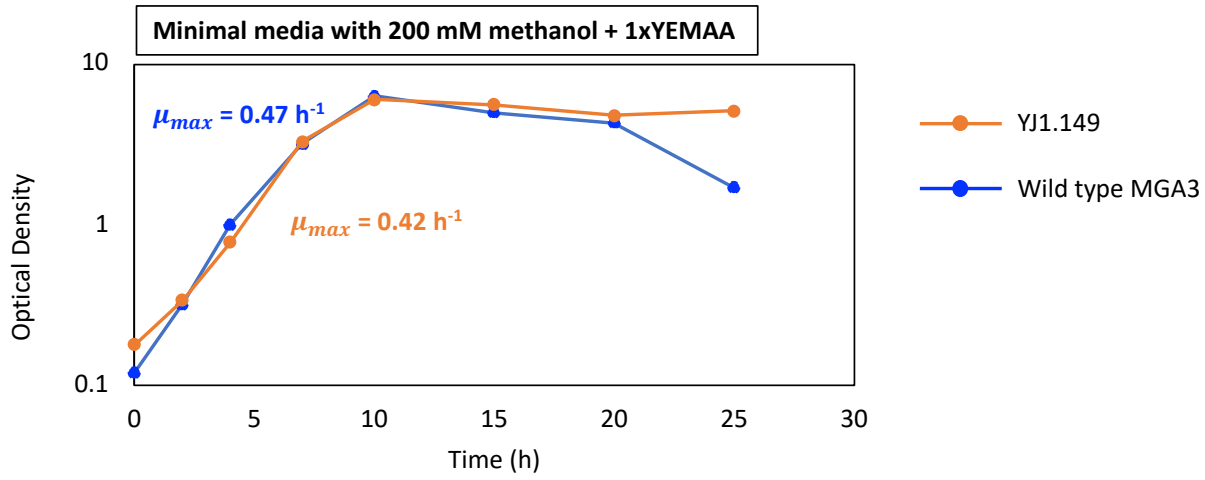

Figure 4.9. YJ1.149 vs. MGA3 with 1X YEMAA growth of YJ1.149 (orange) compared to growth of wild-type MGA3 (blue) on minimal media containing 200 mM methanol and 1X YEMAA.

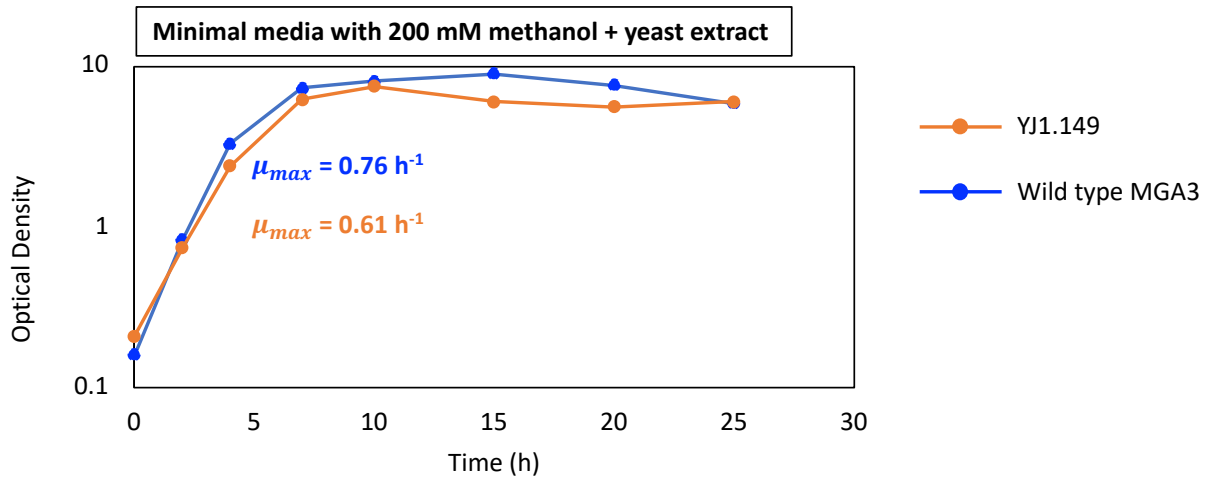

Figure 4.10. YJ1.149 vs MGA3 with yeast extract growth of YJ1.149 (orange) compared to growth of wild-type MGA3 (blue) on minimal media containing 200 mM methanol and 5 g L^{-1} yeast extract.

Ultimately, when grown on liquid media, YJ1.149 was capable of growing in the absence of aromatic supplementation on methanol. However, a diminished growth rate was witnessed, so the strain's physiological properties were investigated further. For growth on MVcM supplemented with 200 mM methanol, YJ1.149 had diminished growth with a μ_{max} of 0.09 h^{-1} whereas wild-type MGA3 had a μ_{max} of 0.32 h^{-1}. The deficit of YJ1.149 in growth was remedied when 1X YEMAA supplementation was introduced to the media. For growth on MVcM supplemented with 200 mM methanol and 1X YEMAA, YJ1.149 had a μ_{max} of 0.42 h^{-1} whereas wild-type MGA3 had a μ_{max} of 0.47 h^{-1}. The fact that YJ1.149 recovered its specific growth rate after supplementation of non-aromatic amino acids signified the strain likely wasn't exhibiting any form of shikimate pathway auxotrophy or gene silencing. For growth on MVcM supplemented with 5 g L^{-1} yeast extract, YJ1.149 had a μ_{max} of 0.61 h^{-1} whereas wild-type MGA3 had a μ_{max} of 0.76 h^{-1}. The data show that although growth was not observed in YJ1.149 without aromatic supplementation on solid media, a difference in physiological properties was observed in a system that was not oxygen mass transfer-limited. In liquid media, it is possible to add agitation with baffled flasks, which greatly enhances dissolved oxygen levels and cellular growth rate. MGA3 is

Table 4.2. Kill curve for mutagenesis of YJ1.149 YJ1.149 exposure to varying levels of EMS.

	Concentration (*v/v* % EMS)		
Time (min)	*0*	*0.8*	*1.0*
10	-	29 %	7.3 %
20	100 %	13 %	1.8 %

a highly aerobic methylotroph that does not grow well in oxygen-limited systems, which increases the likelihood of identifying false positive phenotypes when screening on solid media.[6,15] Nonetheless, YJ1.149 was selected as a candidate for further mutagenesis experiments.

It was hypothesized that if MGA3 was continuously exposed to mutagen while SA was exogenously present in the media, *aroE* could become a non-essential gene for the mutant. An assumption must be made here, however, that MGA3 is capable of transporting SA from the external media to its intracellular environment. The organism might eventually demonstrate a growth dependence on SA that has been supplemented to the media over several generations of growth. Such a growth phenotype may also begin to accumulate DHS in the cell. While strains with mutations in essential genes would either grow more slowly or not at all, strains with mutations in non-essential genes would continue growing. Phenotypic screening in between consecutive rounds of mutagenesis is essentially for finding an *aroE* knockout or knockdown mutant before the strain's specific growth rate becomes unusably low. Cells underwent multiple rounds of chemical mutagen exposure. After each round of exposure to chemical mutagen cultures were diluted and immediately plated onto rich media. Colonies were gridded and screened for auxotrophy. If auxotrophy for shikimate pathway supplementation was not observed, colonies with

less growth on selective media than on control media were selected and re-exposed to mutagen (and the aforementioned procedure was repeated).

Table 4.2 shows the kill curve for mutagenesis using EMS on YJ1.149. It can be seen that the survival rates of YJ1.149 even at lower concentrations of EMS are lower than the survival rates of MGA3. YJ1.149 underwent four additional rounds of mutagenesis in the presence of 80 mg L^{-1} SA. Strains YJ1.150, YJ1.151E, YJ1.152, YJ1.153, and YJ1.154B underwent a total of two, three, four, five, and six rounds of mutagenesis, respectively. With each round of mutagenesis, hundreds of mutants were screened on minimal solid media for growth dependence on SA. The colonies with the lowest growth rate on media lacking SA supplementation compared to media containing SA supplementation were chosen for further rounds of mutagenesis. All candidates were also grown up and stored at -80℃. The growth of YJ1.150 and YJ1.154B were compared to the growth of MGA3 in liquid media with and without SA supplementation (**Fig 4.11**). The results of the growth experiments continued to show a lack of growth dependence on SA when examined in liquid media where oxygen mass transfer was not limiting. YJ1.154B inexplicably showed lower growth rates in the presence of SA compared to when SA was missing in the media. Ultimately, MGA3 is a highly oxygen-demanding organism and phenotypic screening of the strain on solid media was highly erroneous. All strains selected during chemical mutagenesis and screening

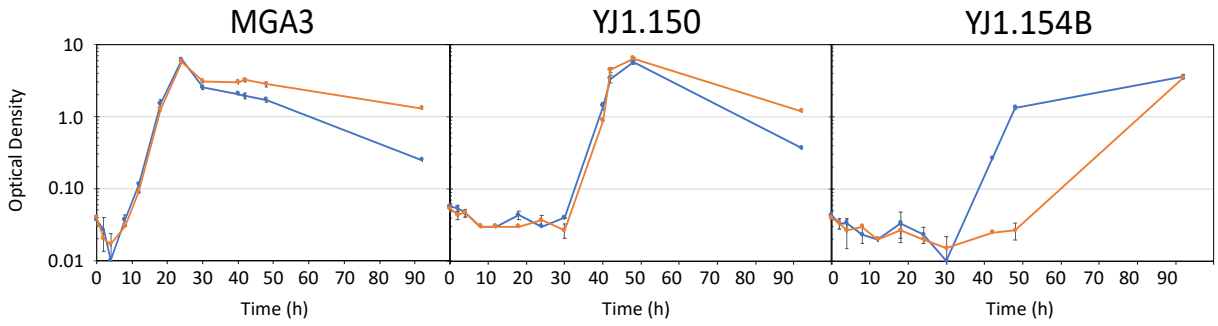

Figure 4.11. Growth of MGA3, YJ1.150, and YJ1.154B growth on MVcM media containing 200 mM methanol and MVcM containing 200 mM methanol and 80 mg L^{-1} SA.

experiments for a positive phenotype were shown to be false-positive phenotypes upon further examination.

4.2.3. Attempt to Isolate Shikimate Dehydrogenase Knockdown in MGA3

Two methods for gene knockdown of *aroE* were examined: RNAi and CRISPRi. During RNAi, plasmids were designed to express synthetic stem-loop-structured *as*RNA molecules regulated by the methanol-inducible promoter, P_{mdh}. The stem-loop structure transcribed during RNAi is illustrated in **Fig. 4.12**. The stem segment of the structure is two reverse-complimentary strands of RNA with high guanine and cytosine (GC) content containing higher hydrogen bonding energy than adenine and thymine hydrogen bonding. Thus, the paired termini are bound together strongly to avoid translation of the RNA in the stem-loop structure into protein or degradation of the transcript. The loop segment encodes RNA that is antisense to transcripts of *aroE* thereby inhibiting translation of the gene to protein. The cloning vector used was pTH1mp.[34] The plasmid pTH1mp_null was an intermediate plasmid that would synthesize paired-termini *m*RNAs with no targeting *as*RNA. Gibson assembly details for inserting paired termini encoding DNA into pTH1mp in order to generate pTH1mp_null are provided in the experimental section. The plasmid pTH1mp_*as*aroE1B synthesized *as*RNA antisense to the center of the shikimate dehydrogenase

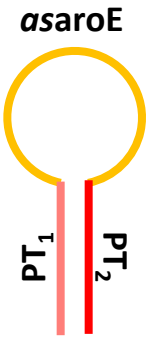

Figure 4.12. Stem-loop structure antisense and paired-termini components of *as*RNA structure.

gene. The plasmid pTH1mp_*as*aroE3C, on the other hand, targets the start codon and ribosome binding site (RBS) of shikimate dehydrogenase. Gibson assembly details for insertion of the antisense encoding regions of plasmids pTH1mp_*as*aroE1B and pTH1mp_*as*aroE3C into pTH1mp_null are provided in the experimental section as well as sequencing data for these two antisense regions. Plasmid pTH1mp_null was used as a control vector throughout these experiments.Each plasmid was transformed separately into wild-type MGA3 and transformants were grown in two types of media: the first was MVcM media containing 50 mM mannitol to test growth when the promotor region, P_{mdh}, controlling *as*RNA transcription was turned off (a second type of control). The second was MVcM media containing 200 mM methanol to test growth when the promotor region, P_{mdh}, controlling *as*RNA transcription was turned on. Promoter P_{mdh} is induced when methanol is introduced to the media. In case the knockdown strategies were successful and the cell needed exogenously added SA to be more viable, SA was supplemented to all media. Chloramphenicol was also supplemented in all media for plasmid maintenance. Samples were cold-quenched as they were collected at each timepoint for 48 hours then mixed with a 40:40:20 (*v*/*v*) mixture of acetonitrile:methanol:0.1 M formic acid to lyse the cells and sample their intracellular environment as well as the extracellular environment. This method of cold-quenching and sampling for whole-broth analysis was previously reported by Carnicer et al and used in this study.[16] Cold-quenching of shake flask samples affords a so-called "snapshot" of the intracellular metabolome so no metabolites are degraded during the sampling process. Further details are provided in the experimental section. HPLC analysis of the whole broth samples detected no peaks at the elution time for DHS. **Fig. A.6.5** is an HPLC calibration curve for DHS at varying concentrations of DHS with their respective integrations. A typical HPLC chromatogram containing DHS is shown in **Fig. A.6.6**. Cellular growth data during the shake flask experiments

are shown in **Fig. 4.13**. When grown on methanol, MGA3/pTH1mp_null (blue), MGA3/pTH1mp_*as*aroE1B (orange), and MGA3/pTH1mp_*as*aroE3C (green) had μ_{max} values of 0.29 h^{-1}, 0.45 h^{-1}, and 0.16 h^{-1}, respectively. When grown on mannitol, MGA3/pTH1mp_null (light blue), MGA3/pTH1mp_*as*aroE1B (light orange), and MGA3/pTH1mp_*as*aroE3C (light green) had μ_{max} values of 0.32 h^{-1}, 0.31 h^{-1}, and 0.29 h^{-1}, respectively.

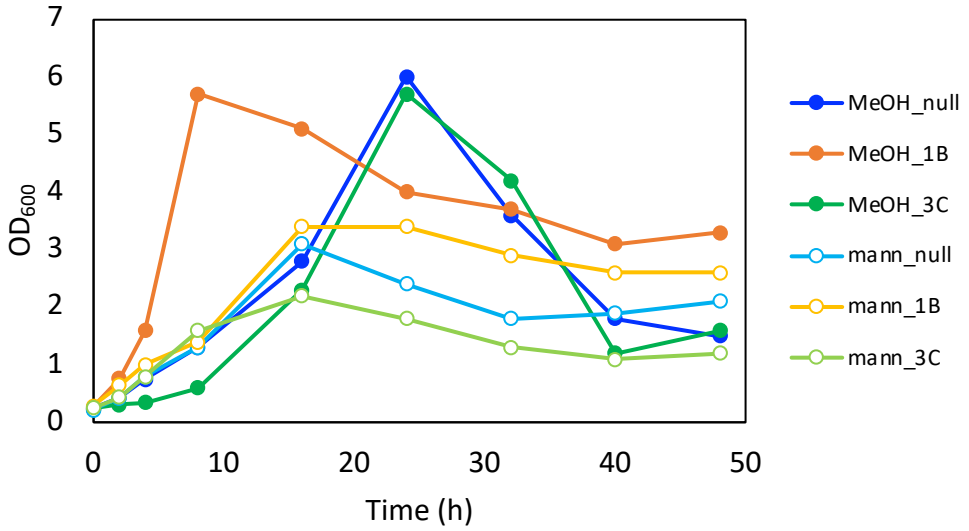

Figure 4.13. Growth curves for MGA3 carrying RNAi plasmids MGA3/pTH1mp_null, MGA3/pTH1mp_asaroE1B, and MGA3/pTH1mp_asaroE3C were tested for growth in MVcM media supplemented with 80 mg L^{-1} SA and either 200 mM methanol or 50 mM mannitol.

A second method for knocking down *aroE* was investigated known as CRISPRi. Plasmids designed for CRISPRi expressed Cas9 protein that was inactive. However, the gene-targeting *sg*RNA also encoded by these plasmids still guides the dead enzyme, or *d*Cas9, to the gene of interest. The enzyme still interacts with regions of chromosomal DNA with specificity and inhibits ribosomal transcription, but does not create double-stranded breaks in the DNA. The piCas plasmid was used as the cloning vector for CRISPRi and also as a control vector during shake flask experiments.[19] Transcription of *d*Cas9 and gene-targeting *sg*RNA are activated by mannitol-inducible promoters P_{m2p}.[34] One *aroE*-targeting piCas plasmid was generated known as

piCas_aroEsgRNA1 with *sg*RNA targeting the center of the *aroE* gene following a PAM sequence as outlined by Schultenkämper et al.[19] Cloning and construction of piCas_aroEsgRNA1 is described further in the experimental section. Transformations were performed to generate MGA3/piCas and MGA3/piCas_aroEsgRNA1 strains, and their growth phenotypes were compared in minimal MVcM media containing 200 mM methanol, 12.5 mM mannitol for induction, and 80 mg L^{-1} SA. Whole broth samples were collected at each time point as described previously and no traces of DHS were detected using HPLC analytics. Cellular growth patterns and titers of mannitol and SA detected using HPLC are plotted in **Fig. 4.14**. The maximum cellular growth rate of MGA3/piCas_aroEsgRNA1, μ_{max} equal to 0.35 h^{-1}, was lower than that of MGA3/piCas, μ_{max} equal to 0.49 h^{-1}. The diminished growth rate of MGA3/piCas_aroEsgRNA1 upon activation of its CRISPRi system could be indicative of some interaction between *d*Cas9 and *aroE*, which could burden cellular metabolism. However, no detectable levels of DHS were ever observed in the whole broth lysates.

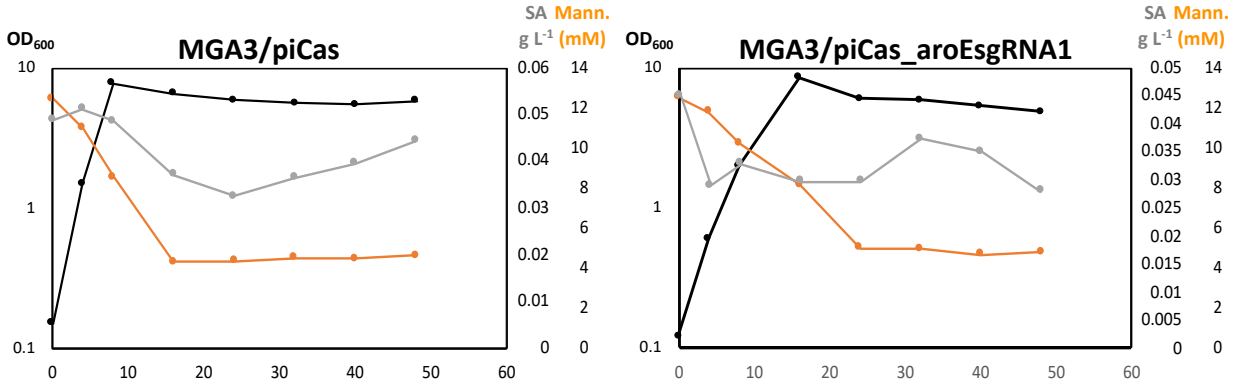

Figure 4.14. Growth curves for MGA3 carrying synthetic CRISPRi plasmids optical density (black), SA titer (grey), and mannitol titer (orange) plotted over time for MGA/piCas and MGA3/piCas_aroEsgRNA1 grown in minimal media containing 200 mM methanol and chloramphenicol supplementation.

4.3. Summary & Future Work

The shikimate pathway precursor to SA, DHS, is an intermediate for producing a plethora of valuable compounds including catechol, vanillin, and adipic acid. Data presented encompass an effort to add to the "methanol economy", utilizing methanol for DHS biosynthesis. *Bacillus methanolicus* MGA3 was exposed to up to six rounds of chemical mutagenesis for obtaining a knockout or knockdown of *aroE*. Chemical mutagenesis strategies failed due to the lack of an effective screening method. Most mutants in this study were screened using selective agar plates where oxygen mass transfer is limited for a highly aerobic organism like MGA3. Interpreting growth signals in such a substrate-limited environment created erroneous readings and many "false positive" results. Strategies for knocking down *aroE* using RNAi and CRISPRi were also employed. The growth of MGA3 strains carrying RNAi and CRISPRi plasmids was tested in liquid media. Samples were cold-quenched and lysed with a chemical mixture of acetonitrile:methanol:0.1 M formic acid (40:40:20 *v*/*v*) to test the intracellular and extracellular environments. No DHS was detected during RNAi and CRISPRi shake flask studies although reduced growth rates were observed in strains expressing *as*RNA and *d*Cas9.

REFERENCES

[1] Zhang, Y.; Xiao, J.; Shen, L. "Simulation of Methanol Production from Biomass Gasification in Interconnected Fluidized Beds" *Ind. Eng. Chem. Res.* **2009**, *48*, 5351-5359.

[2] Holmgren, K. M.; Berntsson, T.; Andersson, E.; Rydberg, T. "System aspects of biomass gasification with methanol synthesis – Process concepts and energy analysis" *Energy* **2012**, *45*, 817-828.

[3] de Fournas, N.; Wei, M. "Techno-economic assessment of renewable methanol from biomass gasification and PEM electrolysis for decarbonization of the maritime sector in California" *Energy Conversion and Management* **2022**, *257*, 115440.

[4] Yang, R.; Fu, Y.; Zhang, Y.; Tsubaki, N. "In situ DRIFT study of low-temperature methanol synthesis mechanism on Cu/ZnO catalysts from CO_2-containing syngas using ethanol promoter" *Journal of Catalysis* **2004**, *228*, 23-35.

[5] Bae, J. W.; Kasipandi, S. "Recent Advances in Direct Synthesis of Value-Added Aromatic Chemicals from Syngas by Cascade Reactions over Bifunctional Catalysts" *Advanced Materials* **2019**, *31*, 1803390.

[6] Brautaset, T.; Jakobsen, Ø. M.; Josefsen, K. D.; Flickinger, M. C.; Ellingsen, T. E. "*Bacillus methanolicus*: a candidate for industrial production of amino acids from methanol at 50°C" *Appl. Microbiol. Biotechnol.* **2007**, *74*, 22-34.

[7] Komives, C. F.; Cheung, L. Y.-Y.; Pluschkell, S. B.; Flickinger, M. C. "Growth of Bacillus methanolicus in Seawater-Based Media" **2005**, *J. Ind. Microbiol. Biotechnol.*, *32*(2), 61–66.

[8] Sant'Ana, A. S.; Brexó, R. P. "Impact and significance of microbial contamination during fermentation for bioethanol production" **2017**, *Renewable and Sustainable Energy Reviews*, *73*, 423–434.

[9] Brautaset, T.; Heggeset, T. M. B.; Krog, A.; Balzer, S.; Wentzel, A.; Ellingsen, T. E. "Genome Sequence of Thermotolerant *Bacillus methanolicus:* Features and Regulations Related to Methylotrophy and Production of L-Lysine and L-Glutamate from Methanol" **2012**, *Applied and Environmental Microbiology*, *78*(15), 5170-5181.

[10] Niu, W.; Draths, K. M.; Frost, J. W. "Benzene-Free Synthesis of Adipic Acid" *Biotechnol. Prog.* **2002**, *18*(2), 201–211.

[11] Skoog, E.; Shin, J. H.; Saez-Jimenez, V.; Mapelli, V.; Olsson, L. Biobased Adipic Acid - The Challenge of Developing the Production Host. Biotechnol. Adv. **2018**, *36*(8), 2248–2263.

[12] Deng, Y.; Ma, L.; Mao, Y. Biological Production of Adipic Acid from Renewable Substrates: Current and Future Methods. Biochem. Eng. J. **2016**, *105*, 16–26.

[13] Li, K.; Frost, J. W. "Synthesis of Vanillin from Glucose" *J. Am. Chem. Soc.* **1998,** *120,* 10545-10546.

[14] Draths, K. M.; Frost, J. W. "Environmentally Compatible Synthesis of Catechol from *D*-Glucose" J. Am. Chem. Soc., **1995**, *117*, 2395-2400.

[15] Pfeifenschneider, J.; Brautaset, T.; Wendisch, V. F. Methanol as Carbon Substrate in the Bio-Economy: Metabolic Engineering of Aerobic Methylotrophic Bacteria for Production of Value-Added Chemicals: Methanol as Carbon Substrate in the Bio-Economy. Biofuels Bioprod. Biorefin. **2017**, *11*(4), 719–731.

[16] Schendel, F. J.; Bremmon, C. E.; Flickinger, M. C.; Guettler, M.; Hanson, R. S. "L-Lysine Production at 50 Degrees C by Mutants of a Newly Isolated and Characterized Methylotrophic Bacillus sp." Appl. Environ. Microbiol. **1990**, *56*(4), 963–970.

[17] Shah, D.; Kamili, A. N.; Wani, A. A.; Nazir, N.; Sajad, N.; Khan, I.; Parray, J. A.; Shah, S. "Mutagenic Action of Ethyl Methanesulphonate (EMS): A Review" *Journal of Research & Development* **2016**, *16*, 63-68.

[18] Nestmann, E. R. "Mutagenesis by nitrosoguanidine, ethyl methanesulfonate, and mutator gene *mutH* in continuous cultures of *Escherichia coli**" *Mutation Research* **1975**, *28*, 323-330.

[19] Schultenkämper, K.; Brito, L. F.; López, M. G.; Brautaset, T.; Wendisch, V. F. "Establishment and Application of CRISPR Interference to Affect Sporulation, Hydrogen Peroxide Detoxification, and Mannitol Catabolism in the Methylotrophic Thermophile Bacillus methanolicus." Appl. Microbiol. Biotechnol. **2019**, *103*(14), 5879–5889.

[20] Kolev, N. G.; Atayde, V. D.; Ullu, E. "A single-cloning-step procedure for the generation of RNAi plasmids producing long stem-loop RNA" Molecular & Biochemical Parasitology 184 **2012**, 55–58.

[21] Yang, Y.; Lin, Y.; Wang, J.; Wu, Y.; Zhang, R.; Cheng, M.; Shen, X.; Wang, J.; Chen, Z.; Li, C.; Yuan, Q.; Yan, Y. "Sensor-regulator and RNAi based bifunctional dynamic control network for engineered microbial synthesis" *Nature Comm.* **2018**, 9, 3043.

[22] Wang, Q.; Li, L.; Tu, R.; Song, G.; Cheng, J. Chen, W.; Li, L.; Wang, L. "Development of a Synthetic 3-Dehydroshikimate Biosensor in *Escherichia coli* for Metabolite Monitoring and Genetic Screening" *ACS Synth. Biol.* **2019**, *8*, 297–306.

[23] Vorholt, J. A.; Müller, J. E. N.; Meyer, F.; Litsanov, B.; Kiefer, P. "Core pathways operating during methylotrophy of *Bacillus methanolicus* MGA3 and induction of a bacillithiol-dependent detoxification pathway upon formaldehyde stress" *Molecular Microbiology* **2015**, *98*(6), 1089–1100.

[24] Delépine, B.; López, M. G.; Carnicer, M.; Vicente, C. M.; Wendisch, V. F.; Heux, S. "Charting the metabolic landscape of the facultative methylotroph *Bacillus methanolicus*" *mSystems* **2020**, *5*(5), (e00745-20).

[25] Whitaker, W. B.; Sandoval, N. R.; Bennett, R. K.; Fast, A. G.; Papoutsakis, E. T. "Synthetic Methylotrophy: Engineering the Production of Biofuels and Chemicals Based on the Biology of Aerobic Methanol Utilization" *Curr. Opin. Biotechnol.* **2015**, *33*, 165–175.

[26] Brautaset, T.; Nærdal, I.; Netzer, R.; Irla, M.; Krog, A.; Heggeset, T. M. B.; Wendisch, V. F. "L-lysine production by *Bacillus methanolicus*: Genome-based mutational analysis and L-lysine secretion engineering" *Journal of Biotechnology*. **2017**, 244, 25-33.

[27] Wendisch, V. F.; Nærdal, I.; Pfeifenschneider, J.; Brautaset, T. "Methanol-based cadaverine production by genetically engineered *Bacillus methanolicus* strains" *Microbial Biotechnology,* **2015**, *8*, 342–350.

[28] Wendisch, V. F.; Irla, M.; Nærdal, I.; Brautaset, T. "Methanol-based γ-aminobutyric acid (GABA) production by genetically engineered Bacillus methanolicus strains" Industrial Crops and Products **2017**, *106*, 12–20.

[29] Brautaset T., Williams M. D., Dillingham R. D., Kaufmann C., Bennaars A., Crabbe E., et al. "Role of the *Bacillus methanolicus* citrate synthase II gene, *citY*, in regulating the secretion of glutamate in L-Lysine-Secreting mutants" *Appl. Environ. Microbiol.* **2003**, 69 3986–3995. 10.1128/AEM.69.7.3986-3995.2003

[30] Kopec, D. "Control of Critical Process Parameters Using In-Situ Analytics" *Bioprocess International*, **2017**, *15*, 11.

[31] Jakobsen, Ø. M.; Brautaset, T.; Degnes, K. F.; Heggeset, T. M. B.; Balzer, S.; Flickinger, M. C.; Valla, S.; Ellingsen, T. E. "Overexpression of Wild-Type Aspartokinase Increases L-Lysine Production in the Thermotolerant Methylotrophic Bacterium *Bacillus methanolicus*" *Applied and Environmental Microbiology* **2009**, *75*(3), 652-661.

[32] Schendel, F. J.; Bremmon, C. E.; Flickinger, M. C.; Guettler, M.; Hanson, R. S. "L-Lysine Production at 50°C by Mutants of a Newly Isolated and Characterized Methylotrophic *Bacillus sp*." **1990**, *Applied and Environmental Microbiology*, *56*(4), 963-970.

[33] Gibson, D. G. "Enzymatic Assembly of Overlapping DNA Fragments" *Methods in Enzymology* **2011**, *498*, 349-361.

[34] Irla, M.; Heggeset, T. M.; Nærdal, I.; Paul, L.; Haugen, T.; Le, S. B.; Brautaset, T.; Wendisch, V. F. "Genome-Based Genetic Tool Development for Bacillus methanolicus: Theta- and Rolling Circle-Replicating Plasmids for Inducible Gene Expression and Application to Methanol-Based Cadaverine Production" *Front. Microbiol.* **2016**, *7*, 1481.

[35] Gibson, D. G. "Enzyme Assembly of Overlapping DNA Fragments" *Methods in Enzymology*, Chapter 15 **2011**, *498*, 349-361.

[36] *RNAfold Web Server*, Institute for Theoretical Chemistry, University of Vienna. http://rna.tbi.univie.ac.at/cgi-bin/RNAWebSuite/RNAfold.cgi

[37] Jakobsen, Ø. M., Benichou, A., Flickinger, M. C., Valla, S., Ellingsen, T. E., Brautaset, T. "Upregulated transcription of plasmid and chromosomal ribulose monophosphate pathway genes is critical for methanol assimilation rate and methanol tolerance in the methylotrophic bacterium *Bacillus methanolicus*" *J. Bacteriol*. **2006**, *188*, 3063–3072.

[38] Carnicer, M.; Vieira, G.; Brautaset, T.; Portais, J. C.; Heux, S. "Quantitative metabolomics of the thermophilic methylotroph *Bacillus methanolicus*" *Microb Cel Fact* **2016**, *15*, 92.

[39] Baena-Moreno, Francisco M., et al. "Carbon capture and utilization technologies: a literature review and recent advances." *Energy Sources, Part A: Recovery, Utilization, and Environmental Effects* 41.12, **2019**, 1403-1433.

[40] Choi, Sisun, et al. "Recent advances in microbial production of cis, cis-muconic acid." *Biomolecules* 10.9, **2020**, 1238.

[41] Weber, Christian, et al. "Biosynthesis of cis, cis-muconic acid and its aromatic precursors, catechol and protocatechuic acid, from renewable feedstocks by Saccharomyces cerevisiae." *Applied and environmental microbiology* 78.23, **2012**, 8421-8430.

[42] Wang, Guokun, et al. "Improvement of cis, cis-muconic acid production in Saccharomyces cerevisiae through biosensor-aided genome engineering." *ACS synthetic biology* 9.3, **2020**, 634-646.

[43] Cooper, Stephen, and Therese Ruettinger. "A temperature sensitive nonsense mutation affecting the synthesis of a major protein of *Escherichia coli* K12." *Molecular and General Genetics MGG* 139.2, **1975**, 167-176.

[44] Najafi, Mohammad B. Habibi, and Parnian Pezeshki. "Bacterial mutation; types, mechanisms and mutant detection methods: a review." *European Scientific Journal*, **2013**.

[45] Ishino, Y.; Shinagawa, H.; Makino, K.; Amemura, M.; Nakata, A. "Nucleotide sequence of the iap gene, responsible for alkaline phosphatase isozyme conversion in *Escherichia coli*, and identification of the gene product" *J Bacteriol*, **1987**, 169: 5429– 5433.

[46] Mojica, F.J.; Díez-Villaseñor, C.; Soria, E.; Juez, G. "Biological significance of a family of regularly spaced repeats in the genomes of Archaea, Bacteria and mitochondria." *Molecular microbiology* 36.1, **2000**, 244-246.

[47] Jansen, R.; Embden, J.D.V.; Gaastra, W.; Schouls, L.M. "Identification of genes that are associated with DNA repeats in prokaryotes." *Molecular microbiology* 43.6, **2002**, 1565-1575.

[48] Mojica, F.J.; Díez-Villaseñor, C.; García-Martínez, J.; Soria, E. "Intervening sequences of regularly spaced prokaryotic repeats derive from foreign genetic elements." *Journal of molecular evolution* 60.2, **2005**, 174-182.

[49] Barrangou, R.; Fremaux, C.; Deveau, H.; Richards, M.; Boyaval, P.; Moineau, S.; Romero, D.A.; Horvath, P. "CRISPR provides acquired resistance against viruses in prokaryotes." *Science* 315.5819, **2007**, 1709-1712.

[50] Jinek, M.; Chylinski, K.; Fonfara, I.; Hauer, M.; Doudna, J.A.; Charpentier, E. "A programmable dual-RNA–guided DNA endonuclease in adaptive bacterial immunity." *science* 337.6096, **2012**, 816-821.

[51] Prather, K. L. J.; Reisch, C. R. "The no-SCAR (Scarless Cas9 Assisted Recombineering) system for genome editing in *Escherichia coli*" *Science Reports* **2015**, 5:15096.

[52] Markert, B.; Stolzenberger, J.; Brautaset, T.; Wendisch, V.F. "Characterization of two transketolases encoded on the chromosome and the plasmid pBM19 of the facultative ribulose monophosphate cycle methylotroph Bacillus methanolicus." *BMC microbiology*, **2014**, 14(1), 1-11.

CHAPTER FIVE: CONCLUSIONS

5.1. Conclusions

The natural product shikimic acid (SA) is the starting material for the synthesis of oseltamivir phosphate (Tamiflu®), an antiviral agent effective against influenza.[1-3] Data presented in the second chapter encompass an effort to add to the "agricultural residue economy", utilizing mixed sugars derived from lignocellulosic corn stover for SA biosynthesis. *Escherichia coli* K-12 strains expressing different glucose transport systems – native phosphotransferase (PTS), heterologously expressed *Z. mobilis* GlF and GlK, and an uncharacterized evolved uptake mechanism – were examined in a fed-batch fermenter for their abilities to co-utilize glucose and xylose for SA synthesis. Strain YJ1.144/pSC6.090B expressing GlF and GlK performed better than a strain expressing the native glucose PTS and another PTS^- strain evolved to take up glucose. YJ1.144/pSC6.090B achieved a SA titer of 91.7 g L^{-1} when grown on a 70:30 (*w*/*w*) mixture of glucose/xylose. An evolved strain that took up glucose with an uncharacterized glucose transport system native to *E. coli* achieved a 102 g L^{-1} titer of SA, although with lower selectivity than YJ1.144/pSC6.090B. YJ1.144/pSC6.090B was grown on corn stover-derived hydrolysates for the biosynthesis of SA, achieving a titer of 55.6 g L^{-1}. QA production was higher when converting hydrolysates in comparison to commercial sugars. It is proposed that this reduction in selectivity is due to the presence of acetate. Quinate/shikimate dehydrogenase, YdiB, reportedly plays a role in the production QA in engineered SA overproducing strains with *ydiB* inactivation resulting in a 75% decrease in QA yield and a 6.17% reduction in the yield of QA relative to SA.[17] Regulation of this gene could improve selectivity for SA relative to QA in the strains reported here.

CO_2 emission data collected from the fed-batch fermentations were used to perform a comparative life-cycle assessment (LCA) and techno-economic analysis (TEA). LCA and TEA

compared SA biosynthesis from corn stover using developmental methods to corn grain via dry milling in the third chapter of this body of work. Corn stover or corn grain feedstocks were funneled into a milling facility central to neighboring farms. A ball mill was used in the corn stover process whereas a dry mill was used for corn grain. After the sugar intermediates were spray dried and trucked to a second off-site refinery, they underwent a SA fermentation/refining process to then be sold to consumers. Only when stover was treated completely as a waste feedstock, could advantages in land use, water use, and eutrophication potential be realized. Realistically, corn stover does have inherent value and SA biosynthesis from stover became more environmentally burdensome than biosynthesis from grain when allocating burdens/benefits based on economic value of the feedstocks. With allocation based on economic value of the feedstocks, stover contributed 64% more than grain to global warming and had eutrophication, water usage, and land usage impacts that were over 20-fold higher than that of corn grain. SA sourced from both stover

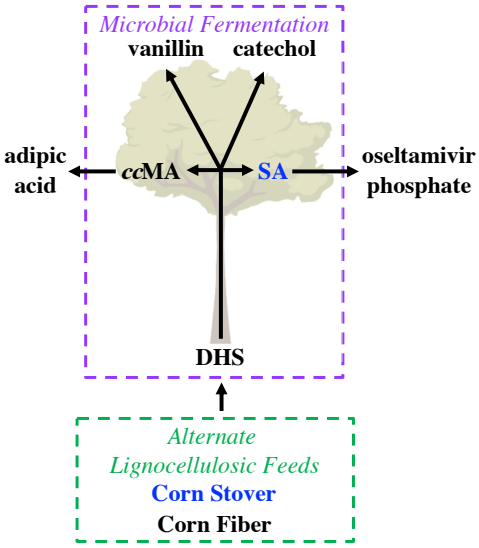

Figure 5.1. Pictorial representation of future project plan feeds and products in blue font have already been tested preliminary to this proposal: DHS, 3-dehydroshikimic acid; SA, shikimic acid; *cc*MA, *cis*, *cis*-muconic acid.

and grain can be profitable. However, higher volumes of feed necessary for stover processing result in higher equipment costs and production costs per pound of SA produced. It is hypothesized that ball milling technology can someday be of interest to farmers looking for whole-crop utilization to marginally benefit profit margins of their land rather than use agricultural residues for soil nutrients and animal feed. Currently, it is not recommended the corn stover process be adopted before barriers of acetic acid inhibition are overcome and environmental impacts and technoeconomics are further improved. The TEA model quantifies improvements needed to make the market for stover-derived glucose and xylose mixtures more competitive with that of grain-derived glucose. Minimizing the economic gap between these processes requires higher sugar yields from milled corn stover and improved SA yields from stover-derived sugar feeds.

A first objective moving forward with this work is to continue production of sugar intermediates, namely glucose and xylose, sourced from agricultural residues other than corn stover (**Fig. 5.1**) such as corn fiber. Furthermore, engineering new bacterial fermentation organisms will afford biosynthesis of other bioprivileged molecules with applications not limited to insecticides, food additives, and polymers. Namely, the shikimate pathway precursor to SA, 3-dehydroshikimate (DHS), is an intermediate for producing a plethora of valuable compounds including catechol, vanillin, and adipic acid in *Escherichia coli* K-12 strains.[4-7] Finally, life cycle

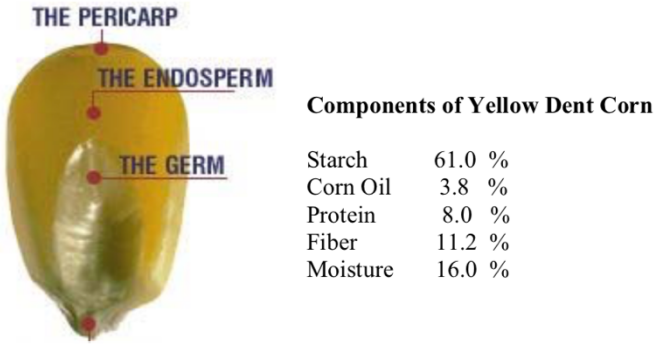

Figure 5.2. Corn kernel corn grain components and composition by weight[17].

assessment (LCA) and technoeconomic analysis (TEA) is to be coupled with each combination of alternative feedstock to compound of interest. It is hypothesized that these milling technologies will be of interest to farmers interested in whole-crop utilization on their land. Whole-crop utilization will add value to their land rather as opposed to using these agricultural residues for soil nutrients and animal feed. inherent drawbacks of corn stover can sway process engineers from its prospect as a feed source. The greater the slope of the fields, the less stover is available for harvest before wind erosion causes considerable damage to the soil. A portion stover cultivated must be left on the fields for the recycling of their nutrients. [8,9] Unpredictable weather patterns during harvesting season can result in elevated moisture levels in the stover leading to unstable product during storing and the growth of mold.[10] Meanwhile, corn fiber is a component of corn the corn grain that is simply a by-product of the dry milling process, which is not susceptible to some of the unpredictable patterns of harvesting corn stover. Corn fiber mainly comes from the pericarp of the grain (**Fig. 5.2**), and it is separated from digested starches after saccharification as a component of distillers dried grains and solubles (DDGS).[11,12] We seek funds to investigate the biosynthetic performance of bacterial strains producing chemicals from sugar sourced from corn fiber. LCA and TEA comparisons will also be made to assess the feasibility of extending a dry milling process with added ball milling processing of DDGS.

The shikimate pathway precursor to SA, DHS, is an intermediate for producing a plethora of valuable compounds including catechol, vanillin, and adipic acid.[1-4] The fourth chapter of this piece presented encompassing an effort to add to the "methanol economy", utilizing methanol for DHS biosynthesis. *Bacillus methanolicus* MGA3 was exposed to up to six rounds of chemical mutagenesis for obtaining a knockout or knockdown of *aroE*.[13] Chemical mutagenesis strategies failed due to the lack of an effective screening method. Most mutants in this study were screened

using selective agar plates where oxygen mass transfer is limited for a highly aerobic organism like MGA3. Interpreting growth signals in such a substrate-limited environment created erroneous readings and many "false positive" results. Strategies for knocking down *aroE* using RNAi and CRISPRi were also employed.[14-16] The growth of MGA3 strains carrying RNAi and CRISPRi plasmids was tested in liquid media. Samples were cold-quenched and lysed with a chemical mixture of acetonitrile:methanol:0.1 M formic acid (40:40:20 *v*/*v*) to test the intracellular and extracellular environments. No DHS was detected during RNAi and CRISPRi shake flask studies although reduced growth rates were observed in strains expressing *as*RNA and *d*Cas9. Genetic tools for recombineering and mutant screening methods/analytical techniques must be further developed with this project in order to accelerate the rate for discovering novel mutants in *B. methanolicus* MGA3.

REFERENCES

[1] Estévez, A. M.; Estévez, R. J. "A Short Overview on the Medicinal Chemistry of (—)-Shikimic Acid" *Mini-Reviews in Medicinal Chemistry*, **2012**, 12, 1443-1454

[2] Diaz Quiroz, D. C.; Carmona, S. B.; Bolivar, F.; Escalante, A. "Current perspectives on applications of shikimic and aminoshikimic acids in pharmaceutical chemistry" *Research and Reports in Medicinal Chemistry*, **2014**, 4, 35-46

[3] Rawat, G.; Tripathi, P.; Saxena, R. K. "Expanding horizons of shikimic acid: Recent progresses in production and its endless frontiers in application and market trends" *Appl. Microbiol Biotechnol.*, **2013**, 97, 4277-4287

[4] Niu, W.; Draths, K. M.; Frost, J. W."Benzene-Free Synthesis of Adipic Acid" Applied and Environmental Microbiology **2012**, *78*(15), 5170-5181.

[5] Li, K.; Frost, J. W. "Synthesis of Vanillin from Glucose" *J. Am. Chem. Soc.* **1998,** *120,* 10545-10546.

[6] Draths, K. M.; Frost, J. W. "Environmentally Compatible Synthesis of Catechol from *D*-Glucose" J. Am. Chem. Soc., **1995**, *117*, 2395-2400.

[7] Chandran, S. S.; Yi, J.; Draths, K. M.; von Daeniken, R.; Weber, W.; Frost, J. W. "Phosphoenolpyruvate Availability and the Biosynthesis of Shikimic Acid" *Biotechnology Progress* **2008**, *19*(3), 808-814.

[8] Pennington, D.; Jean, M.; Thelen, K.; Rust, S.; Anderson, E.; Gould, K. "Michigan Corn Stover Project: Cattle, Storage and Bioenergy" **2017**, MSU Extension Bulletin E-3354, 1-15

[9] Wortmann, C.; Klein, R.; Shapiro, C. "Harvesting Crop Residues" *NebGuide*, **2012**, Nebraska Extension, G1846.

[10] Smith, W. A.; Wendt, L. M.; Bonner, I. J.; Murphy, J. A. "Effects of Storage Moisture Content on Corn Stover Biomass Stability, Composition, and Conversion Efficacy" *Front. Bioeng. Biotechnol.*, **2020**, 8:716

[11] Wang, P.; Singh, V.; Xu, L.; Johnston, D. B.; Rausch, K. D.; Tumbleson, M. E. "Comparison of Enzymatic (E-Mill) and Conventional Dry-Grind Corn Processes Using a Granular Starch Hydrolyzing Enzyme" *Cereal Chem.*, **2005**, 82(6):734-738

[12] Davis, K. S. "Corn Milling, Processing and Generation of Co-products" Presented at the 62nd Minnesota Nutrition Conference and Minnesota Corn Growers Association Technical Symposium, **2001**, Chippewa Valley Ethanol Company: Benson, MN

[13] Brautaset, T.; Jakobsen, Ø. M.; Josefsen, K. D.; Flickinger, M. C.; Ellingsen, T. E. "*Bacillus methanolicus*: a candidate for industrial production of amino acids from methanol at 50°C" *Appl. Microbiol. Biotechnol.* **2007**, *74*, 22-34.

[14] Schultenkämper, K.; Brito, L. F.; López, M. G.; Brautaset, T.; Wendisch, V. F. "Establishment and Application of CRISPR Interference to Affect Sporulation, Hydrogen Peroxide Detoxification, and Mannitol Catabolism in the Methylotrophic Thermophile Bacillus methanolicus." Appl. Microbiol. Biotechnol. **2019**, *103*(14), 5879–5889.

[15] Kolev, N. G.; Atayde, V. D.; Ullu, E. "A single-cloning-step procedure for the generation of RNAi plasmids producing long stem-loop RNA" Molecular & Biochemical Parasitology 184 **2012**, 55–58.

[16] Yang, Y.; Lin, Y.; Wang, J.; Wu, Y.; Zhang, R.; Cheng, M.; Shen, X.; Wang, J.; Chen, Z.; Li, C.; Yuan, Q.; Yan, Y. "Sensor-regulator and RNAi based bifunctional dynamic control network for engineered microbial synthesis" *Nature Comm.* **2018**, 9, 3043.

[17] García, Sofía, et al. "The role of the ydiB gene, which encodes quinate/shikimate dehydrogenase, in the production of quinic, dehydroshikimic and shikimic acids in a PTS-strain of *Escherichia coli*." *Microbial Physiology* 27.1, **2017**, 11-21.

CHAPTER SIX: EXPERIMENTAL

6.1. General Materials and Methods

6.1.1. Escherichia coli – Media and Materials

Chemicals, biochemicals, nutrient broth media components and buffer salts were purchased from MilliporeSigma, Becton, Dickinson and Company, and Thermo Fisher Scientific. 0.22 μm and 0.45 μm syringe filters were purchased from MilliporeSigma. M9 minimal media were used for seed culturing before fermentation and shake flask phenotyping experiments.[1] M9 salts (1 L) contained 6 g Na_2HPO_4, 3 g KH_2PO_4, and 1 g NH_4Cl, 0.5 g NaCl. For M9 minimal medium, the following were filter-sterilized and added to autoclaved M9 salts (1 L): 20% (*w/v*) *D*-glucose (20 mL), 1 M $MgSO_4$ (2 mL), and 1 mg mL^{-1} thiamine·HCl (1 mL). During shake flask seed culturing, M9 minimal media were supplemented with 4 g rather than 10 g *D*-glucose. When culturing strains unable to synthesize aromatic amino acids and vitamins, M9 minimal media (1 L) was supplemented with sterile-filtered 40 mg phenylalanine, 40 mg tyrosine, 40 mg tryptophan, 10 mg *p*-hydroxybenzoic acid, 10 mg potassium *p*-aminobenzoate, and 10 mg 2, 3-dihydroxybenzoic acid. When necessary, 40 mg serine was added. When preparing solid media (i.e. agar plates), twice concentrated liquid media were combined with 3.0% (w/v) agar in equal volumes. LB media were prepared as follows (1 L): 10 g tryptone, 5 g yeast extract, and 10 g NaCl. SOC media contained (1 L): 20 g tryptone, 5 g yeast extract, 0.5 g NaCl, and 0.186 g KCl. Pre-sterilized 20% (*w/v*) *D*-glucose (10 mL) and 1 M $MgSO_4$ (2 mL) were added after the SOC was autoclave sterilized. Commercial SOC media were used for the recovery of transformed cells. 2XYeast-Tryptone (2XYT) media (1 L) contained tryptone (16 g), yeast extract (10 g) and NaCl (5 g) and was sterilized by autoclaving. When necessary, sterile-filtered antibiotics were added (1 L): 50 mg mL^{-1} ampicillin (Ap, 1 mL), 25 mg mL^{-1} chloramphenicol (Cm, 1 mL), 50 mg mL^{-1} spectinomycin

(Sp, 1 mL), 25 mg mL^{-1} kanamycin (Kn, 1 mL), and 100 mg mL^{-1} anhydrotetracycline (aTc, 1 mL). When used for induction, autoclave-sterilized 20% (*w*/*v*) L-arabinose was added to 0.2% (*w*/*v*) of the media. Solid LB media were prepared the same as solid minimal media. QIAprep Spin Miniprep and Maxiprep kits were purchased from Qiagen. UltraPure™ agarose was purchased from Thermo Fisher. dNTPs were purchased from Promega. Restriction enzymes, Gibson® Assembly Cloning Kits, Monarch® PCR and DNA Cleanup Kits, Q5® High-Fidelity DNA Polymerase, and Taq DNA Polymerase were purchased from New England Biolabs.

Fermentation media included (1 L): 7.5 g K_2HPO_4, 0.3 g ammonium iron citrate, 1.92 g citric acid, 0.7 g L-phenylalanine, 0.7 g L-tyrosine, and 0.35 g L-tryptophan, and initial substrate with supplements. Initial substrate was autoclaved separately, combined with filter-sterilized supplements, and added to the media via an external pump. The initial substrate contained 20 g carbohydrates (20 g *D*-glucose, 14 g *D*-glucose and 6 g *D*-xylose, or hydrolysate-derived sugars) per liter of fermentation media. Initial acetic acid was supplemented at 0.72 g per liter of fermentation media when appropriate. Initial substrate supplements contained 1 M $MgSO_4$ (2 mL), 1 mg mL^{-1} thiamine·HCl (1 mL), 10 mg mL^{-1} *p*-hydroxybenzoic acid (1 mL), 10 mg mL^{-1} potassium *p*-aminobenzoate (1 mL), 10 mg mL^{-1} 2, 3-dihydroxybenzoic acid (1 mL), 3.7 mg $(NH_4)_6(Mo_7O_{24})\cdot 4H_2O$, 2.9 mg $ZnSO_4\cdot 7H_2O$, 24.7 mg $B(OH)_3$, 2.5 mg $CuSO_4\cdot 5H_2O$, and 15.8 mg $MnCl_2\cdot 4H_2O$. Feed substrate stock was added during fermentation via an external pump, and contained 60% (*w*/*v*) *D*-glucose; 42% (*w*/*v*) *D*-glucose, and 18% (*w*/*v*) *D*-xylose; 42% (*w*/*v*) *D*-glucose, 18% (*w*/*v*) *D*-xylose, and 2.2% (*w*/*v*) acetic acid; or 75% (*w*/*v*) hydrolysate-derived sugars.

6.1.2. Bacillus methanolicus – Media and Materials

MGA3 strains were cultivated in MVcM minimal media.[4] MVcM salts (1L) contained 4.09 g K_2HPO_4, 1.30 g NaH_2PO_4, and 2.11 g $(NH_4)_2SO_4$. MVcM salts (1 L) were supplemented with 0.25

g yeast extract for MGA3 precultures to make MVcMY salts. To make MVcM or MVcMY minimal medium, the following were filter-sterilized and added to autoclaved MVcM or MVcMY salts: Vitamins {per liter: 0.1 mg *D*-biotin, 0.1 mg thiamine·HCl, 0.1 mg flavin mononucleotide, 0.1 mg pyridoxine·HCl, 0.1 mg pantothenate, 0.1 mg nicotinamide, 0.1 mg *p*-aminobenzoic acid, 0.02 mg folic acid, and 0.1 mg vitamin B12}, trace metals {per liter: 5.56 mg $FeSO_4 \cdot 7H_2O$, 0.04 mg $CuSO_4 \cdot 5H_2O$, 7.35 mg $CaCl_2 \cdot 2H_2O$, 0.04 $CoCl_2 \cdot 6H_2O$, 9.9 mg $MnCl_2 \cdot 4H_2O$, 0.288 mg $ZnSO_4 \cdot 7H_2O$, 0.011 mg $(NH_4)_2MoO_4 \cdot 4H_2O$, and 0.031 mg H_3BO_3}, 0.12 g $MgSO_4$, and appropriate substrate {8 mL methanol or 9.11 g mannitol}. For growth in rich media, MGA3 strains were cultivated in autoclaved SOBsuc containing (1 L): 20 g tryptone, 5 g yeast extract, 0.5 g NaCl, 0.186 g KCl, and 85.58 g sucrose. 2.4 g filter-sterilized $MgSO_4$ was added after autoclave sterilization. When necessary, 10 mg Cm was added per liter of SOBsuc. EP buffer consisted of 1 mM HEPES and 25% polyethylene glycol 8000 at pH 7.0.

When preparing solid media for MGA3, twice-concentrated liquid media were combined with 3.0% (*w*/*v*) agar in equal volumes. Two recipes of selective media were used for screening for *aroE* mutants after chemical mutagenesis. Each method contained one selective media that lacked any supplementation of metabolites from the common pathway for aromatic biosynthesis. Another non-selective plate supplemented either yeast extract or SA. Initially, selective plates contained K_2HPO_4 (40.93 g L^{-1}), KH_2PO_4 (12.96 g L^{-1}), $(NH_4)_2SO_4$ (21.14 g L^{-1}), 1X trace metals, 4X trace vitamins excluding p-aminobenzoic acid, 1X yeast extract mimic amino acids (YEMAA), 0.1 mM Mg_2SO_4, and 100 mM mannitol. YEMAA (1000X) contained L-alanine (10.25 mg mL^{-1}), L-asparagine (7.0 mg mL^{-1}), L-cystine (1.5 mg mL^{-1}), L-glutamate (27.5 mg mL^{-1}), L-glycine (6.25 mg mL^{-1}), L-histidine (2.75 mg mL^{-1}), L-isoleucine (6.5 mg mL^{-1}), L-leucine (9.25 mg mL^{-1}), L-lysine (10.5 mg mL^{-1}), L- methionine (2.0 mg mL^{-1}), L-proline (5.5 mg mL^{-1}), L-serine (6.75 mg

mL^{-1}), L-threonine (6.5 mg mL^{-1}), L-valine (7.75 mg mL^{-1}). Solutions of Mg_2SO_4 and mannitol were autoclaved separately and added to sterile media as needed. Solutions of YEMAA were sterilized separately by passage through a 0.22 μm syringe filter and added to sterile media as needed. The respective non-selective plates contained 5 g L^{-1} of yeast extract and included p-aminobenzoic acid. The second recipe for selective plates contained K_2HPO_4 (40.93 g L^{-1}), KH_2PO_4 (12.96 g L^{-1}), $(NH_4)_2SO_4$ (21.14 g L^{-1}), 1X trace metals, 4X trace vitamins excluding p-aminobenzoic acid), 0.1 mM Mg_2SO_4, and 100 mM mannitol. The respective non-selective plates contained 80 mg L^{-1} of SA and included p-aminobenzoic acid. When preparing rich solid media, no sucrose was added. Meaning, twice concentrated SOB media were combined with 3.0% (*w*/*v*) agar in equal volumes.

Monarch gel extraction kit, Monarch DNA clean-up kit, Q5 DNA polymerase, HiFi master mix, and 1 kb DNA ladder were purchased from New England Biolabs. The 1 kb+ DNA ladder was purchased from Promega. Pre-cast 4-20 % (w/v) acrylamide Mini-PROTEAN TGX gels and Precision Plus Protein All Blue Ladder were purchased from BioRad. Plasmid extraction kits were purchased from Qiagen. B. methanolicus MGA3 was received as a gift from Dr. Trygve Brautaset (Norwegian University of Science and Technology, Trondheim, Norway). Gibson assembly master mixes were made first by preparing a 5X ISO reaction buffer. The buffer consisted of 25% PEG-8000, 500 mM Tris-HCl, pH 7.5, 50 mM $MgCl_2$, 50 mM DTT, 1 mM each of the four dNTPs, and 5 mM NAD. The 5X ISO reaction buffer was stored at -20°C.[9] Next, an enzyme-reagent master mixture was prepared by combining 320 μL of 5X ISO buffer, 0.64 μL of 10 U μL^{-1} T5 exonuclease, 20 μL of 2 U μL^{-1} Phusion polymerase 160 μL of 40 U μ μL^{-1} Taq ligase, and water up to a final volume of 1.2 mL. The mixture was aliquoted into 15 μL stocks and stored at -20°C.[9]

6.1.3. PCR Amplification

Table 6.1. Reaction components of PCR components, volumes, and final concentrations.

Component	Volume (μL)	Final Concentration
5X Q5 reaction buffer	10	1X
10 mM dNTPs	1	200 μM
10 μM forward primer	2.5	0.5 μM
10 μM reverse primer	2.5	0.5 μM
Template DNA	Varies	1-5 ng
Q5 High-Fidelity DNA polymerase	0.5	0.02 U μL^{-1}
Deionized water	Up to 50 μL	-

Unless otherwise specified, all PCR amplifications were conducted in a Bio-Rad DNA Engine® Peltier Thermal Cycler with a final reaction volume of 50 μL using Q5® High-Fidelity DNA Polymerase with other components as listed in **Table 6.1**. Routine PCR was conducted using the thermocycling conditions in **Table 6.2**. The PCR samples were quenched with 10 μL of 6X loading dye containing SDS (NEB) before visualization on a 0.7% agarose gel.

Table 6.2. Thermocycling conditions for PCR thermocycling steps, temperatures, and rest times

Step	Temperature (°C)	Time
Initial Denaturation	98	30 sec
	98	10 sec
30 cycles	*50-72	30 sec
	72	30 sec kb^{-1}
Final Extension	72	2 min
Hold	4	-

6.2. *Escherichia coli* Methods

6.2.1. Electrocompetent Bacterial Cell Generation and Transformation

Electrocompetent cells were prepared using standard operating procedures from the laboratory which were adapted from Sambrook and Russell.[2] A single bacterial colony from a freshly streaked

plate (<5 days old) of the desired strain was used to inoculate a 5 mL LB culture and incubated overnight with shaking (37 °C, 200 rpm). An aliquot of the overnight culture (2 mL) was used to inoculate 100 mL of sterile 2xYT media in a 500 mL baffled shake flask and incubated at 37 °C until an OD_{600} of 0.5-0.7 was reached. The cells were collected by centrifugation using a FiberliteTM F12-6x500LEX fixed angle rotor (4,500 x *g*, 5 min, 4 °C) and gently resuspended in 100 mL cold, sterile deionized water to remove residual salts from the culture media. The cells were pelleted by centrifugation (4,500 x *g*, 5 min, 4 °C) and the sample was carefully decanted to remove the supernatant. The wash step was repeated with an additional 100 mL cold, sterile deionized water. The cell pellet was resuspended in 100 mL cold, sterile 10% aqueous (*v*/*v*) glycerol and centrifuged at (4,500 x *g*, 5 min, 4 °C). The supernatant was discarded and the cell pellet was resuspended in 0.5 mL 10% (*v*/*v*) glycerol. Aliquots (50 µL) were prepared in pre-chilled, sterile microcentrifuge tubes on ice and flash-frozen in liquid nitrogen prior to storage at -80 °C.

For the transformation of electrocompetent *E. coli* cells, plasmid DNA (2 µL of 1-5 ng μL^{-1} in sterile deionized water) or purified, de-salted PCR or ligation products were combined with 50 µL of electrocompetent cells thawed on ice. Gentle pipetting was carried out to ensure sufficient mixing, and the sample was transferred to a cold, sterile Gene Pulser® electroporation cuvette (0.2 cm electrode gap). Electroporation was carried out using a Bio-Rad Gene Pulser II electroporation system (2.5 kV, 25 mF and 200 Ω), which resulted in a time constant in the range of 5.16–5.25 ms. The cuvette was immediately placed on ice, 1 mL room temperature SOC media was added. The resulting recovery culture was incubated at 37 °C with shaking (1 h, 200 rpm). The cells were harvested by centrifugation at 13,000 rpm in a microcentrifuge, and 800 µL of the supernatant was

discarded. The cell pellet was resuspended in the remaining media and 20 μL and 80 μL aliquots were plated onto LB solid media containing the appropriate antibiotic.

6.2.2. Strains, Plasmids, Primers, and Oligonucleotides

Table 6.3. Strains, plasmids, and oligonucleotides itemized biological materials used in *E. coli* studies.

Strain/Plasmid/Oligo.	Relevant Characteristics	Ref.
	Strains	
DH5α	Δ(lacZ)M15 Δ*hsdR* Δ*recA*	Invitrogen
RB791	$lacI^q$	ATCC 53622
RB791 *serA::aroB*	$lacI^q$ *serA::aroB*	[19]
JW1087-2	*ptsG::kn*^{R}	CGSC 9031
RB791 *serA::aroB* Δ*aroL*	$lacI^q$ *serA::aroB* Δ*aroL*	This study
YJ1.130	RB791 *serA::aroB* Δ*aroL* Δ*aroK*	This study
YJ1.144	YJ1.130 Δ*ptsG*	This study
YJ1.148	YJ1.144 evolved to take up glucose	This study
	Plasmids	
pCas9-cr4	p15a_ori, *cas9*, cm^R	Addgene, [5]
pKDsgRNA-ack	Rep101(Ts), *gam*, *beta*, *exo*, sp^R	Addgene, [5]
pKDsgRNA-p15	p15a sgRNA in pKDsgRNA-ack	Addgene, [5]
pKDsgRNA-aroL	*aroL* sgRNA in pKDsgRNA-ack	This study
pKDsgRNA-aroK	*aroK sg*RNA in pKDsgRNA-ack	This study
pCP20	Rep101(Ts), *flp*, ap^R, λ_{rep}(Ts)	[6, 7]
pKD12.138A	$aroF^{FBR}$, P_{tac}, *aroE*, *serA*, *tktA*, ap^R	[19]
pSC6.090B	*glf*, *glk*, $aroF^{FBR}$, P_{tac}, *aroE*, *serA*, *tktA*	[3]
	Oligonucleotides	
HSS011	For homologous recombination of Δ*aroL*	This study
YJ003	For homologous recombination of Δ*aroK*	This study

Oligonucleotides were purchased from Integrated DNA Technologies. DH5α strains were used for cloning. RB791 *serA::aroB* was the microbial host used in this study, which was generated

from *E. coli* K-12 strain RB791 in a separate study.[19] JW1087-2 was used for homologous recombination of a *ptsG* deletion into our host strain. YJ1.130 is a host strain carrying deletions in both shikimate kinase isozymes as well as an additional copy of DAHP synthase inserted into the genomic *serA* vector. Deletion of *ptsG* in YJ1.130 afforded a second host strain of interest, YJ1.144. Shake flasks containing M9 minimal media, serine, glucose, and aromatic supplementation were prepared and inoculated with strain YJ1.144. After two days, the media turned turbid. The culture of mutants was reinoculated into another shake flask of M9 minimal media serine, and glucose to an initial OD_{600} of 0.01 and grown to a final optical density of 1. The culture was then reinoculated to an initial OD_{600} of 0.01 and grown to a final optical density of 1-2 five more times. It was observed that after approximately 40 generations the maximum specific growth, μ_{max}, rate stopped increasing with each subsequent reinoculation. The new strain, YJ1.148, was frozen in 20% (*v*/*v*) glycerol and stored at -80℃. Strains, plasmids, and oligonucleotides used to employ the no-SCAR method in this study are listed in **Table 6.3** and described in further detail in the *Section 6.2.3*. This method was used to generate deletions in the genes *aroL* and *aroK*. A deletion was made in *ptsG* by P1 transduction – recombination of a homologous *ptsG::kan*^{R} locus carrying an excisable kanamycin resistance cassette as described by Saragliadis et al.[6,7] Plasmids pKD12.138A and pSC6.090B were used for the expression of shikimate pathway genes to engineer SA overproduction. In a previous study, pSC6.090B was constructed from pKD12.138A.[4] Linearization of pKD12.138A occurs after removing Ap^R using NcoI digestion enzymes. A fragment containing P_{tac}, *glf*, and *glk* is ligated into its place. The resulting pSC6.090B lacks Ap^R and expresses facilitated diffusion transport enzymes GlF and GlK (**Fig. 6.1**).[4] Primer and oligonucleotide sequences are provided in **Table 6.4**. Lowercase letters in the sequences of HSS006 and HSS007 signify regions of homology between the two

oligonucleotides that encode a gene-targeting protospacer sequence. Lowercase letters in the sequences of HSS009 and HSS010 also signify regions of homology between the two oligonucleotides that encode a gene-targeting protospacer sequence. More primer and oligonucleotide descriptions are provided in **Table 6.5**.

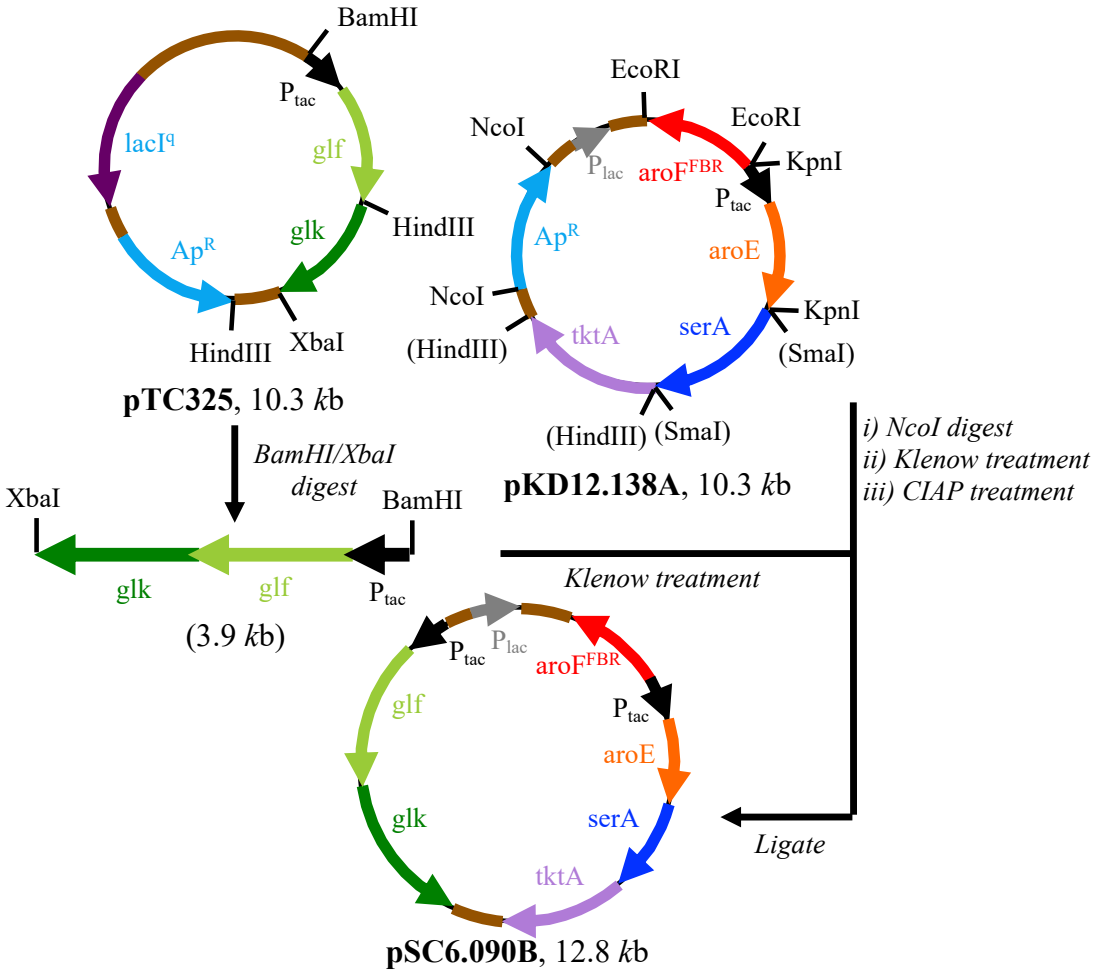

Figure 6.1. Cloning pSC6.090B flow chart for preparation of plasmid pSC6.090B from pKD12.138A.

Table 6.4. Primer and oligonucleotide sequences sequences of primers used in *E. coli* studies.

Oligo. name	Sequence (5' to 3')
HSS006	attgtgctggctactggcggGTTTTAGAGCTAGAAATAGCAAG
HSS007	ccgccagtagccagcacaatGTGCTCAGTATCTCTATCACTGA
HSS009	accgttatcgctacaggcggGTTTTAGAGCTAGAAATAGCAAG
HSS010	ccgcctgtagcgataacggtGTGCTCAGTATCTCTATCACTGA
YJ003	TGGCCAACGCTTCCAGAACTTCACGCGGCGGTGTTTCAACGTGCAG CAACATTGATGACCTTTTCTTCGCGATCGCGGAAGCCTTCTTCG
HSS011	GTGCCAGGGCGCTGCGAATTTCAGAAATCACCTGGCTGGGTCGAC GGTTAAGCG
YJ015	GCGGGTTTATCATTAACGAATAGTC
YJ016	CGACATCCACCTTAATTACTGTAC
YJ017	GATCGCTATTCTCATGACAC
YJ018	CTTCCTTATTTCACGGGATG
YJ032	TTAGTCTCCCCAACGTCTTA
YJ033	CCATACTCAGGAGCACTCTC

Table 6.5. Primer and oligonucleotide descriptions descriptions of primers used in *E. coli* studies.

Oligo.	PCR Fragment Length (bp)	Description
HSS006 HSS007	-	Primers containing protospacer to generate pKDsgRNA-aroK. Lowercase letters in sequence signify 20 bp region of homology between HSS006 and HSS007.
HSS009 HSS010	-	Primers containing protospacer to generate pKDsgRNA-aroL. Lowercase letters in sequence signify 20 bp region of homology between HSS009 and HSS010
YJ003	-	For homologous recombination of Δ*aroK*
HSS011	-	For homologous recombination of Δ*aroL*
YJ015	620 w/o deletion	Forward primer for *aroK* amplification
YJ016	340 w/ deletion	Reverse primer *aroK* amplification
YJ017	650 w/o deletion	Forward primer *aroL* amplification
YJ018	260 w/ deletion	Reverse primer *aroL* amplification
YJ032	1400 w/ deletion	Forward primer *ptsG* amplification
YJ033	190 w/o deletion	Reverse primer *ptsG* amplification

6.2.3. Targeted Gene-Editing using Scarless Cas9 Assisted Recombineering (no-SCAR)

Deletions were made in *aroL* and *aroK* using the no-SCAR method as described by Prather and Reisch.[5] A rough flow diagram for creating gene deletions using the no-SCAR method is shown in **Fig. 6.2(a)** where a two-plasmid system is used to carry out gene recombination followed by mutant counter-selection to afford an enriched mutant culture. Genes encoded in the two template plasmids, pCas9-cr4 and pKDsgRNA-ack (plasmid maps shown in **Fig. A.6.7** and **Fig. A.6.8**, respectively), are required in this process. The pCas9-cr4 plasmid encodes the Cas9 enzyme (preceded by an aTc-activated promoter region), Cm resistance, and a p15A origin of replication are encoded on the pCas9-cr4 plasmid. The pKDsgRNA-ack plasmid encodes genes for the λ-red recombineering enzymes (exo, beta, and gam components expressed by an L-arabinose-inducible promoter) , Sp resistance, and a thermosensitive replicon. For creating deletions in *aroL* and *aroK*

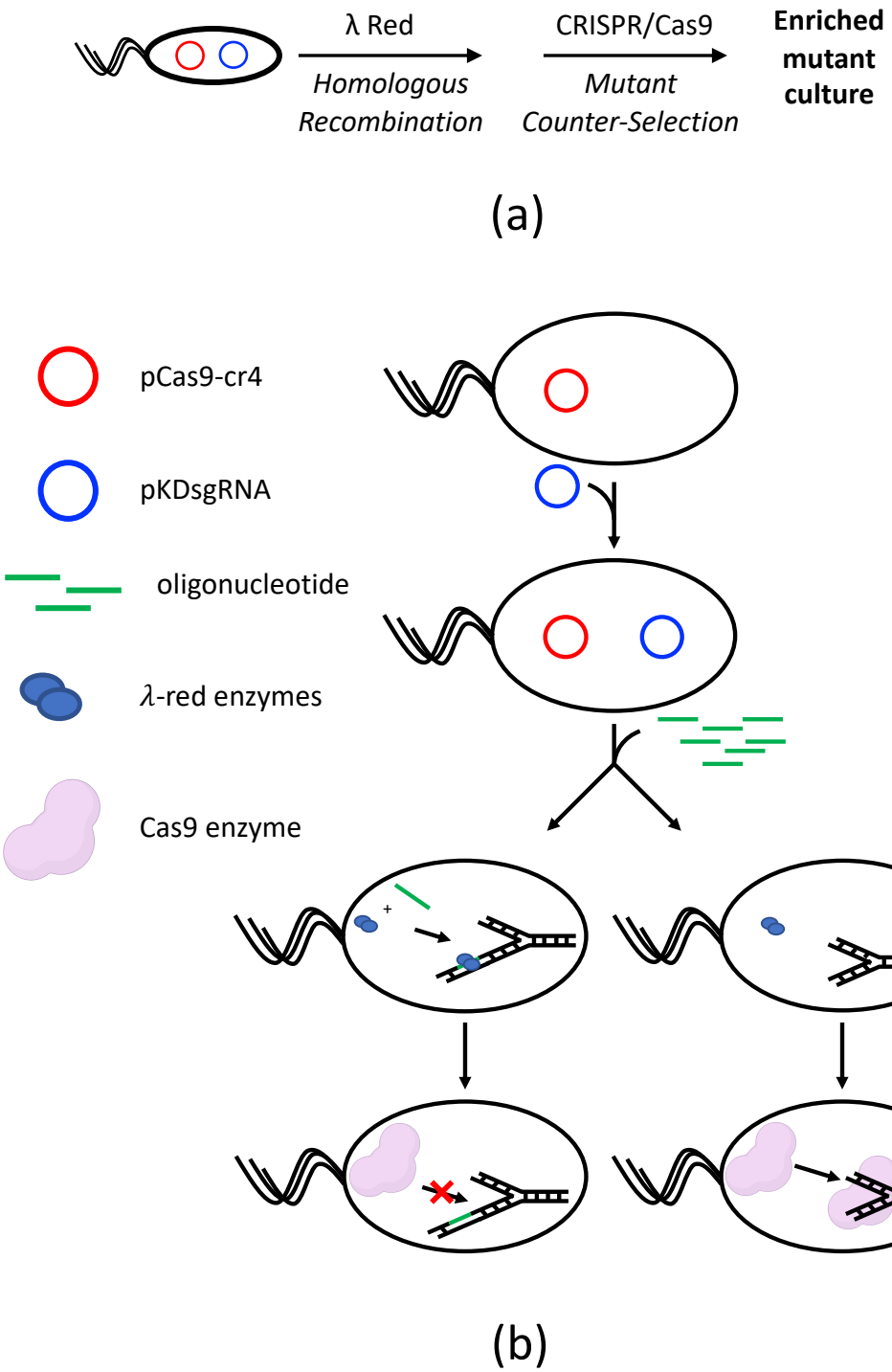

Figure 6.2. No-SCAR method (a) Flow diagram for gene deletion and counter-selection of mutants using the no-SCAR method (b) host strain containing pCas9-cr4 plasmid transformed with pKDsgRNA plasmid expressing λ-red enzymes and sgRNA allowing Cas9 from pCas9-cr4 to target gene of interest. Following λ-red expression, cells are transformed with oligonucleotide DNA that is incorporated at a replication fork at a low frequency. Unsuccessful mutations are selected against after being targeted by Cas9, which generates double stranded breaks in their chromosomal DNA resulting in cell death.

plasmids containing sgRNA targeting their respective genes, pKDsgRNA-aroL and pKDsgRNA-aroK, were prepared. pKDsgRNA-aroK and pKDsgRNA-aroL were generated from pKDsgRNA-ack using circular polymerase extension cloning of their two respective protospacer-encoding primers.[21] This means PCR amplification of pKDsgRNA-ack was performed to include protospacer sequences of *aroL* and *aroK* genes and the linear plasmid was self-ligated.[5] Primers HSS006 and HSS007 (sequences and descriptions in **Table 6.4** and **Table 6.5**, respectively) were primers containing a protospacer used to generate pKDsgRNA-aroK from pKDsgRNA-ack. Lowercase letters in the sequences of HSS006 and HSS007 indicate regions of homology that encode the aroK-targeting protospacer sequence. Primers HSS009 and HSS010 (sequences and descriptions in **Table 6.4** and **Table 6.5**, respectively) were used to generate pKDsgRNA-aroL. Lowercase letters in the sequences of HSS009 and HSS010 indicate regions of homology that encode the aroL-targeting protospacer sequence. **Fig. 6.2(b)** conceptually illustrates a flow diagram of the no-SCAR procedure for gene editing. The no-SCAR procedure begins by transforming the pCas9-cr4 plasmid into the host cell. The pCas9-cr4-containing host strain is then made electrocompetent and transformed with the desired pKDsgRNA plasmid specific to a desired gene mutation. Cells are cultured at 30°C after a pKDsgRNA plasmid is transformed into the cell until procedure calls for the plasmid to be excised. Gene deletions via homologous recombination facilitated by λ-red recombineering enzymes are activated in the pKDsgRNA plasmid first by induction with 0.2 % (*w*/*v*) L-arabinose once the cells reach an OD_{600} of 0.4-0.5. Oligonucleotides HSS011 and YJ003 (sequences and descriptions in **Table 6.4** and **Table 6.5**, respectively) are double-stranded oligonucleotides designed for homologous recombination of deletions in *aroL* and *aroK*, respectively, using the λ-red enzymes. 100 ng to 1 μg of oligonucleotide DNA is combined with a 50 μL aliquot of the host strain harboring the pCas9-cr4 and pKDsgRNA plasmids. The

cells are then pulsed with an electroporator using the same settings used during plasmid transformation (2.5 kV, 25 mF and 200 Ω). The cells are recovered in 1 mL of SOC media at 30°C. Five ten-fold dilutions of the recovered cells were then plated on LB/Cm/Sp/aTc to induce Cas9 counterselection. Successful recombination occurs at a low frequency using the λ-red system, so a counterselection strategy is required to enrich them. Non-mutants containing in-tact *aroL* and *aroK* genes are targeted by the designed sgRNA fragments linked to the Cas9 proteins. The Cas9 protein is induced by an aTc-inducible promotor. This induction step was performed in the dark due to the sensitivity of aTc to light. Due to its lack of an effective heterologous recombination system for gene repair, *E. coli* is not able to survive double-stranded breaks created by Cas9 proteins. Upon activation of the Cas9 protein, non-mutants are unable to continue growth, and mutants are enriched in the culture. Upon deletion of *aroL* and *aroK*, RB791 would become an auxotroph of aromatic molecules. Knockouts in *aroL* and *aroK* were confirmed using both PCR and phenotypic screening (described further in sections specific for each strain construction). YJ015 and YJ016 (sequences and descriptions in **Table 6.4** and **Table 6.5**, respectively) were forward and reverse primers for amplification of *aroK*. **Table 6.5** displays the PCR fragment lengths of *aroK* from the genome of wild-type *E. coli* not carrying the gene deletion and from the genome of a mutant variant carrying the gene deletion. YJ017 and YJ018 (sequences and descriptions in **Table 6.4** and **Table 6.5**, respectively) were forward and reverse primers for amplification of *aroL*. **Table 6.5** also displays the PCR fragment lengths of *aroL* from the genome of wild-type *E. coli* not carrying the gene deletion and from the genome of a mutant variant carrying the gene deletion. Each colony that could be a potential mutant was replica plated onto M9 minimal media lacking aromatic supplementation, M9 minimal media containing aromatic supplementation, and rich media. Mutants that grew with aromatic supplementation but not

without were selected from the rich plate and stored for future steps. All plasmids used to employ the no-SCAR method in this study are listed in **Table 2.3**. Following the selection of a successful mutant, a single isolated colony is inoculated into LB and incubated at 37℃ for 24 h. The culture was then streaked onto LB/Cm and grown overnight at 42℃. Isolated colonies were replica plated onto LB/Cm, LB/Sp, and LB plates and screened for growth on LB/Cm and LB but loss of growth on LB/Sp. With the p15A origin of replication, a pKDsgRNA plasmid containing sgRNA targeting the p15A locus, pKDsgRNA-p15, was used to excise the pCas9-cr4 plasmid. After pKDsgRNA-p15 is transformed into the cell containing a pCas9-cr4 plasmid desired to be excised, the cells are recovered in SOC media at 30℃. Cells are inoculated straight into LB/aTc media used to induce *cas9* and p15A-targeting sgRNA. After 2 h, the cells are then plated onto LB/Sp/aTc media and incubated at 30℃ overnight. Individual colonies are replica plated onto LB only plates and LB/Cm and screened for loss of Cm resistance. The pKDsgRNA-p15 plasmid is then excised in the same way as other pKDsgRNA plasmids as previously described.

6.2.4. Construction of RB791 serA::aroB ΔaroL

Construction of RB791 *serA::aroB ΔaroL* was performed by employing the no-SCAR method on RB791 *serA::aroB* as the microbial host strain. The plasmid containing sgRNA targeting the *aroL* gene was pKDsgRNA-aroL. The protocol for employing targeted gene-editing using scarless Cas9-assisted recombineering is described in Section 6.2.3.

6.2.5. Construction of YJ1.130

Construction of YJ1.130, or RB791 *serA::aroB ΔaroL ΔaroK*, was performed by employing the no-SCAR method on RB791 *serA::aroB ΔaroL* as the microbial host strain. The plasmid containing sgRNA targeting the *aroK* gene was pKDsgRNA-aroK. The protocol for employing targeted gene-editing using scarless Cas9-assisted recombineering is described in Section 6.2.3.

6.2.6. Targeted Gene-Editing using P1 Transduction and Generation of YJ1.144

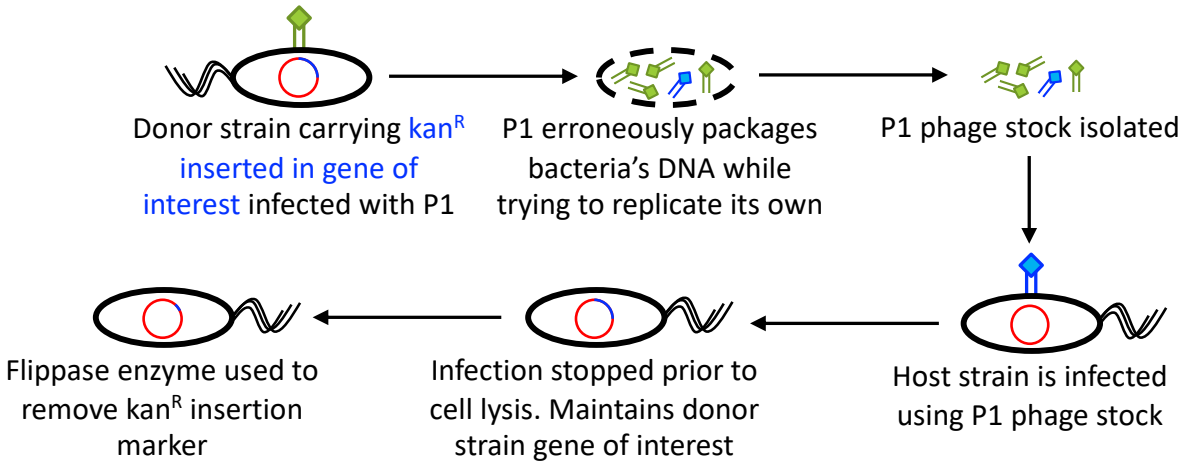

Figure 6.3. P1 transduction and plasmid excision flow diagram for gene deletion using P1 transduction followed by antibiotic resistance cassette excision. the mutation of a donor strain already containing the deletion is transferred to a host strain using the bacteriophage P1. Bacteriophage use the donor cell's machinery to replicate themselves, however, they can erroneously package the cell's own DNA into phage particles at a low frequency. Donor strain P1 cell lysate is used to infect a culture of host strain where the desired mutation from the donor can be transduced to the host. After the desired gene deletion is transduced, a flippase enzyme is expressed to recognize two flanking FRT recognition sites on the antibiotic resistance marker of the deletion. Homologous recombination of these sites excises the antibiotic resistance marker.

A deletion was made in *ptsG* by P1 transduction.[6,7] In this protocol, the mutation of a donor strain already containing the deletion of *ptsG*, JW1087-2, is transferred to a host strain using the bacteriophage P1 (**Fig. 6.3**). After the desired gene deletion is transduced, a flippase enzyme is expressed to recognize two flanking FRT recognition sites on the antibiotic resistance marker of the deletion. Plasmid pCP20 in **Table 6.3** was used to express flippase and excise the kanamycin resistance cassette. JW1087-2 was inoculated in 5 mL of LB/Kn supplemented with 10 mM $CaCl_2$. Cells were incubated with shaking at 200 RPM and 37°C. Once the culture reached an OD_{600} of ~1.0, 100 μL aliquots were partitioned into microfuge tubes. These partitions were infected with 200 μL aliquots of different serial dilutions of a P1 phage stock. After incubating for 20 min at 37°C, 3 mL of sterile soft LB agar containing 0.7% agar (*w*/*v*) was added to the infected donor

cells and the whole solution was spread over solid LB media to harden overnight at 37°C. The following day a semiconfluent cultured plate was selected. Plaques of phage formed in the soft agar were collected in a 1.5 mL microfuge tube using a sterile inoculation loop. The agar material was suspended in 1 mL of LB media and centrifuged for 15 min at 4,000 x g. The supernatant was collected and combined with two drops of chloroform and stored at 4°C.

Next, a culture of YJ1.130 was grown to an OD_{600} of ~1.0 at 37°C and 200 RPM agitation in LB supplemented with 10 mM $CaCl_2$. A 100 μL aliquot of the culture was infected with a 200 μL aliquot of the P1 phage stock prepared from JW1087-2. Infection continued for 20 min at 37°C and was stopped by the addition of sodium citrate (1 M, pH 5.5), to 100 mM. Samples were spun in a microfuge for 1 min. Pelleted cells were washed twice with 1 mL LB containing 100 mM sodium citrate, pH 5.5. The suspension was centrifuged again, and pelleted cells were suspended in 1 mL LB containing 100 mM sodium citrate, pH 5.5, and plated onto LB/Kn plates containing 10 mM sodium citrate. Cells were incubated overnight at 37°C. Colonies that expressed Kn resistance were selected for further screening. Three candidates were made electrocompetent and transformed with pCP20 by electroporation. Cells were recovered in SOC media, plated onto LB/Ap, and incubated overnight at 30°C. A single colony of each candidate was selected and grown in separate LB cultures at 42°C for 6 to 8 h. Dilutions were plated onto LB media and grown overnight at 30°C. A knockout in *ptsG* was confirmed in at least one colony using PCR. YJ032 and YJ033 (sequences and descriptions in **Table 6.4** and **Table 6.5**, respectively) were forward and reverse primers, respectively, for amplification of *ptsG*. **Table 6.5** displays the PCR fragment lengths of *ptsG* from the genome of wild-type *E. coli* not carrying the gene deletion and from the genome of a mutant variant carrying the gene deletion

6.2.7. Escherichia coli Fermentation

Fermentations utilizing commercially purchased sugars as substrate had 0.8 L initial reaction volumes. Fermentations utilizing hydrolysate-derived sugars had 0.5 L initial reaction volumes due to limited quantities of the substrate. Fermentations were fed under "substrate-rich" conditions.[8] Microbes were grown in a 3 L Biostat® B baffled fermenter with a DCU control tower. Parameters pH 7.0, 33°C, an initial agitation of 50 RPM, and an initial aeration rate of 0.06 L min^{-1} were set and controlled using the tower's PID control loops. Once dissolved oxygen (DO) reached 10%, DO was maintained using a two-phase cascade control system. In phase one, agitation was ramped to and held at 750 RPM, followed by ramping of airflow to 1.00 L min^{-1}. In the second phase, airflow was held at 1.00 L min^{-1}, and agitation was ramped up to 1800 RPM. Concentrations of D-glucose in the fermentation broth were monitored throughout fermentations using GlucCell glucose test strips to maintain D-glucose concentrations at above 2 g L^{-1}, although the carbohydrate concentration was usually considerably higher. If D-glucose were too low the external substrate feed rate was increased, and if D-glucose were too high the feed rate was decreased.

Inoculations were prepared by streaking a single colony of an SA-overproducing strain on an agar plate containing M9 minimal glucose media with aromatic supplementation. The plate was incubated for 24-36 h at 37°C. A single colony was introduced into 5 mL of M9 minimal glucose media (liquid) with aromatic supplementation. Cultures were grown at 37°C with agitation at 250 RPM overnight. The next day, cultures were inoculated to an initial OD_{600} of 0.2 into a larger shake flask culture containing M9 minimal glucose media with aromatic supplementation. Agitation was continued at 250 RPM at 37°C. For 0.8 L and 0.5 L fermentations shake flasks contained 80 mL and 50 mL of minimal media, respectively. After the culture reached an appropriate OD_{600}

(approximately 1.0), the inoculant was transferred into the fermentation vessel and the fermentation was initiated (t = 0 h).

Optical density was measured at 600 nm (OD_{600}) using a NanoDrop One^{C} spectrophotometer and converted to dry cell weight (DCW) using a 0.43 g L^{-1} DCW conversion factor per unit of optical density. Water was used as a blank (1 mL), and in samples where $OD_{600} > 1$ a 10- or 100-fold dilution was carried out using water to ensure an absorbance<1. D-Glucose (9 min retention time), D-xylose (9.7 min retention time), SA (13 min retention time), and QA (10.6 min retention time) were quantified by High-Performance Liquid Chromatography (HPLC) refractive index detection (RID). HPLC UV detection was used to quantify DHS (17.2 min retention time) at an absorbance wavelength of 232 nm. An Agilent Technologies 1100 Series HPLC attached to an Aminex HPX-87H column with isocratic elution of 0.01 N H_2SO_4 was used. A 10 μL injection volume was used for the analysis of each sample. Samples were prepared for HPLC analysis using 0.22 μm syringe filters from Millipore Sigma. Titers of DCW, D-glucose, D-xylose, SA, QA, and DHS were multiplied by a dilution factor to account for dilution by the external substrate feed dispensed before samples were taken. Calibration data and a sample HPLC chromatogram are provided in the Appendix section (**Fig. A.6.1 – Fig. A.6.6**). Stock solutions of each analyte (50 g L^{-1} D-glucose, 50 g L^{-1} D-xylose, 80 g L^{-1} SA, 10 g L^{-1} QA, and 10 g L^{-1} DHS) were prepared in filtered water using 5 mL volumetric flasks. Dilutions of the stock solutions were made to generate at least five standard solutions between 0 g L^{-1} and the stock concentration of each analyte. Standards were run using the same sampling method as is used for fermentation samples, and a standard calibration curve was generated for each compound. Headspace exhausts from the fermenter were passed through a condenser and Drierite and then sent to a PASPORT CO_2 Gas Sensor to quantify CO_2. Data reported on SA sourced from hydrolysate sugars were not replicated

due to the limited availability of substrate. Other fermentation data are an average of two replicate experiments.

6.2.8. Hydrolysate Preparation

Ball milled and hydrolyzed sugars derived from corn stover were received as a brown and opaque mixture of solids and liquid. Biomechanical treatment of corn stover was carried out in a 2 L stirred ball mill reactor (JM-2L, Tianchuang Powder Tech Co., Changsha China) as previously described.[22] Hydrolysate sugars were generously donated for this study by Dr. Wei Liao's group from the Biosystems Engineering Department at Michigan State University. Hydrolysates were autoclave sterilized prior to being received by the Liao group. The average titers of D-glucose, D-xylose, and acetate of the received sugars were 55.6 g L^{-1}, 24.0 g L^{-1}, and 2.8 g L^{-1}, respectively. Hydrolysates were spun at 50,000 x g at 4°C for 20 min and their supernatants were stored at -20°C for further separation processes. The pellets were resuspended in autoclave sterilized water and centrifuged once again at 50,000 x g at 4°C for 20 min. Supernatants of both centrifugation steps were combined and sterile filtered through 0.45 μm filters. The filtered solutions were rotary evaporated to a final concentration of 75% (*w*/*v*) of combined D-glucose and D-xylose, which was confirmed using High-Performance Liquid Chromatography (HPLC) refractive index detection (RID) as described previously. A more concentrated external substrate feed was used for the hydrolysate fermentation, because a smaller initial reaction volume was used due to limited availability of hydrolysate sugars. In order for the pH and DO probes to reach further into the broth during fermentation, the external feed was concentrated further and the reaction volume initially charged in the Biostat reactor was increased.

6.3. *Bacillus methanolicus* Methods

6.3.1. Strains, Plasmids, Primers, and Oligonucleotides

All bacterial strains, pla smids, and oligonucleotides are shown in **Table 6.6**. All plasmids were transformed into electrocompetent DH5α and frozen at -80℃ for long-term storage. The host strain used was *B. methanolicus* MGA3. MGA3 was chemically mutagenized in the presence of SA supplementation after which YJ1.149 was selected as a mutant with some growth dependence on SA. YJ1.149 was chemically mutagenized in the presence of SA supplementation after which YJ1.150 was selected as a mutant with the most growth dependence on SA. YJ1.150 was

Table 6.6. Strains, plasmids, and oligonucleotides itemized biological materials used in *E. coli* studies.

Strain/Plasmid/Oligo.	Relevant Characteristics	Ref.
	Strains	
DH5α	Δ(lacZ)M15 Δ*hsdR* Δ*recA*	Invitrogen
MGA3	wild type	[20]
YJ1.149	MGA3 selected for growth in 1% EMS for 20 min	This study
YJ1.150	YJ1.149 selected for growth in 0.8% EMS for 20 min	This study
YJ1.151E	YJ1.150 selected for growth in 0.8% EMS for 20 min	This study
YJ1.152	YJ1.151E selected for growth in 0.8% EMS for 20 min	This study
YJ1.153	YJ1.152 selected for growth in 0.8% EMS for 10 min	This study
YJ1.154B	YJ1.153 selected for growth in 0.8% EMS for 10 min	This study
	Plasmids	
pTH1mp	Cloning vector for RNAi plasmids	[11]
pTH1mp_null	pTH1mp assembled with YJ040 and YJ041	This study
pTH1mp_*as*aroE1B	Targeting central part of MGA3 *aroE*	This study
pTH1mp_*as*aroE3C	Targeting RBS and start codon of MGA3 *aroE*	This study
piCas	Cloning vector for *d*Cas9 expression	[12]
piCas_aroEsgRNA1	Targeting *d*Cas9 gene silencing of *aroE*	This study
	Oligonucleotides	
YJ040	Duplex fragment encoding first paired terminus of stem-loop interfering RNA	This study
YJ041	Duplex fragment encoding second paired terminus of stem-loop interfering RNA	This study

chemically mutagenized in the presence of SA supplementation after which YJ1.151E was selected as a mutant with the most growth dependence on SA. YJ1.151E was chemically mutagenized in the presence of SA supplementation after which YJ1.152 was selected as a mutant with the most growth dependence on SA. YJ1.152 was chemically mutagenized in the presence of SA supplementation after which YJ1.153 was selected as a mutant with the most growth dependence on SA. YJ1.153 was chemically mutagenized in the presence of SA supplementation after which YJ1.154B was selected as a mutant with the most growth dependence on SA.

A Gibson assembly approach was taken for assembling plasmids.[10] The plasmid backbone used for the construction of RNAi plasmids was a low-copy number pTH1mp vector.[11] Two complimentary paired termini, YJ040 and YJ041, were cloned into pTH1mp using the unique SmaI restriction site (the paired termini also had a strategically placed unique XhoI restriction site directly between them). The resulting plasmid was named pTH1mp_null. Antisense RNA (*as*RNA) complementary to a central region of *aroE* in MGA3 was inserted into the unique XhoI site of pTH1mp_null, affording pTH1mp_*as*aroE1B. A second RNAi plasmid, pTH1mp_*as*aroE3C, was constructed similarly and contained *as*RNA complementary to the ribosome binding site (RBS) and start codon of *aroE* in MGA3. For the construction of a CRISPRi plasmid, recombineering followed a procedure outlined by Schultenkämper et al.[12] The piCas plasmid was linearized by performing a double digest using its unique AvaI and XbaI restrictions sites. The plasmid was reassembled with a 20 bp gene-targeting *sg*RNA that targeted *aroE* in MGA3. Sequences of oligonucleotide and primers used for gene amplification and Gibson assembly can be found in **Table 6.8**.

6.3.2. Isolation of Plasmid DNA

For small scale purification of plasmid DNA, a single colony from a freshly transformed plate of *E. coli* was inoculated into 5 mL LB media containing the appropriate antibiotic and incubated overnight with shaking (37 °C, 200 rpm). Cells were harvested using a microcentrifuge (13,000 rpm, 1 min, rt). For large scale purification, a single colony from a freshly transformed plate of *E. coli* was inoculated into 100 mL LB media containing the appropriate antibiotic and incubated overnight with shaking (37 °C, 200 rpm). Cells were harvested using by centrifugation (4,500 x g, 10 min, room temperature). Isolation and purification of the plasmid DNA was carried out using the Qiagen Plasmid Miniprep and Midiprep Kit's following the manufacturer's instructions. For the small scale purification, DNA was eluted from the spin column with 50 µL sterile, deionized water. For the large scale purification of DNA, the air-dried plasmid pellet was dissolved in 100–200 µL sterile, deionized water. All purified plasmids were stored at 4 °C.

6.3.3. Restriction Digestion of DNA

Table 6.7. Components of restriction digests components, volumes and final concentrations.

Component	Volume (μL)	Final Concentration
Plasmid DNA	varies	500-600 ng
10X Buffer*	2	1X
Restriction enzyme 1	1	10 U
Restriction enzyme 2 (optional)	1	10 U
Deionized water	Up to 20 μL	-

A typical restriction digest used to confirm the identity of purified plasmid DNA had a final volume of 20 μL and contained the components listed in **Table 6.7**. For a double digest, 1 μL of each required restriction enzyme was used. If a larger amount of digested plasmid DNA was required for cloning purposes or DNA assembly reaction, the volume was increased to 50 μL and all components were scaled up accordingly. The samples were incubated for 1 h (37 °C) and

quenched with 4 μL 6X loading dye containing SDS (NEB) before visualization on a 0.7% agarose gel containing ethidium bromide (0.5 μg mL^{-1}) in 1X TAE (Tris-Acetate EDTA) buffer. 1X TAE was used as the running buffer with a standard voltage of 98 V (1 h).

6.3.4. Electrocompetent MGA3 Generation and Electroporation

A procedure by Jakobsen et al. was followed for the transformation of plasmid DNA into MGA3.[13] A 100 mL culture of MGA3 was grown overnight in SOBsuc medium. This culture was reinoculated the next day into fresh SOBsuc media. When cells reached an OD_{600} of 0.25, they were harvested by centrifugation at 3,000 x g for 5 min at room temperature. The cell pellet was washed twice in 3.5 mL EP buffer, then resuspended in 0.2 mL EP buffer. Aliquots of 100 μL were stored at -80°C.

To transform competent MGA3 cells, a 100 μL aliquot was mixed with about 1 g of plasmid DNA and incubated on ice for 30 min. The mixture was transferred to an ice-cold electroporation cuvette, and the cells were exposed to a single electrical pulse (200 ; 25 F; 2.5 kV). The cells were recovered in 40 mL of SOBsuc medium for 16 h in a six-baffle, 250 mL shake flask. 10 mL of the cell culture was transferred to a six-baffle, 500 mL shake flask containing 100 mL of prewarmed SOBsuc media supplemented with the appropriate antibiotic. Growth was continued for 6 h, and the culture was plated on solid media with the same antibiotic and then incubated overnight. Transformants would appear by the following day.[13]

6.3.5. MGA3 Fed-Batch Fermentations

Fermentations with *B. methanolicus* MGA3 were performed in 1.0 L reaction volumes using a 3 L Biostat® B baffled fermenter with a DCU control tower. Fermentations were run in MVcMY media supplemented with 6 mg L^{-1} *D*-biotin and 0.01 mg L^{-1} vitamin B_{12}. Methanol was maintained at 150 mM in situ using BIOPAT MultiTrace.[14] MVcM minimal medium supplemented with 5 g

L^{-1} yeast extract was used as a control reaction containing aromatic amino acids. Growth in a fermentation containing MVcM minimal medium supplemented with (per liter) L-alanine (205 mg), L-asparagine (140 mg), L-cystine (30 mg), L-glutamate (550 mg), L-glycine (125 mg), L-histidine (55 mg), L-isoleucine (130 mg), L-leucine (185 mg), L-lysine (210 mg), L-methionine (40 mg), L-proline (110 mg), L-serine (135 mg), L-threonine (130 mg), L-valine (155 mg) would signify the ability for MGA3 to produce its aromatic supplements. External methanol feeds were supplemented with 50 mL CKNFD trace metals per liter of methanol as described by Jakobsen et al.[15] Fermentation media were autoclave-sterilized before runs. Growth was quantified at conditions of 50℃, pH 6.50, and 30% DO. A two-phase cascade control system was used to maintain DO. In phase one, agitation beginning at 400 RPM was ramped up to 1000 RPM and airflow beginning at 0.50 L min^{-1} was ramped up to 1.00 L min^{-1}. In phase two, agitation was further increased to 1800 RPM and aeration was enriched to 60% O_2. Headspace exhausts from the fermenter were passed through a condenser and Drierite and then sent to a PASPORT CO_2 Gas Sensor to quantify CO_2. Fermentations were run until the CO_2 exhaust concentration dropped considerably. Optical density was measured at 600 nm using a NanoDrop One spectrophotometer and converted to dry cell weight (DCW) using a 0.4 g DCW conversion factor.

6.3.6. Cold-Quenching and Whole-Broth Sampling Shake Flask Cultures for HPLC Analysis

A method of cold-quenching and sampling for whole-broth analysis was previously reported by Carnicer et al and used in this study.[16] Seven 4 mm diameter stainless steel beads were pre-cooled to -20℃ inside a 1 mL syringe barrel. Samples of MGA3 cultures were cold-quenched by pulling directly into the pre-cooled syringe barrel and beads (approximately 0.4 mL culture per sample) and mixed with a 3 mL sample of acetonitrile:methanol:0.1 M formic acid (40:40:20 *v*/*v*).

Samples were stored at -80°C for HPLC analysis. Before HPLC analysis, samples were lyophilized and resuspended in 1 mL of deionized water.

6.3.7. MGA3 Chemical Mutagenesis and Mutant Screening

Two different methods for chemical mutagenesis are proposed here. A procedure by Schendel et al. was modified for mutagenizing and screening *B. methanolicus*.[17] Throughout these procedures assume MGA3 cells are cultured at 50°C with 200 RPM agitation unless otherwise noted. In the first procedure, cells underwent one round of chemical mutagen exposure, were sporulated, were washed, then were screened for shikimate pathway auxotrophy. A 40 mL culture containing MVcM supplemented with 200 mM methanol and 5 g L^{-1} yeast extract was grown to late log phase in a six-baffled, 250 mL Erlenmeyer flask. 2.5 mL of the same culture media supplemented with either EMS or MNNG was combined with 2.5 mL of culture. Mutagen exposure was allowed for up to 20 min in a four-baffled, 50 mL Erlenmeyer flask. For recovery, chemical mutants were subsequently diluted 50-fold to 100 mL in a six-baffled, 500 mL Erlenmeyer flask. After 6 h, 1.5 mg $MnCl_2 \cdot 4H_2O$, 0.1 g $MgCl_2 \cdot 6H_2O$, and 0.08 g $CaCl_2$ were added, and culturing continued at 37°C to induce sporulation. After 48 h of shaking, spores were pelleted at 12,000×g, washed twice with sterile water, and stored at 4°C. It was found that the viability of stored mutant spores would diminish after two weeks. Mutants were screened on the first set of selective media described previously. Minimal media containing 5 g L^{-1} was used as a control plate containing aromatic amino acids, and minimal media lacking aromatic vitamins and containing YEMAA supplementation rather than yeast extract was used as a selective plate. Lack of growth on the selective plate but growth on the control plate would indicate auxotrophy for the shikimate pathway.

In the second procedure for chemical mutagenesis, cells underwent multiple rounds of chemical mutagen exposure. After each round of exposure to chemical mutagen cultures were diluted and immediately plated onto rich media. Colonies were gridded and screened for auxotrophy. If auxotrophy for shikimate pathway supplementation was not observed, colonies with less growth on selective media than on control media were selected and re-exposed to mutagen (and the aforementioned procedure was repeated). **Fig. 6.4** is an example of selective plates containing mutant candidates, with a candidate for further screening boxed in blue.

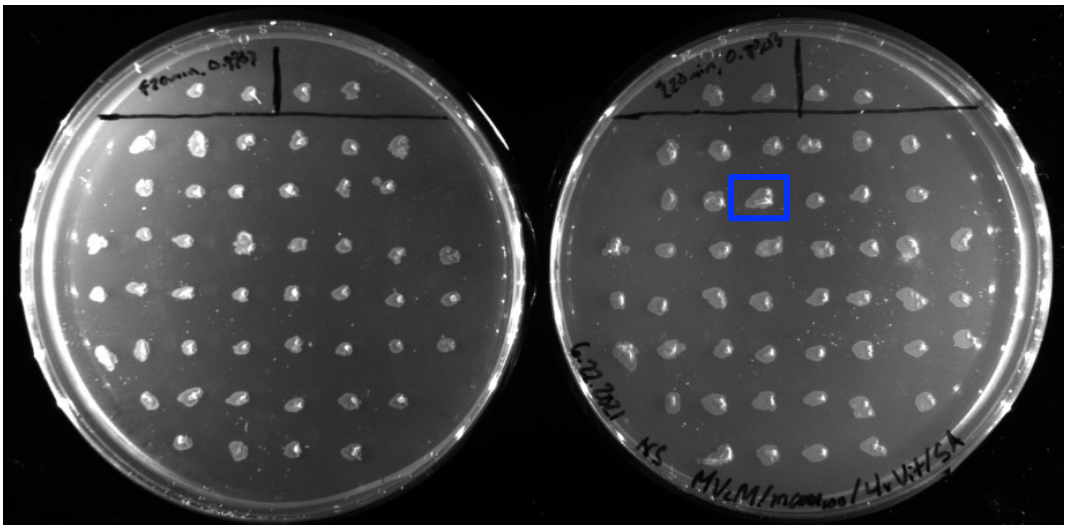

Figure 6.4. Colony screening for growth dependence on SA after replica plating the plate on the left is MVcM containing 100 mM mannitol, and 4X vitamins. The plate on the right is MVcM containing 100 mM mannitol, 4X vitamins, and 80 mg L^{-1} SA. The colony boxed in blue is YJ1.152.

A 40 mL culture containing MVcM supplemented with 200 mM methanol and 80 mg L^{-1} SA was grown to late log phase in a six-baffled, 250 mL Erlenmeyer flask. 2.5 mL of the same culture media supplemented with either EMS or MNNG was combined with 2.5 mL of culture. Mutagen exposure was allowed for up to 20 min in a four-baffled, 50 mL Erlenmeyer flask. For recovery, chemical mutants were subsequently diluted 50-fold to 100 mL with fresh media supplemented with 80 mg L^{-1} in a six-baffled, 500 mL Erlenmeyer flask. After 2 h, dilutions of mutants were plated on rich solid media. Plates that contained individually resolvable CFU were gridded onto a

second plate of rich media. Colonies were subsequently replica plated using the second set of selective media described in Section 4.2.1. Minimal media containing 80 mg L^{-1} SA was used as a control plate containing aromatic amino acids, and minimal media lacking aromatic vitamins and SA was used as a selective plate. Lack of growth on the selective plate but growth on the control plate would indicate auxotrophy with respect to the shikimate pathway. If no auxotrophy was observed, mutagenesis was continued on colonies that grew less on selective media and more on the control media.

6.3.8. Kill Curve Generation

Cells were grown to late log phase in media with aromatic supplementation in the form of either 5 g L^{-1} yeast extract or 80 mg L^{-1} SA. 2.5 mL of the same culture media supplemented with either EMS or MNNG was combined with 2.5 mL of the cell culture. A control experiment was conducted where 2.5 mL of fresh culture with no mutagen was combined with 2.5 mL of the same cell culture. Following mutagenesis, dilutions of the mutants were plated onto SOB solid media. Dilutions of the control culture were similarly plated out. The following day, plates that had distinguishable CFU were tallied.

$$\mathrm{SR}_{C,t} = 100\% \cdot \frac{CFU_M}{CFU_C} \cdot \frac{D_M}{D_C} \qquad \textbf{(6.1)}$$

Eq. 6.1 shows how survival rate, SR, for a given mutagen concentration, C, and exposure time, t. CFU_M is the number of CFU formed on a given plate of mutants. D_M is the dilution factor for that plate. CFU_C is the number of CFU formed on a plate of non-mutants. D_C is the dilution factor for that plate.

6.3.9. Construction of RNAi Knockdown Plasmids

The two-step strategy employed for the construction of RNAi plasmids is shown in **Fig. 6.5**. The low copy-number pTH1mp plasmid is used as the backbone for the construction of *as*RNA expression via a stem-loop structure. The backbone contains a methanol-inducible promotor region followed by a unique SmaI restriction site used for cloning. The plasmid also can express Cm resistance and Em resistance and contains a pUC9 origin of replication. First, reverse complementary paired termini are inserted into the SmaI restriction site of pTH1mp. The resulting pTH1mp_null plasmid contains a strategically located XhoI restriction site in between the two paired termini for insertion of an *as*RNA coding region. In the second step, an antisense region complementary to the *aroE* gene on the genome of *B. methanolicus* MGA3 is inserted into the XhoI site of pTH1mp_null.

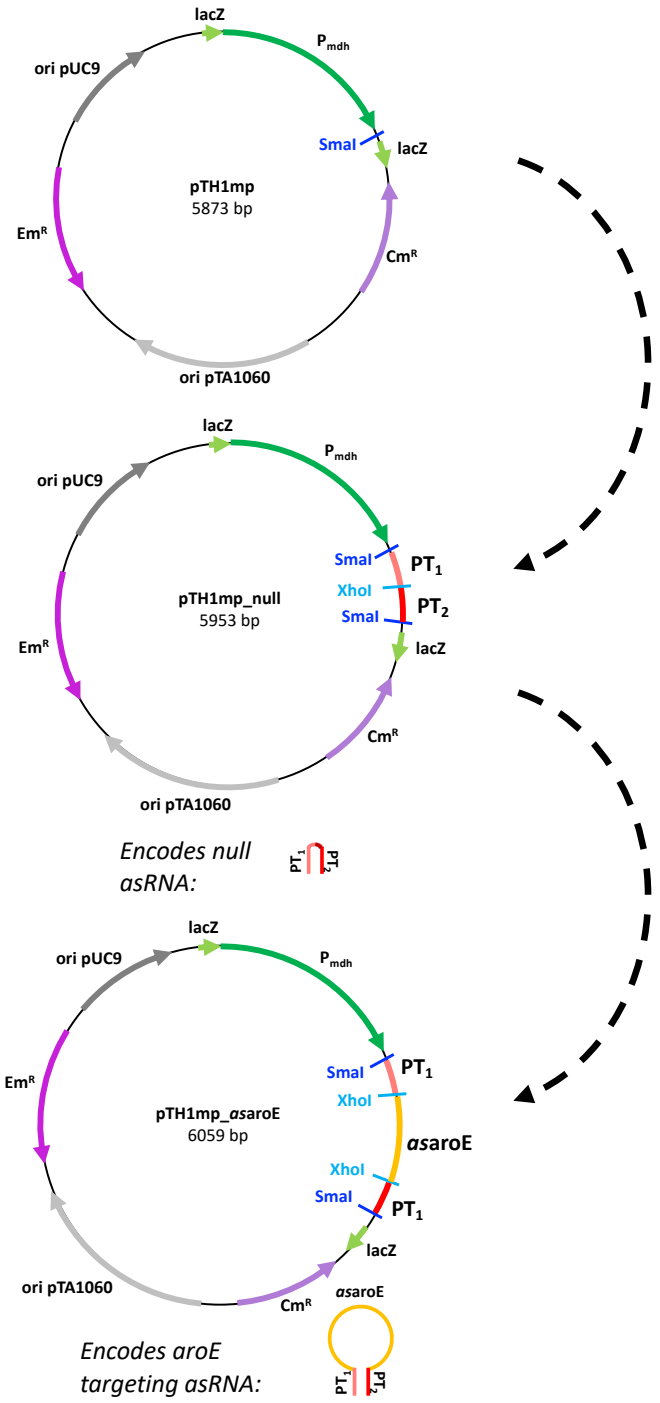

Figure 6.5. Construction of pTH1mp_*as*aroE plasmids two step strategy to construct plasmid for gene knockdown of B. methanolicus MGA3 aroE gene using asRNA. Both cloning steps involve single pot, isothermal reaction for combining overlapping DNA fragments. Step 1: reverse-complementary paired termini (PT) pieces of asRNA step-loop structure cloned into unique SmaI restriction site existing immediately after P_{mdh} promoter. Step 2: loop segment of stem-loop structure cloned into XhoI restriction site existing in center of two PT fragments. Loop segment is complementary to aroE gene on genome of B. methanolicus MGA3.

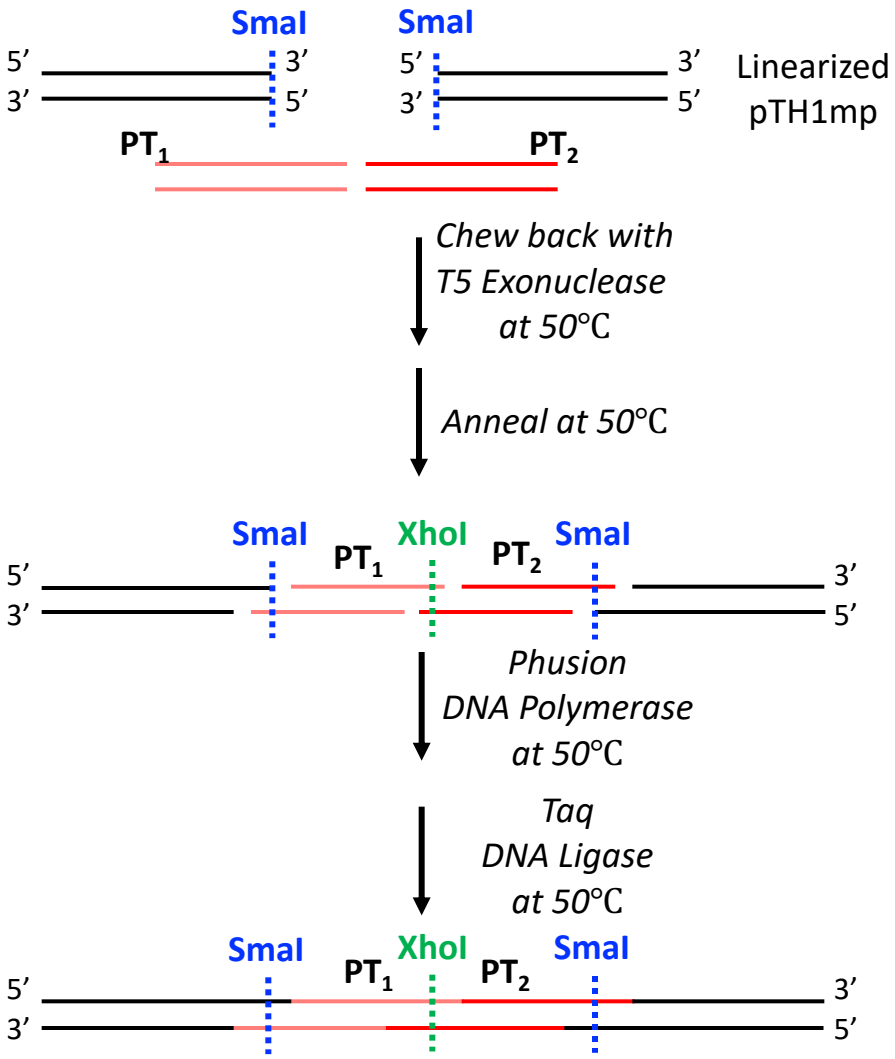

Figure 6.6. Gibson assembly of pTH1mp_null Gibson assembly of SmaI linearized pTH1mp, YJ040, and YJ041 to afford pTH1mp_null.

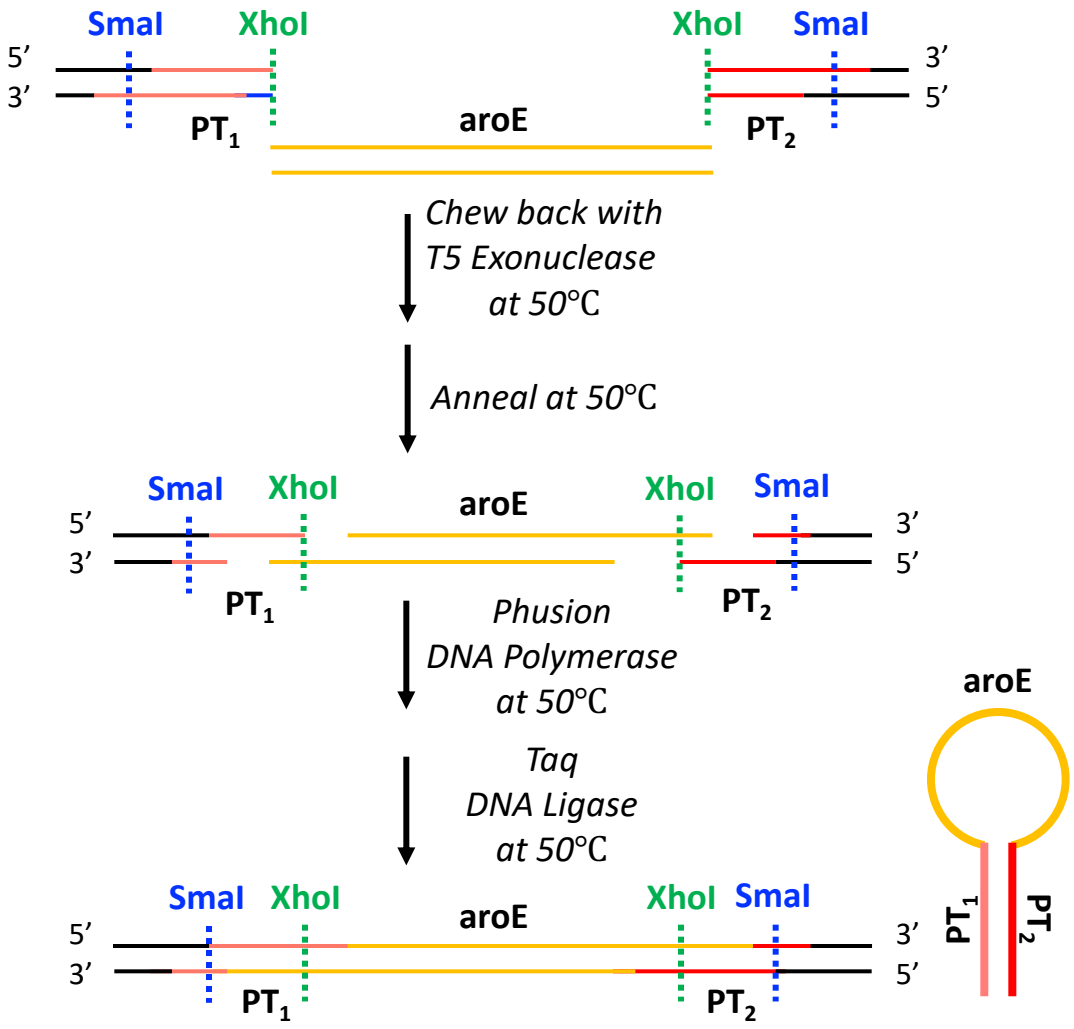

Figure 6.7. Gibson assembly of pTH1mp_*as*aroE plasmids Gibson assembly of XhoI linearized pTH1mp_null and PCR amplified asRNA region complementary to aroE transcript.

The method of Gibson assembly was adopted for a single-step isothermal assembly of overlapping double-stranded DNA (dsDNA) fragments.[9] Synthetic paired termini *ds*DNA fragments YJ040 and YJ041 (**Table 6.7**) were purchased from IDT. After pTH1mp was linearized with SmaI, 5 μL of DNA containing 50 ng each of YJ040, YJ041, and linearized pTH1mp was combined with 15 μL of Gibson assembly master mix. The reaction mixture was incubated at 50°C for 1 h. During this time T5 exonuclease would chew back the 5' ends of all *ds*DNA fragments, and the complementary 3' end overhangs would be assembled and ligated by Phusion DNA

polymerase and Taq ligase (**Fig. 6.6**). The assembly of pTH1mp_null was designed such that a unique XhoI restriction site would exist between the two paired termini for future assembly with *as*RNA coding regions. Upon induction with methanol, pTH1mp_null would express only the stem structure of the total stem-loop structure that would be expressed for RNAi. **Fig. A.6.9** shows the minimum free energy structure of the stem found using RNA Fold.[18]

The Gibson assembly method was also used for the single-step isothermal assembly of pTH1mp_null and antisense region-encoding *ds*DNA fragments.[9] The *ds*DNA encoding the *as*RNA loop region of the stem-loop structure was PCR-amplified and gel-purified. Primers YJ042 and YJ043 (**Table 6.7**) were forward and reverse primers used to amplify *ds*DNA for targeting the central part of the MGA3 *aroE* gene. Primers YJ046 and YJ047 (**Table 6.7**) were forward and reverse primers used to amplify *ds*DNA for targeting the RBS, start codon, and part of the central part of *aroE*. After pTH1mp_null was linearized with XhoI, 5 μL of DNA containing 50 ng each of the respective amplified PCR fragments and linearized pTH1mp_null was combined with 15 μL of Gibson assembly master mix. The reaction mixture was incubated at 50℃ for 1 h. T5 exonuclease, Phusion DNA polymerase, and Taq ligase assembled the two fragments as described before. Upon induction with methanol, these plasmids would express the total stem-loop structure for RNAi. **Fig. A.6.10** shows the minimum free energy structure of the stem found using RNA Fold.[18]

6.3.10. Construction of CRISPRi Knockdown Plasmids

A second strategy was attempted for the knockdown of the *aroE* gene in MGA3 using CRISPRi. The plasmid backbone used for CRISPRi was the mannitol-inducible piCas (**Fig. 6.8**). Plasmid piCas can also express Cm resistance, Kan resistance, and an inactive form of the Cas9 protein known as dead Cas9 (*d*Cas9). A single-step Gibson assembly strategy was employed for

assembling linearized piCas with two single-stranded DNA (*ss*DNA) fragments encoding sgRNA targeting *aroE*. Linearization of piCas was performed using an AvaI and XbaI double-digest of the two unique restriction sites immediately following the P_{m2p} promoter. Synthetic *ss*DNA fragments YJ065 and YJ066 (**Table 6.7**) were purchased from IDT. 5 μL of DNA containing 50 ng each of YJ065, YJ066, and linearized piCas was combined with 15 μL of Gibson assembly master mix. The reaction mixture was incubated at 50°C for 1 h. During this time T5 exonuclease would chew-back the 5' ends of all *ds*DNA fragments, and the complementary 3' end overhangs would be assembled and ligated by Phusion DNA polymerase and Taq ligase (**Fig. 6.9**). The resulting plasmid was named piCas_aroEsgRNA1. Upon induction with 12.5 mM mannitol, piCas_aroEsgRNA1 would express an inactive Cas9 protein that would target and latch onto DNA encoding *aroE*, presumably knocking down its transcription. The *sg*RNA of piCas_aroEsgRNA1 is of the sequence 5'-TTTTTCAAAAGCGAGCGCTC-3'.

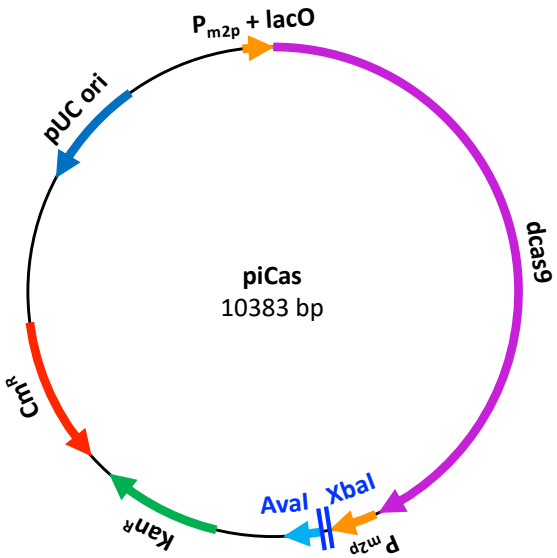

Figure 6.8. Plasmid piCas plasmid map of piCas.

Table 6.8. Primer and oligonucleotide sequences and descriptions primers and oligonucleotide names, sequences, and descriptions of their application to *B. methanolicus* MGA3 studies.

Oligo.	Sequence (5' to 3')	Description
YJ040	TGGTGGTGGTGGTGCTCGAGCACCACCA CCACCACTGCATGGTTAATTCCTCCTCCC GGGAATTCAAGCTTTAAACA	Paired terminus for Gibson assembly
YJ041	CGGGTACCATATGGATCCCCGGGAGGA GGAATTAACCATGCAGTGGTGGTGGTGG TGCTCGAGCACCACCACCACCA	Paired terminus for Gibson assembly
YJ042	TGCAGTGGTGGTGGTGGTGCGCTGCTTT TTCAGCTGTCCGATTACAAAAATC	Forward primer for PCR amplification of 100 bp central segment of *aroE*
YJ043	TGCAGTGGTGGTGGTGGTGCTCATCGGT GCAGGCGGCG	Reverse primer for PCR amplification of 100 bp central segment of *aroE*
YJ046	TGCAGTGGTGGTGGTGGTGCATCATTAT GCATCACAGG	Forward primer for PCR amplification of 100 bp RBS and start codon segment of *aroE*
YJ047	TGCAGTGGTGGTGGTGGTGCTCAAAAAG TCTGTATGGG	Reverse primer for PCR amplification of 100 bp RBS an start codon segment of *aroE*
YJ065	TTTTTCAAAAGCGAGCGCTCATATTTAT CATAAAACGTTT	Synthetic *ss*DNA for assembling *sg*RNA targeting *aroE* gene
YJ066	GAGCGCTCGCTTTTGAAAAAGTTTTAGA GCTAGAAATAGC	Synthetic *ss*DNA for assembling *sg*RNA targeting *aroE* gene

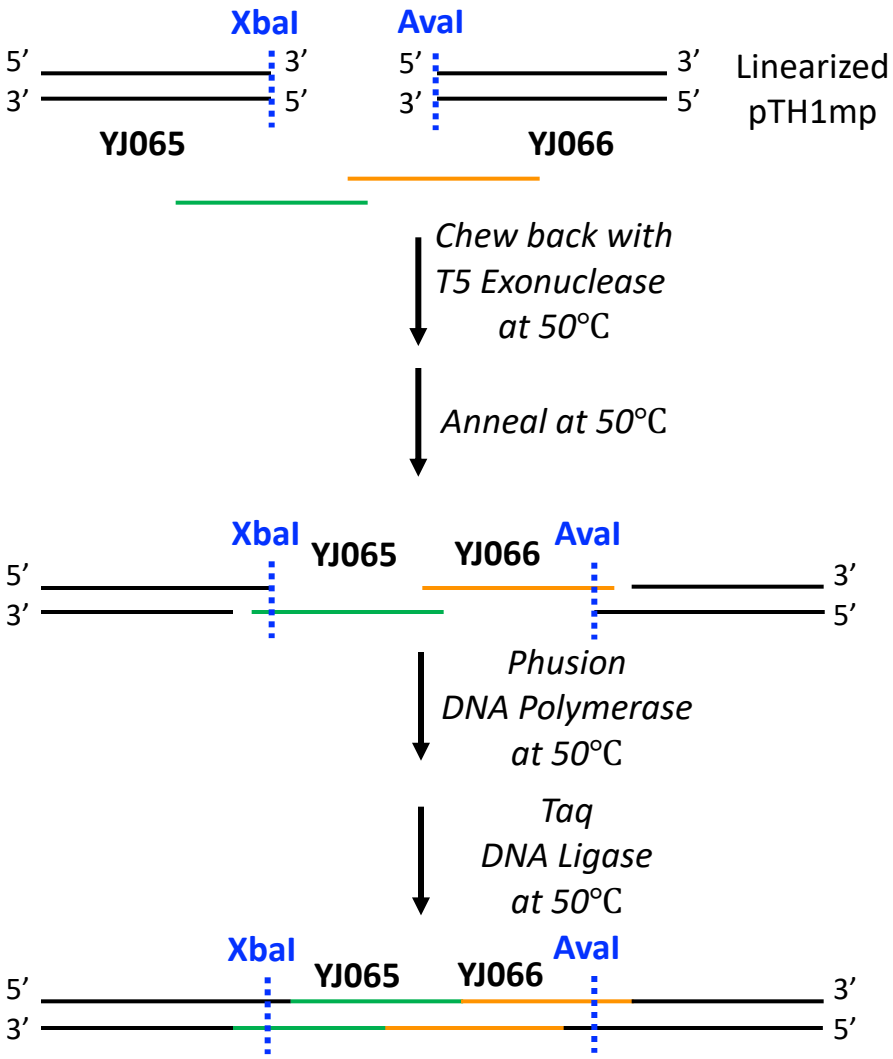

Figure 6.9. Gibson assembly using piCas Gibson assembly of AvaI and XbaI linearized piCas, YJ065, and YJ066 to afford piCas_aroEsgRNA1.

REFERENCES

[1] Niu, W.; Draths, K. M.; Frost, J. W."Benzene-Free Synthesis of Adipic Acid" Applied and Environmental Microbiology **2012**, *78*(15), 5170-5181.

[2] Sambrook, J.; Russell, D. W. Molecular Cloning: A Laboratory Manual 3rd ed.; Cold Spring Harbor Laboratory: Cold Spring Harbor, NY, **2001**.

[3] Chandran, S. S.; Yi, J.; Draths, K. M.; von Daeniken, R.; Weber, W.; Frost, J. W. "Phosphoenolpyruvate Availability and the Biosynthesis of Shikimic Acid" *Biotechnology Progress* **2008**, *19*(3), 808-814.

[4] Chandran, S. S. "Manipulation of genes and enzymes in the shikimate pathway" *A Dissertation*, MSU **2000**, 75.

[5] Prather, K. L. J.; Reisch, C. R. "The no-SCAR (Scarless Cas9 Assisted Recombineering) system for genome editing in *Escherichia coli*" *Science Reports* **2015**, 5:15096.

[6] Saragliadis, A.; Trunk, T.; Leo, J. C. "Producing Gene Deletions in *Escherichia coli* by P1 Transduction with Excisable Antibiotic Resistance Cassettes" *J. Vis. Exp.* **2018**, (139), e58267.

[7] Datsenko, K. A.; Wanner, B. L. "One-step inactivation of chromosomal genes in *Escherichia coli* K-12 using PCR products" *PNAS* **2000**, 97(12), 6640-6645.

[8] Li, K. "Microbial Syntheses of Value-Added Chemicals from *D*-Glucose" **1999**, *A PhD Dissertation*.

[9] Gibson, D. G. "Enzyme Assembly of Overlapping DNA Fragments" *Methods in Enzymology*, Chapter 15 **2011**, *498*, 349-361.

[10] Gibson, D. G. "Enzymatic Assembly of Overlapping DNA Fragments" *Methods in Enzymology* **2011**, *498*, 349-361.

[11] Irla, M.; Heggeset, T. M.; Nærdal, I.; Paul, L.; Haugen, T.; Le, S. B.; Brautaset, T.; Wendisch, V. F. "Genome-Based Genetic Tool Development for Bacillus methanolicus: Theta- and Rolling Circle-Replicating Plasmids for Inducible Gene Expression and Application to Methanol-Based Cadaverine Production" *Front. Microbiol.* **2016**, *7*, 1481.

[12] Schultenkämper, K.; Brito, L. F.; López, M. G.; Brautaset, T.; Wendisch, V. F. "Establishment and Application of CRISPR Interference to Affect Sporulation, Hydrogen Peroxide Detoxification, and Mannitol Catabolism in the Methylotrophic Thermophile Bacillus methanolicus." Appl. Microbiol. Biotechnol. **2019**, *103*(14), 5879–5889.

[13] Jakobsen, Ø. M., Benichou, A., Flickinger, M. C., Valla, S., Ellingsen, T. E., Brautaset, T. "Upregulated transcription of plasmid and chromosomal ribulose monophosphate pathway genes

is critical for methanol assimilation rate and methanol tolerance in the methylotrophic bacterium *Bacillus methanolicus*" *J. Bacteriol.* **2006**, *188*, 3063–3072.

[14] Kopec, D. "Control of Critical Process Parameters Using In-Situ Analytics" *Bioprocess International*, **2017**, *15*, 11.

[15] Jakobsen, Ø. M.; Brautaset, T.; Degnes, K. F.; Heggeset, T. M. B.; Balzer, S.; Flickinger, M. C.; Valla, S.; Ellingsen, T. E. "Overexpression of Wild-Type Aspartokinase Increases L-Lysine Production in the Thermotolerant Methylotrophic Bacterium *Bacillus methanolicus*" *Applied and Environmental Microbiology* **2009**, *75*(3), 652-661.

[16] Carnicer, M.; Vieira, G.; Brautaset, T.; Portais, J. C.; Heux, S. "Quantitative metabolomics of the thermophilic methylotroph *Bacillus methanolicus*" *Microb Cel Fact* **2016**, *15*, 92.

[17] Schendel, F. J.; Bremmon, C. E.; Flickinger, M. C.; Guettler, M.; Hanson, R. S. "L-Lysine Production at 50°C by Mutants of a Newly Isolated and Characterized Methylotrophic *Bacillus sp*." **1990**, *Applied and Environmental Microbiology*, *56*(4), 963-970.

[18] *RNAfold Web Server*, Institute for Theoretical Chemistry, University of Vienna. http://rna.tbi.univie.ac.at/cgi-bin/RNAWebSuite/RNAfold.cgi

[19] Knop, D. R.; Draths, K. M.; Chandran, S. S.; Barker, J. L.; von Daeniken, R.; Weber, W.; Frost, J. W. "Hydroaromatic Equilibration During Biosynthesis of Shikimic Acid" *J. Am. Chem. Soc.*, **2001**, 123, 10173-10182.

[20] Brautaset, T.; Jakobsen, Ø. M.; Josefsen, K. D.; Flickinger, M. C.; Ellingsen, T. E. "*Bacillus methanolicus*: a candidate for industrial production of amino acids from methanol at 50°C" *Appl. Microbiol. Biotechnol.* **2007**, *74*, 22-34.

[21] Quan, J.; Tian, J. "Circular polymerase extension cloning of complex gene libraries and pathways." *PloS one*, **2009**, 4(7), e6441.

[22] Zhong, Y.; Frost, H.; Bustamante, M.; Li, S.; Liu, Y. S.; Liao, W. "A mechano-biocatalytic one-pot approach to release sugars from lignocellulosic materials" *Renewable and Sustainable Energy Reviews* **2020**, *121*, 109675.

Table A.2.1. YJ1.130/pKD12.138A growth on D-glucose raw data time points from each of n = 2 replicate fermentations and their average values. Each time point included titer measurements of DCW, D-glucose, SA, QA, and DHS.

N	Time (h)	DCW_1 (g L^{-1})	DCW_2 (g L^{-1})	DCW_3 (g L^{-1})	D-Gluc (g L^{-1})	D-Xyl (g L^{-1})	SA (g L^{-1})	QA (g L^{-1})	DHS (g L^{-1})
	0	0.1	0.1	0.1	19.5	-	0.0	0.0	0.0
	2	0.1	0.1	0.1	19.0	-	0.0	0.0	0.0
	4	0.2	0.2	0.2	19.2	-	0.0	0.0	0.0
	8	1.0	1.1	1.1	18.0	-	0.3	0.0	0.0
	12	4.7	6.9	5.2	8.9	-	1.0	0.0	0.0
1	18	34.0	35.4	34.9	3.5	-	7.6	0.2	1.0
	24	36.5	33.9	35.4	27.2	-	23.6	0.4	3.4
	30	34.1	31.3	31.3	28.8	-	37.1	0.5	4.8
	36	35.1	32.8	31.6	39.5	-	52.6	1.6	8.8
	42	34.8	36.1	34.8	62.6	-	72.0	1.1	11.7
	48	36.1	32.3	34.2	61.2	-	76.2	1.2	13.2
	0	0.1	0.1	0.1	19.1	-	0.0	0.0	0.0
	2	0.2	0.2	0.2	20.2	-	0.0	0.0	0.0
	4	0.2	0.2	0.2	20.2	-	0.0	0.0	0.0
	8	1.0	1.1	1.0	18.6	-	0.0	0.0	0.0
	12	6.0	6.0	5.6	11.7	-	1.1	0.0	0.0
2	18	34.9	36.3	36.8	2.9	-	5.6	0.2	0.2
	24	36.5	34.9	38.5	27.6	-	24.3	0.4	1.2
	30	34.1	32.4	34.1	27.9	-	36.8	0.5	1.6
	36	35.1	33.9	34.5	38.9	-	55.0	1.5	3.8
	42	34.8	37.4	38.1	66.2	-	80.5	2.8	4.0
	48	36.1	33.5	37.4	61.4	-	79.8	1.8	3.5
	0		0.1		19.3	-	0.0	0.0	0.0
	2		0.1		19.6	-	0.0	0.0	0.0
	4		0.2		19.7	-	0.0	0.0	0.0
	8		1.1		18.3	-	0.2	0.0	0.0
	12		5.7		10.3	-	1.0	0.0	0.0
AVG	18		35.4		3.2	-	6.6	0.2	0.6
	24		36.0		27.4	-	24.0	0.4	2.3
	30		32.9		28.3	-	37.0	0.5	3.2
	36		33.8		39.2	-	53.8	1.6	6.3
	42		36.0		64.4	-	76.2	1.9	7.8
	48		34.9		61.3	-	78.0	1.5	8.4

Table A.2.2. YJ1.130/pKD12.138A growth on D-glucose and D-xylose raw data time points from each of n = 2 replicate fermentations and their average values. Each time point included titer measurements of DCW, D-glucose, D-xylose, SA, QA, and DHS.

N	Time (h)	DCW_1 (g L^{-1})	DCW_2 (g L^{-1})	DCW_3 (g L^{-1})	D-Gluc (g L^{-1})	D-Xyl (g L^{-1})	SA (g L^{-1})	QA (g L^{-1})	DHS (g L^{-1})
	0	0.1	0.1	0.1	12.1	5.3	0.0	0.0	0.0
	2	0.1	0.1	0.1	13.0	5.6	0.0	0.0	0.0
	4	0.2	0.2	0.2	12.8	5.5	0.1	0.0	0.0
	8	1.0	1.0	1.1	11.5	5.5	0.3	0.0	0.0
	12	5.3	5.7	5.7	7.8	7.1	0.9	0.0	0.0
1	18	30.9	31.8	33.3	1.5	26.9	7.4	0.2	0.6
	24	39.7	36.9	39.1	37.3	62.6	21.4	1.1	2.6
	30	39.9	43.7	40.5	51.2	84.4	39.7	1.4	5.1
	36	43.2	37.4	35.5	25.9	84.6	44.9	1.3	4.8
	42	38.1	38.1	35.5	0.4	80.6	56.8	1.9	7.7
	48	30.3	32.3	37.4	0.6	79.4	56.9	2.1	6.4
	0	0.1	0.1	0.1	15.7	7.8	0.0	0.0	0.0
	2	0.1	0.2	0.1	15.6	7.7	0.0	0.0	0.0
	4	0.2	0.2	0.2	14.3	6.1	0.0	0.0	0.0
	8	1.1	1.3	1.2	12.1	6.1	0.2	0.0	0.0
	12	6.2	6.6	5.7	8.8	6.4	0.7	0.0	0.0
2	18	29.4	31.3	32.8	27.2	30.0	8.5	0.2	0.4
	24	33.5	30.6	34.0	49.7	78.5	32.3	0.5	2.4
	30	34.2	34.2	34.8	63.9	95.8	42.9	1.0	3.1
	36	34.2	33.5	33.5	28.2	98.7	56.9	1.4	3.8
	42	30.3	34.2	33.5	0.0	88.4	63.5	2.6	2.7
	48	33.5	32.9	32.9	0.0	88.3	65.9	3.1	3.9
	0		0.1		13.9	6.5	0.0	0.0	0.0
	2		0.1		14.3	6.6	0.0	0.0	0.0
	4		0.2		13.6	5.8	0.0	0.0	0.0
	8		1.1		11.8	5.8	0.2	0.0	0.0
	12		5.9		8.3	6.7	0.8	0.0	0.0
AVG	18		31.6		14.3	28.5	7.9	0.2	0.5
	24		35.6		43.5	70.6	26.8	0.8	2.5
	30		37.9		57.5	90.1	41.3	1.2	4.1
	36		36.2		27.0	91.7	50.9	1.4	4.3
	42		34.9		0.2	84.5	60.1	2.3	5.2
	48		33.2		0.3	83.9	61.4	2.6	5.2

Table A.2.3. YJ1.144/pSC6.090B growth on D-glucose raw data time points from each of n = 2 replicate fermentations and their average values. Each time point included titer measurements of DCW, D-glucose, SA, QA, and DHS.

N	Time (h)	DCW_1 (g L^{-1})	DCW_2 (g L^{-1})	DCW_3 (g L^{-1})	D-Gluc (g L^{-1})	D-Xyl (g L^{-1})	SA (g L^{-1})	QA (g L^{-1})	DHS (g L^{-1})
	0	0.1	0.1	0.1	16.9	-	0.0	0.0	0.0
	2	0.1	0.1	0.1	18.3	-	0.0	0.0	0.0
	4	0.2	0.2	0.2	16.4	-	0.1	0.0	0.0
	8	0.4	0.3	0.3	17.6	-	0.1	0.0	0.0
	12	0.9	1.0	1.0	14.4	-	0.3	0.1	0.0
1	18	4.3	4.4	4.4	19.1	-	1.6	0.8	0.5
	24	21.1	22.1	19.5	17.8	-	9.8	5.4	4.9
	30	35.2	39.0	37.4	13.8	-	26.1	11.8	15.0
	36	32.2	32.2	29.3	7.9	-	44.3	18.0	24.0
	42	31.6	32.3	34.8	39.5	-	63.4	23.1	31.9
	48	31.6	28.4	32.3	56.0	-	62.4	23.2	31.8
	0	0.1	0.1	0.1	13.6	-	0.0	0.0	0.0
	2	0.2	0.2	0.1	13.1	-	0.0	0.0	0.0
	4	0.2	0.2	0.2	13.2	-	0.0	0.0	0.0
	8	0.6	0.6	0.7	13.0	-	0.2	0.0	0.0
	12	1.8	1.8	1.9	12.1	-	0.3	0.1	0.0
2	18	12.9	11.0	9.7	26.3	-	0.9	0.7	0.2
	24	38.5	41.1	39.5	31.6	-	3.0	2.3	1.0
	30	39.6	39.6	41.8	14.7	-	11.7	7.4	3.5
	36	39.8	35.7	34.5	22.4	-	27.5	15.6	7.5
	42	38.7	38.1	34.2	33.3	-	38.2	21.3	9.0
	48	38.7	36.1	36.8	35.4	-	47.3	23.7	10.6
	0		0.1		15.2	-	0.0	0.0	0.0
	2		0.1		15.7	-	0.0	0.0	0.0
	4		0.2		14.8	-	0.1	0.0	0.0
	8		0.5		15.3	-	0.2	0.0	0.0
	12		1.4		13.2	-	0.3	0.1	0.0
AVG	18		7.5		22.0	-	1.2	0.8	0.3
	24		27.8		22.7	-	5.9	3.5	2.7
	30		35.5		13.1	-	17.3	8.8	8.5
	36		30.7		13.7	-	32.5	15.2	14.3
	42		31.8		33.2	-	46.3	20.2	18.6
	48		34.0		45.7	-	54.9	23.5	21.2

Table A.2.4. YJ1.144/pSC6.090B growth on D-glucose and D-xylose raw data time points from each of n = 2 replicate fermentations and their average values. Each time point included titer measurements of DCW, D-glucose, D-xylose, SA, QA, and DHS.

N	Time (h)	DCW_1 (g L^{-1})	DCW_2 (g L^{-1})	DCW_3 (g L^{-1})	D-Gluc (g L^{-1})	D-Xyl (g L^{-1})	SA (g L^{-1})	QA (g L^{-1})	DHS (g L^{-1})
	0	0.1	0.1	0.1	11.9	5.0	0.0	0.0	0.0
	2	0.1	0.1	0.1	11.4	4.8	0.0	0.0	0.0
	4	0.1	0.1	0.1	12.2	4.8	0.1	0.0	0.0
	8	0.3	0.4	0.3	11.8	4.7	0.2	0.0	0.0
	12	1.3	1.1	1.1	8.8	3.2	0.7	0.0	0.0
1	18	8.8	10.3	10.3	5.9	1.8	7.7	0.3	1.8
	24	36.3	35.7	34.6	21.9	4.4	31.1	1.3	8.3
	30	35.5	36.1	38.6	28.9	5.7	52.3	3.0	15.2
	36	36.1	35.5	34.2	16.1	6.1	70.7	4.0	21.5
	42	30.3	32.9	31.6	29.9	9.7	85.4	4.7	24.2
	48	28.4	29.0	31.6	17.8	7.4	96.3	5.0	21.7
	0	0.1	0.1	0.1	13.3	5.5	0.0	0.0	0.0
	2	0.1	0.1	0.2	13.5	5.9	0.0	0.0	0.0
	4	0.2	0.2	0.2	13.3	5.9	0.1	0.0	0.0
	8	0.9	0.9	0.9	12.9	5.6	0.2	0.0	0.0
	12	3.0	3.1	3.3	12.1	5.1	0.4	0.2	0.0
2	18	28.9	27.9	28.9	19.4	6.7	2.8	0.4	0.4
	24	39.7	39.7	40.3	10.4	2.7	17.8	3.1	3.2
	30	38.6	39.2	41.1	9.7	2.9	39.4	6.0	7.1
	36	38.1	38.1	34.8	25.9	9.0	56.7	8.9	7.8
	42	38.1	32.9	35.5	32.3	12.6	75.4	10.8	9.4
	48	37.4	36.1	36.8	11.8	7.8	87.1	11.7	10.5
	0		0.1		12.6	5.2	0.0	0.0	0.0
	2		0.1		12.4	5.4	0.0	0.0	0.0
	4		0.2		12.7	5.4	0.1	0.0	0.0
	8		0.6		12.3	5.1	0.2	0.0	0.0
	12		2.1		10.5	4.1	0.5	0.1	0.0
AVG	18		18.1		12.6	4.2	5.3	0.3	1.1
	24		34.2		16.1	3.5	24.5	2.2	5.8
	30		33.7		19.3	4.3	45.8	4.5	11.2
	36		32.4		21.0	7.5	63.7	6.5	14.7
	42		33.5		31.1	11.1	80.4	7.8	16.8
	48		33.2		14.8	7.6	91.7	8.3	16.1

Table A.2.5. YJ1.148/pKD12.138A growth on D-glucose raw data time points from each of n = 2 replicate fermentations and their average values. Each time point included titer measurements of DCW, D-glucose, SA, QA, and DHS.

N	Time (h)	DCW_1 (g L^{-1})	DCW_2 (g L^{-1})	DCW_3 (g L^{-1})	D-Gluc (g L^{-1})	D-Xyl (g L^{-1})	SA (g L^{-1})	QA (g L^{-1})	DHS (g L^{-1})
	0	0.1	0.1	0.1	18.6	-	0.0	0.0	0.0
	2	0.2	0.2	0.2	21.1	-	0.0	0.0	0.0
	4	0.3	0.2	0.2	17.1	-	0.0	0.0	0.0
	8	0.7	0.7	0.6	17.9	-	0.1	0.0	0.0
	12	2.6	2.5	2.6	13.6	-	0.5	0.0	0.1
1	18	17.7	18.1	18.6	1.9	-	5.3	0.4	1.1
	24	35.5	33.0	32.5	1.1	-	12.9	5.8	5.1
	30	36.1	35.0	35.0	14.9	-	33.7	14.6	14.7
	36	32.2	34.5	35.1	30.9	-	54.6	2.2	10.4
	42	35.3	34.1	32.3	56.0	-	62.8	24.3	24.1
	48	35.5	36.1	33.5	38.9	-	79.1	28.3	29.1
	0	0.1	0.1	0.1	19.9	-	0.0	0.0	0.0
	2	0.2	0.2	0.2	19.3	-	0.0	0.0	0.0
	4	0.2	0.2	0.2	18.9	-	0.0	0.0	0.0
	8	0.6	0.7	0.7	17.2	-	0.0	0.0	0.0
	12	2.6	2.5	2.5	16.1	-	0.0	0.0	0.0
2	18	19.0	18.6	19.0	20.5	-	0.0	0.1	1.3
	24	31.0	33.0	33.0	23.1	-	0.0	1.0	14.6
	30	36.7	40.0	42.2	39.4	-	0.0	1.5	25.4
	36	38.0	40.4	38.6	34.3	-	0.0	1.8	39.3
	42	35.3	37.8	34.7	28.9	-	0.0	1.7	38.8
	48	35.5	36.8	36.8	27.7	-	0.0	3.2	41.0
	0		0.1		19.3	-	0.0	0.0	0.0
	2		0.2		20.2	-	0.0	0.0	0.0
	4		0.2		18.0	-	0.0	0.0	0.0
	8		0.7		17.6	-	0.1	0.0	0.0
	12		2.5		14.8	-	0.5	0.0	0.1
AVG	18		18.5		11.2	-	4.5	0.3	1.2
	24		33.0		12.1	-	18.0	3.4	9.9
	30		37.5		27.2	-	38.7	8.0	20.0
	36		36.5		32.6	-	59.4	2.0	24.9
	42		34.9		42.4	-	67.5	13.0	31.4
	48		35.7		33.3	-	83.9	15.8	35.1

Table A.2.6. YJ1.148/pKD12.138A growth on D-glucose and D-xylose raw data time points from each of n = 2 replicate fermentations and their average values. Each time point included titer measurements of DCW, D-glucose, D-xylose, SA, QA, and DHS.

N	Time (h)	DCW_1 (g L^{-1})	DCW_2 (g L^{-1})	DCW_3 (g L^{-1})	D-Gluc (g L^{-1})	D-Xyl (g L^{-1})	SA (g L^{-1})	QA (g L^{-1})	DHS (g L^{-1})
	0	0.1	0.1	0.1	21.7	9.2	0.0	0.0	0.0
	2	0.1	0.1	0.1	20.5	8.9	0.0	0.0	0.0
	4	0.2	0.2	0.2	21.1	9.3	0.1	0.0	0.0
	8	0.5	0.5	0.6	20.5	9.1	0.2	0.0	0.0
	12	2.4	2.5	2.7	14.9	8.0	1.0	0.2	0.0
1	18	16.8	16.3	17.2	13.8	7.9	8.2	0.9	1.5
	24	33.1	35.2	32.6	18.0	12.0	31.5	3.7	5.8
	30	34.0	32.8	32.8	74.0	43.0	81.1	2.8	10.5
	36	37.4	32.9	32.3	52.0	32.1	87.4	8.1	14.1
	42	31.6	33.5	31.0	67.7	35.6	93.9	8.7	11.7
	48	31.6	31.0	32.9	51.7	26.6	113.3	8.9	20.4
	0	0.1	0.1	0.1	12.7	5.5	0.0	0.0	0.0
	2	0.1	0.1	0.2	12.4	5.1	0.0	0.0	0.0
	4	0.2	0.2	0.2	11.8	5.0	0.1	0.0	0.0
	8	0.6	0.6	0.7	12.4	5.4	0.2	0.0	0.0
	12	2.6	2.7	2.9	9.3	4.9	0.5	0.0	0.0
2	18	20.9	19.1	20.9	10.9	7.7	3.3	0.1	0.6
	24	35.7	34.7	36.8	26.1	16.3	24.2	0.8	8.2
	30	0.0	0.0	0.0	47.1	25.3	46.6	1.0	19.9
	36	36.8	36.1	38.1	54.3	27.8	64.2	1.5	29.3
	42	34.8	34.8	36.8	20.8	15.4	72.8	2.2	31.3
	48	34.2	35.5	34.2	5.7	9.9	89.8	2.7	37.3
	0		0.1		17.2	7.3	0.0	0.0	0.0
	2		0.1		16.4	7.0	0.0	0.0	0.0
	4		0.2		16.4	7.1	0.1	0.0	0.0
	8		0.6		16.5	7.2	0.2	0.0	0.0
	12		2.6		12.1	6.4	0.8	0.1	0.0
AVG	18		18.5		12.4	7.8	5.8	0.5	1.1
	24		34.7		22.0	14.2	27.9	2.3	7.0
	30		33.2		60.6	34.2	63.9	1.9	15.2
	36		35.6		53.2	29.9	75.8	4.8	21.7
	42		33.8		44.3	25.5	83.3	5.4	21.5
	48		33.2		28.7	18.3	101.6	5.8	28.8

Table A.2.7. YJ1.144/pSC6.090B growth on D-glucose, D-xylose, and acetate raw data time points from each of n = 1 replicate fermentations and their average values. Each time point included titer measurements of DCW, D-glucose, D-xylose, SA, QA, and DHS.

N	Time (h)	DCW_1 (g L^{-1})	DCW_2 (g L^{-1})	DCW_3 (g L^{-1})	DCW_{avg} (g L^{-1})	D-Gluc (g L^{-1})	D-Xyl (g L^{-1})	SA (g L^{-1})	QA (g L^{-1})	DHS (g L^{-1})
	0	0.1	0.1	0.1	0.1	20.3	9.0	0.0	0.0	0.0
	3	0.1	0.1	0.1	0.1	22.8	10.1	0.0	0.0	0.0
	6	0.2	0.2	0.2	0.2	22.7	9.9	0.0	0.0	0.0
	9	0.6	0.6	0.6	0.6	21.9	8.9	0.2	0.0	0.0
	13	1.5	1.6	1.7	1.6	20.2	8.1	0.9	0.0	0.0
1	18	12.5	12.5	11.6	12.2	13.2	3.3	2.9	0.6	0.4
	24	29.8	30.7	31.2	30.6	1.7	1.4	10.9	5.9	2.3
	30	29.4	29.4	30.3	29.7	1.5	1.6	18.8	14.6	4.4
	36	31.7	32.7	33.3	32.6	1.7	2.1	34.7	25.4	7.9
	42	39.5	40.1	37.2	38.9	1.8	2.1	50.0	34.7	9.7
	48	32.3	32.9	33.5	32.9	2.4	2.6	59.0	40.2	11.2

Table A.2.8. YJ1.144/pSC6.090B growth on corn stover-derived hydrolysates raw data time points from each of n = 1 replicate fermentations and their average values. Each time point included titer measurements of DCW, D-glucose, D-xylose, SA, QA, and DHS.

N	Time (h)	DCW_1 (g L^{-1})	DCW_2 (g L^{-1})	DCW_3 (g L^{-1})	DCW_{avg} (g L^{-1})	D-Gluc (g L^{-1})	D-Xyl (g L^{-1})	SA (g L^{-1})	QA (g L^{-1})	DHS (g L^{-1})
	0	0.0	0.1	0.1	0.1	19.9	8.6	0.0	0.0	0.0
	2	0.1	0.1	0.1	0.1	20.1	8.5	0.0	0.0	0.0
	4	0.1	0.2	0.2	0.2	21.2	9.0	0.0	0.0	0.0
	8	0.1	0.1	0.1	0.1	21.3	8.9	0.1	0.0	0.0
	14	0.2	0.2	0.2	0.2	21.4	9.3	0.1	0.0	0.0
	20	0.4	0.3	0.2	0.3	21.0	8.8	0.2	0.1	0.0
	24	0.6	0.6	0.7	0.6	19.5	8.8	0.3	0.0	0.0
1	28	1.3	1.3	1.4	1.3	17.9	8.3	0.9	0.0	0.0
	32	2.3	2.4	2.4	2.4	15.1	6.8	2.1	0.0	0.1
	36	9.2	9.6	9.6	9.5	5.4	1.9	5.3	1.2	0.4
	40	23.0	23.0	21.9	22.6	23.5	8.4	10.7	6.6	1.2
	44	32.8	27.3	31.7	30.6	28.9	10.0	20.1	10.2	1.7
	48	28.2	29.3	28.2	28.6	31.0	16.4	32.4	15.9	2.4
	54	25.1	26.3	25.1	25.5	32.0	22.3	45.4	25.0	3.0
	60	29.0	29.0	26.4	28.2	16.8	23.6	55.6	29.4	3.4

Table A.2.9. Cumulative CO_2 emissions raw data for all fermentations CO_2 emissions from YJ1.130/pKD12.138A, YJ1.144/pSC6.090B, and YJ1.148/pKD12.138A grown on D-glucose (G), D-glucose/D-xylose (GX), D-glucose/D-xylose/acetate (GXA), or hydrolysate sugars (H).

Time (h)	YJ1.130/ pKD12.138A G	YJ1.130/ pKD12.138A GX	YJ1.144/ pSC6.090B G	YJ1.144/ pSC6.090B GX	YJ1.148/ pKD12.138A G	YJ1.148/ pKD12.138A GX	YJ1.144/ pSC6.090B GXA	YJ1.144/ pSC6.090B H
1	0.0	0.0	0.0	0.0	0.0	0.0	0.0	0.0
2	0.0	0.0	0.0	0.0	0.0	0.0	0.0	0.0
3	0.0	0.0	0.0	0.0	0.0	0.0	0.0	0.0
4	0.0	0.0	0.0	0.0	0.0	0.0	0.0	0.0
5	0.0	0.0	0.0	0.0	0.0	0.0	0.0	0.0
6	0.1	0.0	0.0	0.0	0.0	0.0	0.0	0.0
7	0.1	0.1	0.0	0.1	0.1	0.1	0.0	0.0
8	0.1	0.1	0.1	0.1	0.1	0.1	0.1	0.0
9	0.1	0.1	0.1	0.1	0.1	0.1	0.1	0.0
10	0.2	0.2	0.1	0.2	0.2	0.1	0.1	0.0
11	0.3	0.3	0.1	0.2	0.2	0.2	0.2	0.0
12	0.4	0.4	0.1	0.3	0.3	0.2	0.2	0.0
13	0.5	0.6	0.2	0.3	0.4	0.3	0.3	0.1
14	1.0	0.9	0.2	0.4	0.4	0.4	0.3	0.1
15	1.7	1.4	0.3	0.8	0.5	0.5	0.4	0.1
16	2.7	2.1	0.3	1.6	0.9	1.2	0.5	0.1
17	3.6	3.0	0.4	2.4	1.6	2.0	0.6	0.1
18	4.8	4.2	0.4	3.3	2.4	2.7	0.8	0.1
19	6.0	5.4	0.5	4.4	3.4	3.7	1.4	0.1
20	7.2	6.4	0.6	5.4	4.7	4.7	2.3	0.2
21	8.3	7.3	0.9	6.3	5.4	5.6	3.1	0.2
22	9.4	8.2	1.6	7.2	6.1	6.5	4.0	0.2
23	10.4	9.1	2.2	8.1	6.7	7.3	4.8	0.2
24	11.4	10.0	2.9	8.9	7.3	8.1	5.5	0.3
25	12.4	11.0	3.6	9.7	8.0	8.8	6.4	0.3
26	13.3	11.9	4.4	10.5	8.7	9.6	7.3	0.4
27	14.3	12.9	5.3	11.3	9.4	10.3	8.2	0.4
28	15.2	13.8	6.2	12.1	11.1	10.1	9.1	0.5
29	16.1	14.7	6.9	12.8	10.7	11.9	10.1	0.6
30	17.1	15.6	7.7	13.6	11.4	12.6	11.0	0.7
31	18.0	16.5	8.4	14.3	12.0	13.3	11.9	0.8
32	18.9	17.4	9.2	15.1	12.7	14.0	12.9	0.9
33	19.8	18.2	9.9	15.8	13.3	14.7	13.8	1.0
34	20.7	19.1	10.7	16.5	14.0	15.3	14.8	1.1
35	21.6	19.9	11.4	17.2	14.6	16.0	15.7	1.2
36	22.5	20.8	12.1	17.9	15.2	16.6	16.7	1.5
37	23.3	21.6	12.8	18.5	15.8	17.3	17.6	2.2
38	24.2	22.4	13.5	19.2	16.5	17.9	18.6	3.2
39	25.0	23.3	14.2	19.8	17.1	18.5	19.6	4.6
40	25.8	24.0	14.9	20.5	17.7	19.1	20.6	5.9
41	26.6	24.8	15.6	21.2	18.3	19.7	21.7	7.1
42	27.4	25.4	16.3	21.8	18.9	20.2	22.7	8.3
43	28.2	25.9	16.9	22.5	19.5	20.8	23.8	9.5
44	28.9	26.2	17.6	23.1	20.1	21.4	24.8	10.5
45	29.7	26.6	18.3	23.7	20.7	22.0	25.9	11.6
46	30.4	27.0	18.9	24.3	21.3	22.5	27.0	12.7
47	31.2	27.4	19.6	24.9	21.8	23.1	28.1	13.7
48	31.9	27.8	20.3	25.5	22.4	23.7	29.3	14.8
49	-	-	-	-	-	-	-	15.7
50	-	-	-	-	-	-	-	16.8
51	-	-	-	-	-	-	-	17.8
52	-	-	-	-	-	-	-	18.8
53	-	-	-	-	-	-	-	19.8
54	-	-	-	-	-	-	-	20.8
55	-	-	-	-	-	-	-	21.8
56	-	-	-	-	-	-	-	22.7
57	-	-	-	-	-	-	-	23.7
58	-	-	-	-	-	-	-	24.6
59	-	-	-	-	-	-	-	25.5
60	-	-	-	-	-	-	-	26.3

Table A.2.10. YJ1.144/pSC6.090B fermentations yields (mol/mol) molar yields of SA, QA, DHS, DCW, and CO_2 on a moles of carbon-to-carbon basis. Calculations began with glucose titer measured using HPLC. From these values, moles of carbon were calculated. The conversion yields of carbon from carbohydrates to carbon in the respective analyte are itemized in the bottom five rows.

Analyte	YJ1.144/pSC6.090B G	YJ1.144/pSC6.090B GX	YJ1.144/pSC6.090B GXA	YJ1.144/pSC6.090B H
Glucose Initial ($g\ L^{-1}$)	15.2	12.6	20.3	19.9
Xylose Initial ($g\ L^{-1}$)	-	5.2	9	8.6
Glucose Final ($g\ L^{-1}$)	45.7	14.8	7.4	16.8
Xylose Final ($g\ L^{-1}$)	-	7.6	6.6	23.6
Shikimate ($g\ L^{-1}$)	54.9	91.7	65.1	55.6
Quinate ($g\ L^{-1}$)	23.5	8.3	34.1	29.4
3-dehydroshikimate ($g\ L^{-1}$)	21.2	16.1	11.9	3.4
Dry Cell Weight ($g\ L^{-1}$)	36.0	34.0	39.0	31.0
Carbon Dioxide ($g\ L^{-1}$)	20	26	29	26
Gluc + Xyl Consumed (mol C)	8.98	9.84	10.5	9.59
Shikimate (mol C)	2.21	3.69	2.62	2.23
Quinate (mol C)	0.86	0.30	1.25	1.08
3-dehydroshikimate (mol C)	0.86	0.65	0.48	0.14
Dry Cell Weight (mol C)	1.57	1.48	1.70	1.35
Carbon Dioxide (mol C)	0.45	0.59	0.66	0.59
Shikimate (%)	0.25	0.37	0.25	0.23
Quinate (%)	0.10	0.03	0.12	0.11
3-dehydroshikimate (%)	0.10	0.07	0.05	0.01
Dry Cell Weight (%)	0.17	0.15	0.16	0.14
Carbon Dioxide (%)	0.05	0.06	0.06	0.06

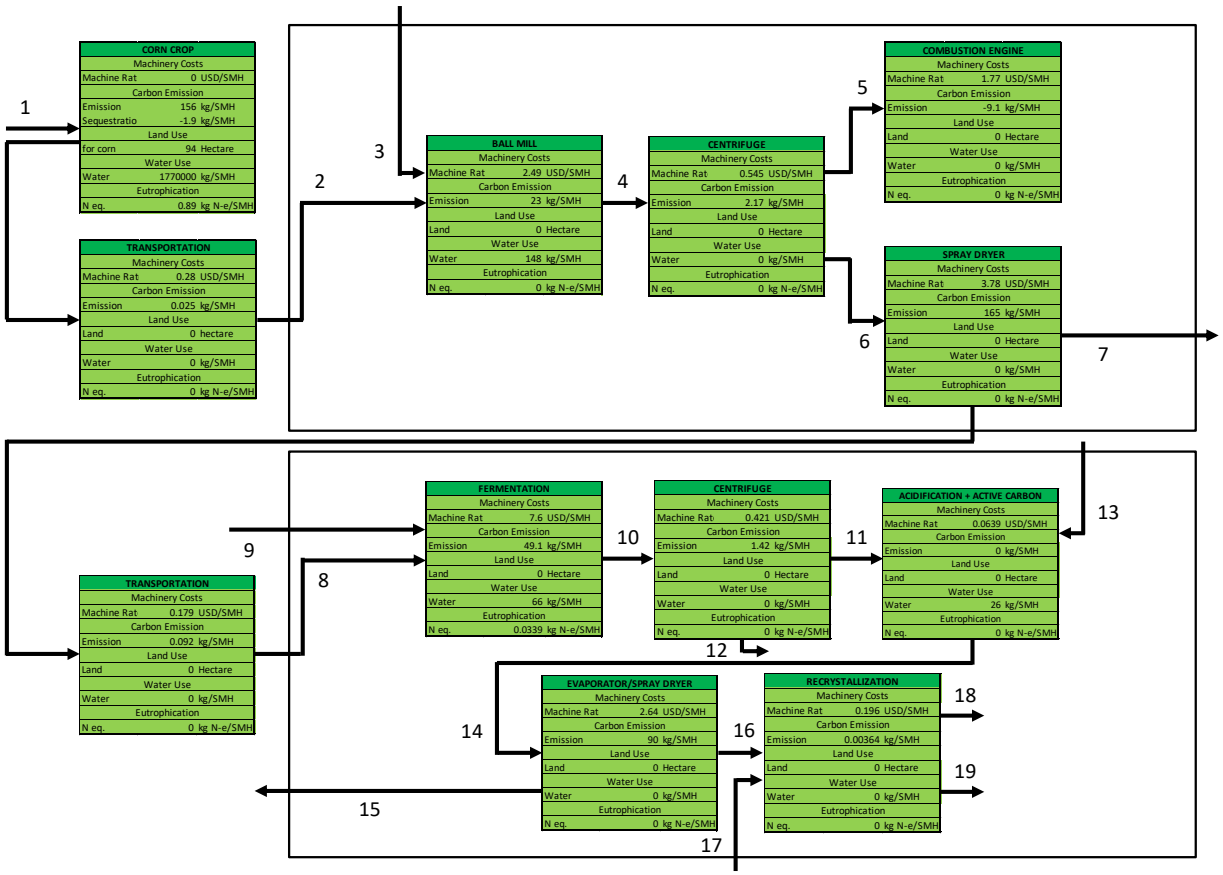

1	N, 13200 kg yr^{-1}; P, 5180 kg yr^{-1}; K, 10700 kg yr^{-1}; Herbicide, 235 kg yr^{-1}; Insecticide, 9 kg yr^{-1}; Lime, 2170 kg yr^{-1}
2	Corn stover, 352000 kg yr^{-1}; 35% (*w*/*w*) moisture
3	Cellulase, 2870 kg yr^{-1}; Xylanase, 454 kg yr^{-1}; Fresh water, 905000 kg yr^{-1}; Backset water, 388000 kg yr^{-1}
4	Glucose, 90900 kg yr^{-1}; Xylose, 33100 kg yr^{-1}; Acetic acid, 2330 kg yr^{-1}; Cellulose, 17500 kg yr^{-1}; Xylan, 14100 kg yr^{-1}; Lignin, 80000 kg yr^{-1}; Ash, 44800 kg yr^{-1}; Water, 1370000 kg yr^{-1}
5	Cellulose, 17500 kg yr^{-1}; Xylan, 14100 kg yr^{-1}; Lignin, 80000 kg yr^{-1}; Ash, 44800 kg yr^{-1}
6	Glucose, 90900 kg yr^{-1}; Xylose, 33100 kg yr^{-1}; Acetic acid, 2330 kg yr^{-1}; Water, 1370000 kg yr^{-1}
7	Water, 1370000 kg yr^{-1}
8	Glucose, 90900 kg yr^{-1}; Xylose, 33100 kg yr^{-1}; Acetic acid, 2330 kg yr^{-1}
9	Conc. NH_4OH, 4850 kg yr^{-1}; K_2HPO_4, 2820 kg yr^{-1}; Ammonium Iron Citrate, 113 kg yr^{-1}; Citric acid, 722 kg yr^{-1}; Tyrosine, 263 kg yr^{-1}; Phenylalanine, 263 kg yr^{-1}; Tryptophan, 132 kg yr^{-1}; Benzoic acids, 4 kg yr^{-1}; $MgSO_4$, 45 kg yr^{-1}; Thiamine, 0.4 kg yr^{-1}; $(NH_4)_6(Mo_7O_{24})\cdot 4H_2O$, 1 kg yr^{-1}; $ZnSO_4\cdot 7H_2O$, 1 kg yr^{-1}; $B(OH)_3$, 8 kg yr^{-1}; $CuSO_4\cdot 5H_2O$, 0.8 kg yr^{-1}; $MnCl_2\cdot 4H_2O$, 5 kg yr^{-1}; Water, 576000 kg yr^{-1}
10	Shikimic acid, 34500 kg yr^{-1}; Biomass, 12500 kg yr^{-1}; 3-Dehydroshikimate, 6050 kg yr^{-1}; Quinic acid, 3120 kg yr^{-1}; Water, 526000 kg yr^{-1}
11	Shikimic acid, 34500 kg yr^{-1}; 3-Dehydroshikimate, 6050 kg yr^{-1}; Quinic acid, 3120 kg yr^{-1}; Water, 526000 kg yr^{-1}
12	Biomass, 12500 kg yr^{-1}
13	Active carbon, 75200 kg yr^{-1}; 6 N H_2SO_4, 226000 kg yr^{-1}
14	Shikimic acid, 34500 kg yr^{-1}; 3-Dehydroshikimate, 6050 kg yr^{-1}; Quinic acid, 3120 kg yr^{-1}; Water, 752000 kg yr^{-1}
15	Water, 752000 kg yr^{-1}
16	Shikimic acid, 34500 kg yr^{-1}; 3-Dehydroshikimate, 6050 kg yr^{-1}; Quinic acid, 3120 kg yr^{-1}; Water, 1300 kg yr^{-1}
17	n-butanol, 180 kg yr^{-1}
18	95% (*w*/*w*) Shikimic acid, 30000 kg yr^{-1}
19	Shikimic acid, 4470 kg yr^{-1}; 3-Dehydroshikimate, 4470 kg yr^{-1}; Quinic acid, 3120 kg yr^{-1}

Figure A.3.1. Stover flow diagram stream summary table for 30 MT SA yr^{-1} capacity corn stover refinery system.

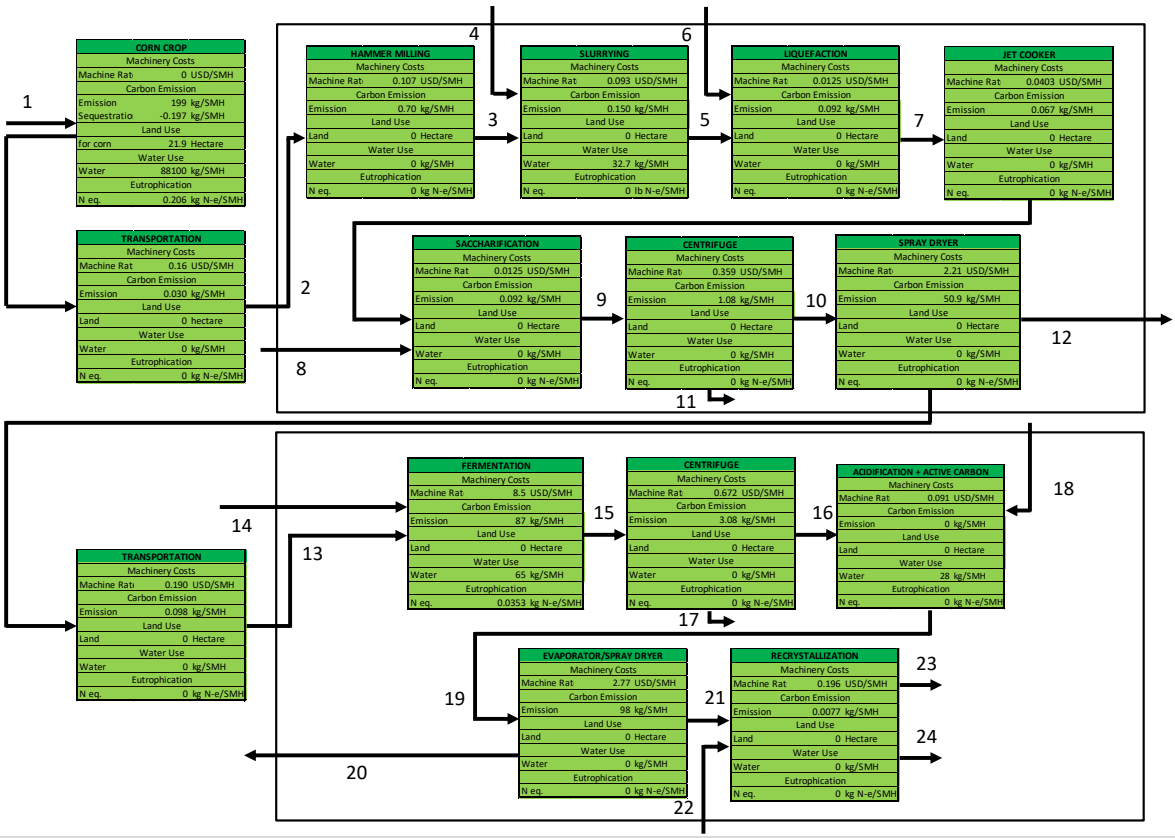

1	N, 3060 kg yr^{-1}; P, 1200 kg yr^{-1}; K, 2490 kg yr^{-1}; Herbicide, 55 kg yr^{-1}; Insecticide, 2 kg yr^{-1}; Lime, 503 kg yr^{-1}
2	Corn grain, 202000 kg yr^{-1}; 15.5% (*w*/*w*) moisture
3	Dry corn meal, 170000 kg yr^{-1}
4	Fresh water, 286000 kg yr^{-1}; Backset water, 102000 kg yr^{-1}
5	Starch, 125000 kg yr^{-1}; Water, 434000 kg yr^{-1}
6	Alpha amylase, 125 kg yr^{-1}
7	Dextrins, 125000 kg yr^{-1}; Alpha amylase, 125 kg yr^{-1}; Water, 434000 kg yr^{-1}
8	Glucoamylase, 680 kg yr^{-1}
9	Dextrose, 136000 kg yr^{-1}; Glucoamylase, 680 kg yr^{-1}; Alpha amylase, 125 kg yr^{-1}; Water, 423000 kg yr^{-1}
10	Dextrose, 227000 kg yr^{-1}; Water, 705000 kg yr^{-1}
11	DDGS, 240000 kg yr^{-1}
12	Water, 419000 kg yr^{-1}
13	Glucose, 135000 kg yr^{-1}
14	Conc. NH_4OH, 5050 kg yr^{-1}; K_2HPO_4, 3060 kg yr^{-1}; Ammonium Iron Citrate, 122 kg yr^{-1}; Citric acid, 784 kg yr^{-1}; Tyrosine, 286 kg yr^{-1}; Phenylalanine, 286 kg yr^{-1}; Tryptophan, 143 kg yr^{-1}; Benzoic acids, 4 kg yr^{-1}; $MgSO_4$, 49 kg yr^{-1}; Thiamine, 0.4 kg yr^{-1}; $(NH_4)_6(Mo_7O_{24})\cdot 4H_2O$, 2 kg yr^{-1}; $ZnSO_4\cdot 7H_2O$, 1 kg yr^{-1}; $B(OH)_3$, 10 kg yr^{-1}; $CuSO_4\cdot 5H_2O$, 1 kg yr^{-1}; $MnCl_2\cdot 4H_2O$, 6 kg yr^{-1}; Water, 571000 kg yr^{-1}
15	Shikimic acid, 31800 kg yr^{-1}; Biomass, 14700 kg yr^{-1}; 3-Dehydroshikimate, 3420 kg yr^{-1}; Quinic acid, 608 kg yr^{-1}; Water, 571000 kg yr^{-1}
16	Shikimic acid, 31800 kg yr^{-1}; 3-Dehydroshikimate, 3420 kg yr^{-1}; Quinic acid, 608 kg yr^{-1}; Water, 571000 kg yr^{-1}
17	Biomass, 24500 kg yr^{-1}
18	Active carbon, 81600 kg yr^{-1}; 6 N H_2SO_4, 245000 kg yr^{-1}
19	Shikimic acid, 31800 kg yr^{-1}; 3-Dehydroshikimate, 3420 kg yr^{-1}; Quinic acid, 608 kg yr^{-1}; Water, 816000 kg yr^{-1}
20	Water, 815000 kg yr^{-1}
21	Shikimic acid, 31800 kg yr^{-1}; 3-Dehydroshikimate, 3420 kg yr^{-1}; Quinic acid, 608 kg yr^{-1}; Water, 1070 kg yr^{-1}
22	n-butanol, 180 kg yr^{-1}
23	95% (*w*/*w*) Shikimic acid, 30000 kg yr^{-1}
24	Shikimic acid, 1840 kg yr^{-1}; 3-Dehydroshikimate, 1840 kg yr^{-1}; Quinic acid, 608 kg yr^{-1}

Figure A.3.2. Grain flow diagram stream summary table for 30 MT SA yr^{-1} capacity corn grain refinery system.

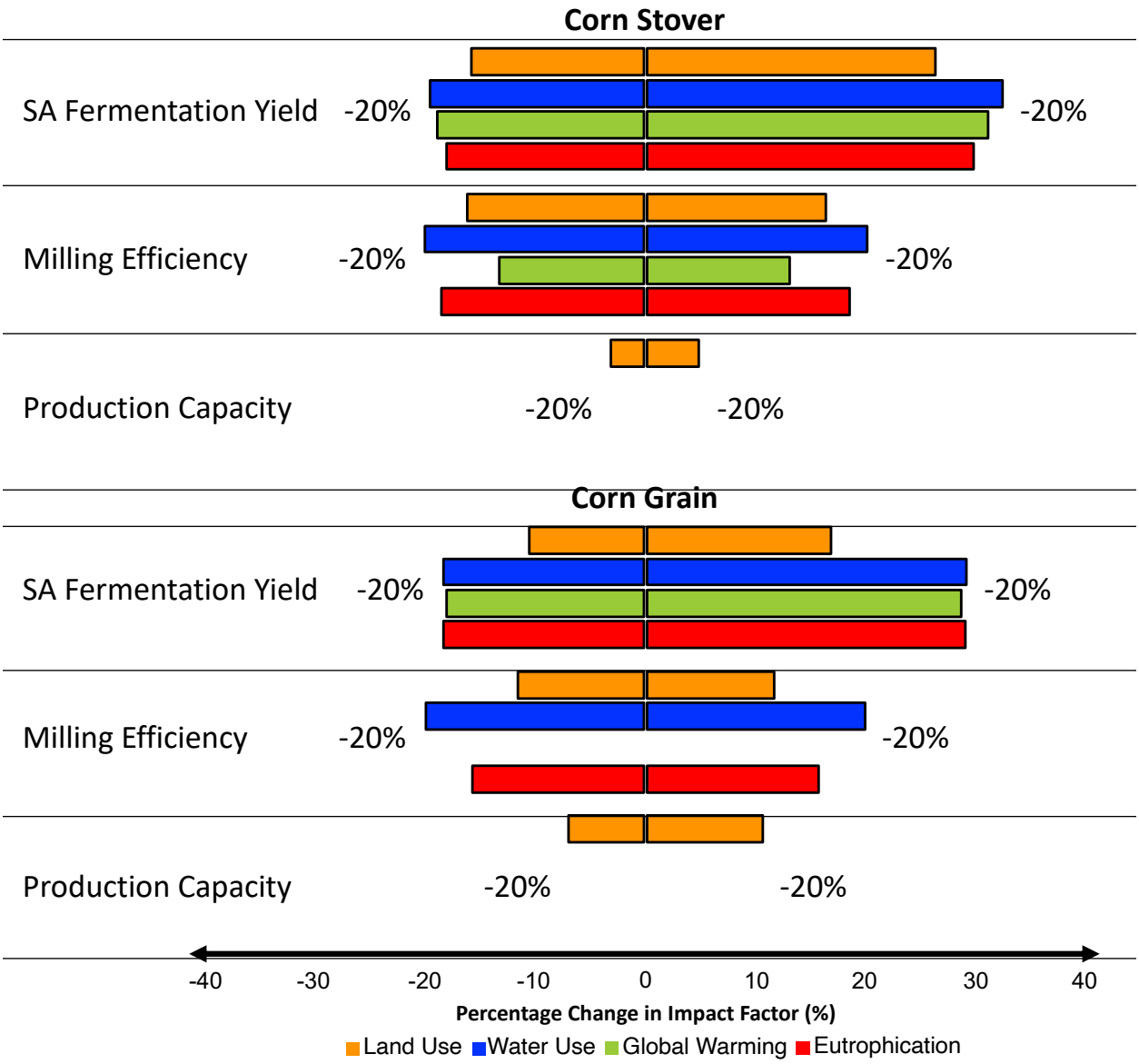

Figure A.3.3. LCA sensitivity (percentage) tornado plot of the sensitivities of key contributing variables to LCI categories.

Table A.3.1. Data quality indicators (DQI) DQIs for cultivation, ball mill, dry mill, spray drying, and fermentation data.

Data	Ref.	Reliability	Completeness	Temporal Correlation	Geographical Correlation	Technological Correlation	DQI
Cultivation	[53]	1	1	3	3	2	2.0
Ball Mill	[8]	1	1	1	1	1	1.0
Dry Mill	[19, 20]	1	1	4	1	2	1.8
Spray Drying	[54]	1	1	5	1	2	2.0
Fermentation	This study	1	1	1	1	1	1.0

Table A.3.2. Equipment summary table equipment costing, sizing, and emission rates.

Equipment	Price (USD)	Sizing	Machine Rate (USD SMH^{-1})	Emission Rate (kg CO_2 SMH^{-1})	Ref.
Corn Stover					
Ball Mill 1	38,200	1980 L	0.83	7.57	[8]
Ball Mill 2	38,200	1980 L	0.83	7.57	[8]
Ball Mill 3	38,200	1980 L	0.83	7.57	[8]
Centrifuge 1	25,100	3.07 kW	0.54	2.17	[19, 20]
Combustion Engine	49,800	12.8 kW	1.08	-9.07	[55, 56]
Gasifier	32,000	-	0.69	0	[55, 56]
Spray Dryer	174,000	15700 L	3.78	165	[54]
Fermenter 1	117,000	5530 L	2.54	16.4	This study
Fermenter 2	117,000	5530 L	2.54	16.4	This study
Fermenter 3	117,000	5530 L	2.54	16.4	This study
Centrifuge 2	19,400	2 kW	0.42	1.42	[19, 20]
Mixing Tank	2,940	1550 L	0.06	0	[19, 20]
Spray Dryer 2	121,000	8580 L	2.64	90	[54]
Cold Room	9,000	0.0052 kW	0.20	0.004	[57]
Transportation	-	-	0.46	0.12	-
Corn Grain					
Hammer Mill	4,940	0.98 kW	0.11	0.70	[23, 24]
Slurry Tank	4,290	96 L	0.09	0.150	[23, 24]
Liquefaction Tank	574	96 L	0.012	0.092	[23, 24]
Jet Cooker	1,860	0.094 kW	0.04	0.067	[23, 24]
Saccharification	575	96 L	0.01	0.092	[23, 24]
Centrifuge 1	16,500	1.53 kW	0.36	1.08	[23, 24]
Spray Dryer 1	102,000	6380 L	2.21	50.9	[54]
Fermenter 1	130,000	6580 L	2.82	29.2	This study
Fermenter 2	130,000	6580 L	2.82	29.2	This study
Fermenter 3	130,000	6580 L	2.82	29.2	This study
Centrifuge 2	30,900	4.36 kW	0.67	3.08	[23, 24]
Mixing Tank	4,170	2780 L	0.09	0	[23, 24]
Spray Dryer 2	127,000	9310 L	2.77	98	[54]
Cold Room	9,000	0.011 HP	0.20	0.008	[57]
Transportation	-	-	0.35	0.128	-

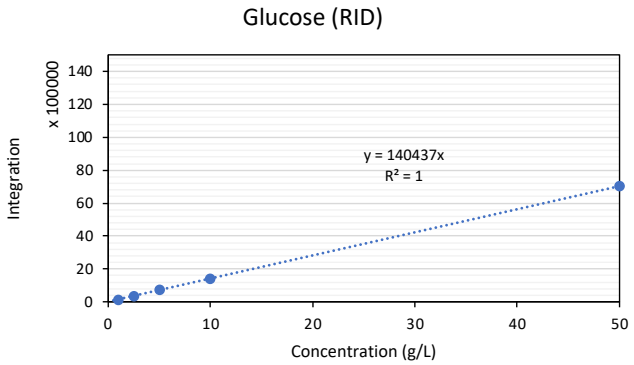

Figure A.6.1. Glucose HPLC calibration curve D-glucose HPLC-RID calibration data.

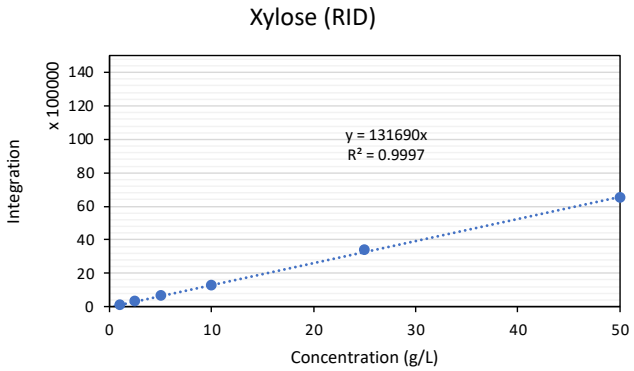

Figure A.6.2. Xylose HPLC calibration curve: D-xylose HPLC-RID calibration data.

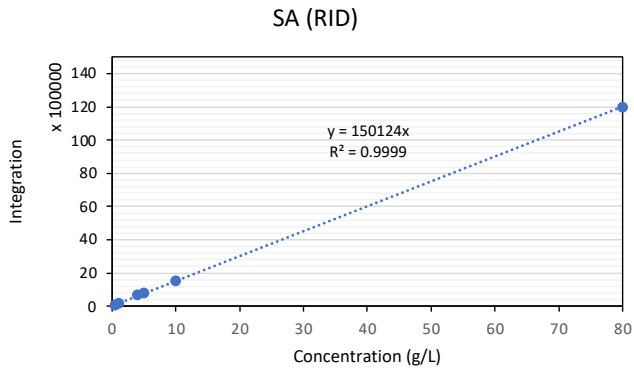

Figure A.6.3. SA HPLC calibration curve SA HPLC-RID calibration data.

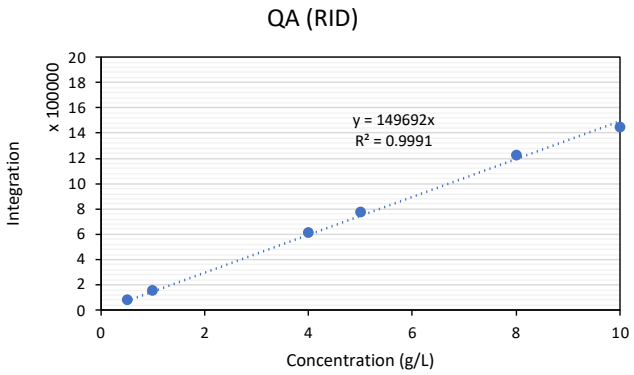

Figure A.6.4. QA HPLC calibration curve QA HPLC-RID calibration data.

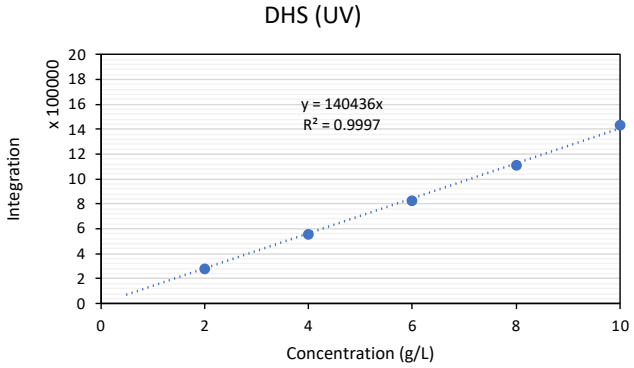

Figure A.6.5. DHS HPLC calibration curve DHS HPLC-UV calibration data.

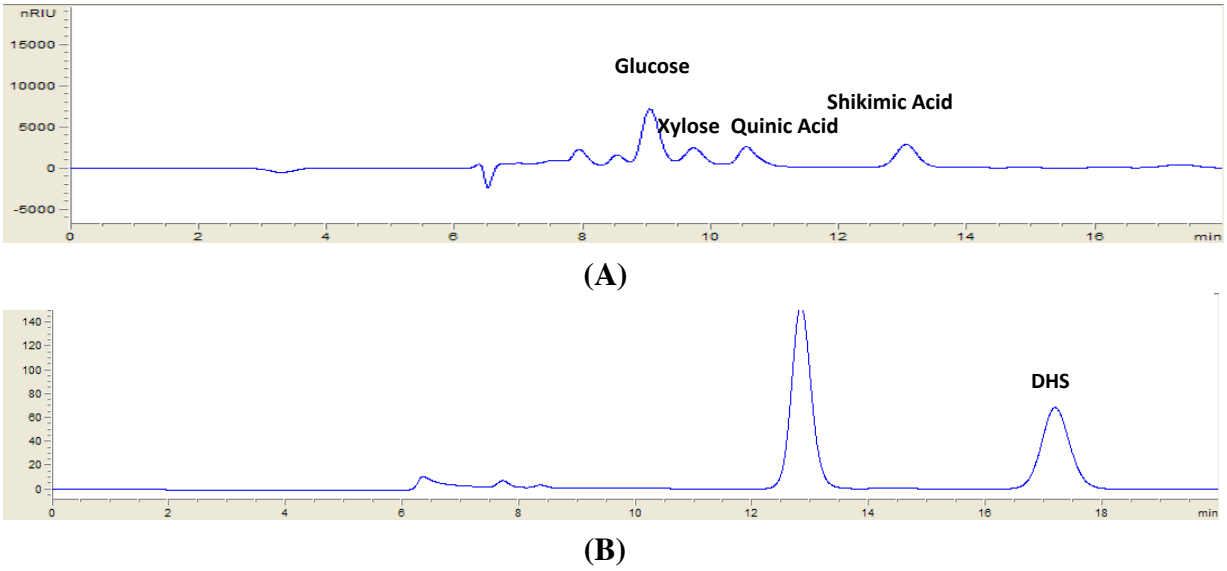

Figure A.6.6. Hydrolysate HPLC chromatogram (a) RID chromatogram (b) UV chromatogram.

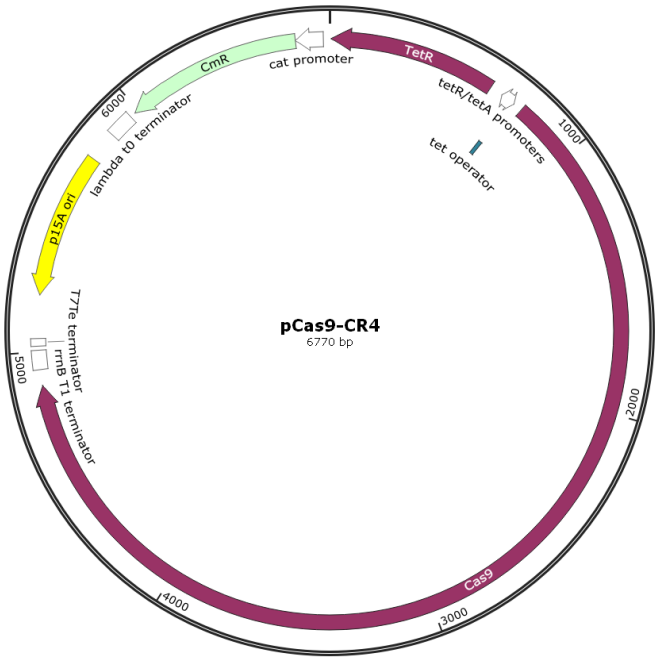

Figure A.6.7. Plasmid pCas9-cr4 plasmid map of pCas9-cr4.

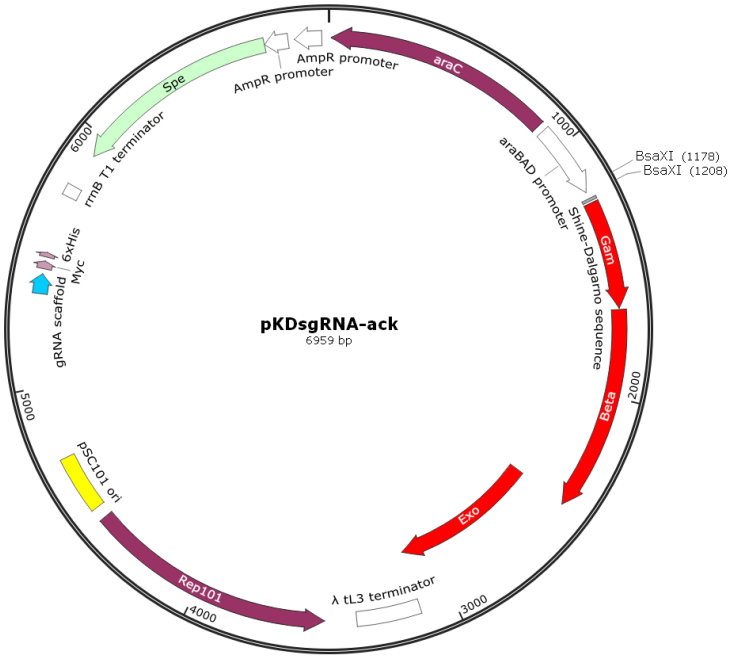

Figure A.6.8. Plasmid pKDsgRNA-ack plasmid map of pKDsgRNA-ack.

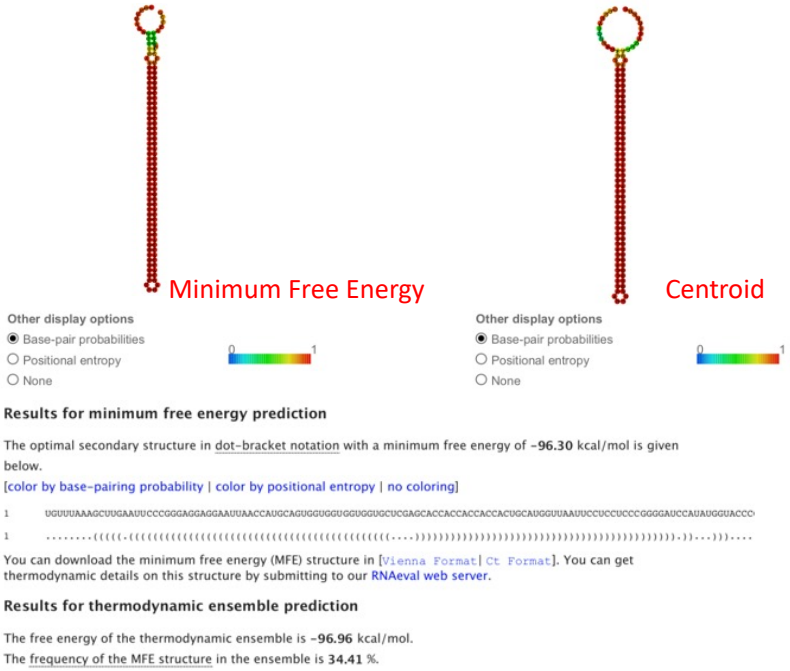

Figure A.6.9. Minimum free energy (MFE) of stem structure MFE of paired termini lacking *as*RNA region of stem-loop structure.

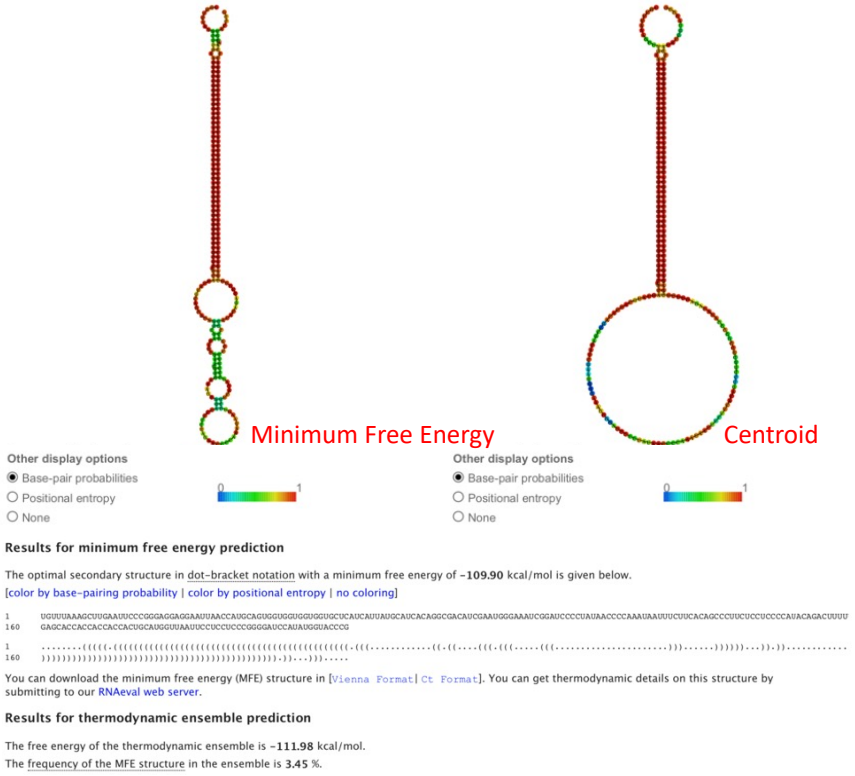

Figure A.6.10. MFE of stem-loop structure MFE of paired termini carrying *as*aroE region of stem-loop structure. Both MFE and centroid structures are displayed.